

Corrosivity of Water-Base Drilling Fluids in Deep, Hot Wells

by

Olawake Surajudeen Shokoya

A Thesis Presented to the

FACULTY OF THE COLLEGE OF GRADUATE STUDIES

KING FAHD UNIVERSITY OF PETROLEUM & MINERALS

DHAHRAN, SAUDI ARABIA

In Partial Fulfillment of the
Requirements for the Degree of

MASTER OF SCIENCE

In

PETROLEUM ENGINEERING

December, 1994

INFORMATION TO USERS

This manuscript has been reproduced from the microfilm master. UMI films the text directly from the original or copy submitted. Thus, some thesis and dissertation copies are in typewriter face, while others may be from any type of computer printer.

The quality of this reproduction is dependent upon the quality of the copy submitted. Broken or indistinct print, colored or poor quality illustrations and photographs, print bleedthrough, substandard margins, and improper alignment can adversely affect reproduction.

In the unlikely event that the author did not send UMI a complete manuscript and there are missing pages, these will be noted. Also, if unauthorized copyright material had to be removed, a note will indicate the deletion.

Oversize materials (e.g., maps, drawings, charts) are reproduced by sectioning the original, beginning at the upper left-hand corner and continuing from left to right in equal sections with small overlaps. Each original is also photographed in one exposure and is included in reduced form at the back of the book.

Photographs included in the original manuscript have been reproduced xerographically in this copy. Higher quality 6" x 9" black and white photographic prints are available for any photographs or illustrations appearing in this copy for an additional charge. Contact UMI directly to order.

UMI

A Bell & Howell Information Company
300 North Zeeb Road, Ann Arbor, MI 48106-1346 USA
313/761-4700 800/521-0600



**CORROSIVITY OF WATER-BASE DRILLING
FLUIDS IN DEEP, HOT WELLS**

BY

OLAWALE SURAJUDEEN SHOKOYA

A Thesis Presented to the
FACULTY OF THE COLLEGE OF GRADUATE STUDIES
KING FAHD UNIVERSITY OF PETROLEUM & MINERALS
DHAHRAN, SAUDI ARABIA

In Partial Fulfillment of the
Requirements for the Degree of

MASTER OF SCIENCE
In
PETROLEUM ENGINEERING

December 1994

UMI Number: 1375313

**UMI Microform 1375313
Copyright 1995, by UMI Company. All rights reserved.**

**This microform edition is protected against unauthorized
copying under Title 17, United States Code.**

UMI
300 North Zeeb Road
Ann Arbor, MI 48103

KING FAHD UNIVERSITY OF PETROLEUM AND MINERALS
DHAHRAN 31261, SAUDI ARABIA

COLLEGE OF GRADUATE STUDIES

This thesis, written by **Olawale Surajudeen Shokoya** under the direction of his Thesis Advisor and approved by his Thesis Committee, has been presented to and accepted by the Dean of the College of Graduate Studies, in partial fulfillment of the requirements for the degree of **MASTER OF SCIENCE**.

Thesis Committee

M. A. Marhoun

Dr. Muhammad A. Al-Marhoun
Thesis Advisor

H. Y. Al-Yousef

Dr. Hasan Y. Al-Yousef
Member

[Signature]

Dr. Khalid Al-Fossail
Member

[Signature]

Dr. Khalid Al-Fossail
Department Chairman

[Signature]

Dr. Ala H. Al-Rabeh
Dean, College of Graduate Studies



Date:

30.1.95

Dedication

To my wife and daughter

ACKNOWLEDGEMENT

Praise be to Almighty Allah, the beneficent and the merciful. Acknowledgement is due to King Fahd University of Petroleum and Minerals (KFUPM) for support of this research. The Divisions I and V of KFUPM's Research Institute (RI) are also acknowledged for making their equipment and personnel available for supervision of part of this study.

I wish to express my gratitude and appreciation to Dr. Muhammad Ali Al-Marhoun who served as my major advisor for his constant guidance and beneficial advice, not only during the course of this research; but since I joined KFUPM. I owe the other members of my committee, Dr. Hasan Y. Al-Yousef and Dr. Khalid Al Fossail, a debt of gratitude for their effective contribution and unflinching support that made the timely and successful completion of this research possible.

Acknowledgement is also due to Dr. Oluwatoyin A. Ashiru of division V, KFUPM/RI for his invaluable contribution to the outcome of this research. Special thanks to the staff of the Petroleum Engineering Department Laboratory for their collective and individual efforts that saw to the timely and successful completion of the experimental work. The assistance of Mr. Abdul Quddus Mehr-ud-din and Mr. Nizar Reda Jarrah, both of division V, KFUPM/RI; in conducting part of the experimental work is hereby acknowledged.

Several individuals deserve to be mentioned for various forms of assistance; before, during, and after this work. I am greatly indebted to Mr. Abdul Samad Idrissu and Mr. Abdul Rahim Muhammadain for their kindness. To other friends and well wishers too numerous to mention, I say thank you all. Thanks to Mr. Varkey Paulose for typing part of this thesis.

Finally, I would like to thank my family, both here and in Nigeria for having stood solidly by me these past two years. Special thanks to my wife for her understanding, constant encouragement and full support during the past two years when all my time was spent for my studies. I also acknowledge her help in preparing the script of this thesis.

TABLE OF CONTENTS

	Page No.
List of Tables	viii
List of Figures	xi
Thesis Abstract: English	xv
Arabic	xvi
CHAPTER 1 INTRODUCTION	1
CHAPTER 2 FUNDAMENTALS OF CORROSION	4
2.1 Types of Corrosion	4
2.2 Corrosion Mechanism	6
2.3 Corrosive Environments and Their Effect	9
2.3.1 Dissolved Oxygen	9
2.3.2 Temperature	9
2.3.3 pH	10
2.3.4 Carbon Dioxide	10
2.3.5 Hydrogen Sulfide	11
2.3.6 Stress Cracking and Hydrogen Embrittlement	12
2.4 Corrosion Monitoring	13
2.4.1 Weight-Loss Method	14
2.4.2 Polarization Resistance	19
2.4.3 Potentiodynamic Polarization Diagrams	21
2.4.4 AC Impedance Polarization	23
2.5 Factors Affecting Reproducibility of Corrosion Rate Measurements	27
CHAPTER 3 LITERATURE REVIEW	29
CHAPTER 4 EXPERIMENTAL SET-UP AND PROCEDURE	43

4.1	Experimental Set-Up	43
4.1.1	Mud Formulation	43
4.1.2	Equipment	44
4.2	Procedure	54
4.2.1	Mud Preparation	54
4.2.2	Preparation of Corrosion Coupons	55
4.2.3	HPHT Viscometer	56
4.2.4	Roller Oven	56
4.2.5	Flow Loop	57
4.2.6	Potentiodynamic Polarization Tests	61
4.2.7	AC Impedance Tests	64
4.2.8	Scanning Electron Microscope (SEM) Investigation	64
CHAPTER 5 RESULTS AND DISCUSSION		65
5.1	Thermal Stability of Mud	65
5.2	Effect of Temperature and Exposure Time on Mud Corrosivity	81
5.3	Effect of pH and Exposure Time on Mud Corrosivity	90
5.4	Potentiodynamic Polarization Results	95
5.5	AC Impedance Results	98
5.6	Analysis of Scanning Electron Micrographs	106
CHAPTER 6 CONCLUSIONS AND RECOMMENDATIONS		118
6.1	Conclusions	118
6.2	Recommendations	119
NOMENCLATURE		122
REFERENCES		124
APPENDICES		130

A	Experimental Data for Thermal Stability Tests	131
B	Experimental Data for Roller Oven and Flow Loop Tests	138
C	Experimental Data for Potentiodynamic and AC Impedance Tests.	151
VITA		161

LIST OF TABLES

TABLE		Page No.
I	Literature Review Summary.	39
A1	Consistency Curve Data Obtained at 3000 psi after Preparation of Mud (no Aging).	132
A2	Consistency Curve Data Obtained at 3000 psi after Aging for 5 days.	132
A3	Consistency Curve Data Obtained at 3000 psi after Aging for 10 days.	133
A4	Consistency Curve Data Obtained at 3000 psi after Aging for 15 days.	133
A5	Consistency Curve Data Obtained at 3000 psi after Aging for 20 days.	134
A6	Consistency Curve Data Obtained at Ambient Conditions after Aging at 250 °F.	134
A7	Effective Viscosity Data Obtained at 3000 psi, Different Temperature and Aging Period.	135
A8	Plastic Viscosity Data Obtained at 3000 psi, Different Temperature and Aging period.	135
A9	Yield Strength Data Obtained at 3000 psi, Different Temperature and Aging period.	136
A10	Gel Strength Data Obtained at 3000 psi, Different Temperature and Aging period.	136
A11	Power Law Exponent, n' Obtained from all Tests at 3000 psi, Different Temperature and Aging period.	137
A12	Consistency Index, k Obtained from all Tests at 3000 psi, Different Temperature and Aging period.	137

B1	Corrosion Rate Data of Mild Steel (1018) Coupons Exposed to Mud in the Roller Oven at 200 °F. pH of Mud = 10.9.	138
B2	Corrosion Rate Data of Mild Steel (1018) Coupons Exposed to Mud in the Roller Oven at 250 °F. pH of Mud = 10.9.	139
B3	Corrosion Rate Data of Mild Steel (1018) Coupons Exposed to Mud in the Roller Oven at 300 °F. pH of Mud = 10.9.	140
B4	Corrosion Rate Data of Mild Steel (1018) Coupons Exposed to Mud in the Roller Oven at 400 °F. pH of Mud = 10.9.	141
B5	Corrosion Rate Data of Mild Steel (1018) Coupons Exposed to Mud in the Roller Oven at pH of 7.9. Temperature = 250 °F.	142
B6	Corrosion Rate Data of Mild Steel (1018) Coupons Exposed to Mud in the Roller Oven at pH of 6.1. Temperature = 250 °F.	143
B7	Corrosion Rate Data of Mild Steel (1018) Coupons Exposed to Mud in the Roller Oven at pH of 4.9. Temperature = 250 °F.	144
B8	Corrosion Rate Data of Mild Steel (1018) Coupons Exposed to Mud in the Cold Section of Flow Loop at 3000 psi for 8 hours. pH of Mud = 9.5.	145
B9	Corrosion Rate Data of Mild Steel (1018) Coupons Exposed to Mud in the Hot Section of Flow Loop at 3000 psi for 8 hours. pH of Mud = 9.5.	146
B10	Corrosion Rate Data of Mild Steel (1018) Coupons Exposed to Mud in the Cold Section of Flow Loop at 3000 psi for 8 hours.	147
B11	Corrosion Rate Data of Mild Steel (1018) Coupons Exposed to Mud in the Hot Section of Flow Loop at 3000 psi for 8 hours. Temperature = 161 °F.	148
B12	Polarization Resistance Corrosion Rate Data of Mild Steel (1018) Coupons Exposed to Mud in the Cold Section of Flow Loop at Different Temperature and 3000 psi over an 8 hour period. pH of Mud = 9.5.	149
B13	Polarization Resistance Corrosion Rate Data of mild steel (1018) Coupons Exposed to Mud in the Hot Section of Flow Loop at	

	Different Temperature and 3000 psi over an 8 hour period. pH of Mud = 9.5.	149
B14	Polarization Resistance Corrosion Rate Data of Mild Steel (1018) Coupons Exposed to Mud in the Cold Section of Flow Loop at Different pH and 3000 psi over an 8 hour period.	150
B15	Polarization Resistance Corrosion Rate Data of Mild Steel (1018) Coupons Exposed to Mud in the Cold Section of Flow Loop at Different pH and 3000 psi over an 8 hour period. Temperature = 161 °F.	150
C1	Potentiodynamic Polarization Data Measured Under Static and Ambient Conditions at Different Mud pH.	151
C2	Hydrodynamic Data Obtained at Equilibrium Corrosion Potential of 500 mV for Mud pH 4.1.	151
C3	Hydrodynamic Data Obtained at Equilibrium Corrosion Potential of 500 mV for Mud pH 10.9.	152
C4	AC Impedance Data Obtained Under Static Condition for Mud pH 10.9	153
C5	AC Impedance Data Obtained at 500 rpm for Mud pH 10.9.	154
C6	AC Impedance Data Obtained at 1000 rpm for Mud pH 10.9.	155
C7	AC Impedance Data Obtained at 2000 rpm for Mud pH 10.9.	156
C8	AC Impedance Data Obtained Under Static Condition for Mud pH 4.1.	157
C9	AC Impedance Data Obtained at 500 rpm for Mud pH 4.1.	158
C10	AC Impedance Data Obtained at 1000 rpm for Mud pH 4.1.	159
C11	AC Impedance Data Obtained at 2000 rpm for Mud pH 4.1.	160

LIST OF FIGURES

Figure		Page No.
2.1	Hypothetical Cathodic and Anodic Polarization Plot Showing the Extrapolation of Tafel Slopes to the Corrosion Potential to Obtain Corrosion Current Density.	17
2.2	Impedance Technique for Corrosion Measurements.	26
4.1	Schematic Diagram of the Dynamic Flow Loop.	45
4.2	Schematic Diagram of the Test Section.	48
4.3	Flow Loop Corrosion Cells.	49
4.4	FANN-70 High Pressure-High Temperature Viscometer.	51
4.5	Baroid Roller Oven with 500 ml Aging Cells.	53
4.6a	Experimental Set-Up of the Dynamic Flow Loop showing the Test Section, the Heating and Cooling system, and the Heater Control Panel.	58
4.6b	Experimental Set-Up of the Dynamic Flow Loop showing the Pumping Unit, the Mud Reservoir, Mixer and pH Meter.	59
4.6c	Experimental Set-up of the Dynamic Flow Loop showing the Control Panel with Petrolite Corrosion Meter, other Measuring Instruments and Recorders.	60
4.7	Experimental Set-Up of Potentiodynamic and AC Impedance Tests.	63
5.1	Consistency Curve Obtained at 3000 psi after Aging in Roller Oven at 200 °F.	67
5.2	Consistency Curve Obtained at 3000 psi after Aging in Roller Oven at 250 °F.	68
5.3	Consistency Curve Obtained at 3000 psi after Aging in Roller Oven	

	at 300 °F.	69
5.4	Consistency Curve Obtained at 3000 psi after Aging in Roller Oven at 400 °F.	70
5.5	Comparison of Consistency Curves Obtained Under Downhole (250 °F, 3000 psi) and Surface Conditions.	71
5.6	Effect of Temperature on Effective Viscosity Measured at 1022 s ⁻¹ Shear Rate.	72
5.7	Effect of Aging on Effective Viscosity Measured at 1022 s ⁻¹ Shear Rate.	73
5.8	Effect of Temperature on Plastic Viscosity.	74
5.9	Effect of Aging on Plastic Viscosity.	75
5.10	Effect of Temperature on Yield Strength.	77
5.11	Effect of Aging on Yield Strength.	78
5.12	Effect of Temperature on Gel Strength.	79
5.13	Effect of Aging on Gel Strength.	80
5.14	Effect of Temperature on Weight Loss Measured Using the Roller Oven at Mud pH of 10.9.	82
5.15	Effect of Exposure Time on Weight Loss Measured Using the Roller Oven at Mud pH of 10.9.	83
5.16	Effect of Temperature and Corrosion on Mud pH Under Roller Oven Conditions.	84
5.17	Effect of Exposure Time on Mud pH Under Roller Oven Conditions in the Presence of Corroded Samples.	85
5.18	Effect of Temperature on Corrosion Rate Measured at the COLD Section of Flow Loop. Mud pH = 9.5.	87
5.19	Effect of Temperature on Corrosion Rate Measured at the HOT Section of Flow Loop. Mud pH = 9.5.	88
5.20	Effect of pH on Weight Loss of Coupons Exposed at 250 °F for 20	

	days in the Roller Oven.	91
5.21	Effect of Exposure Time on Weight Loss of Coupons Exposed at 250 °F in the Roller Oven.	92
5.22	Effect of pH on Corrosion Rate Measured at the COLD Section of Flow Loop.	93
5.23	Effect of pH on Corrosion Rate Measured at the HOT Section of Flow Loop. Mud Temperature = 161 °F.	94
5.24	Potentiodynamic Polarization Diagram Obtained Under Static and Ambient Conditions.	96
5.25	Effect of pH on Corrosion Rate Measured Under Static and Ambient Conditions by Potentiodynamic Polarization.	97
5.26	Potentiodynamic Curves in the Anodic Region at Different Rotation Speed of the RCE to Show the Effect of Diffusion. Mud pH = 10.9.	99
5.27	Potentiodynamic Curves in the Anodic Region at Different Rotation Speed of the RCE to Show the Effect of Diffusion. Mud pH = 4.1.	100
5.28	Anodic Limiting Current Density vs Square Root of Angular Velocity for Mud pH 4.1 and 10.9.	101
5.29	Impedance Spectra of Mild Steel (1018) in Water-Base Drilling Fluid at 500 mV (vs SCE) and pH 10.9.	102
5.30	Impedance Spectra of Mild Steel (1018) in Water-Base Drilling Fluid at Different RPM and pH 4.1.	103
5.31	Impedance Spectrum of Mild Steel (1018) in Water-Base Drilling Fluid at Static Condition and pH 4.1.	105
5.32	Impedance Spectrum of Mild Steel (1018) in Water-Base Drilling Fluid at 500 RPM and pH 4.1.	107
5.33	Impedance Spectrum of Mild Steel (1018) in Water-Base Drilling Fluid at 1000 RPM and pH 4.1.	108
5.34	Impedance Spectrum of Mild Steel (1018) in Water-Base Drilling Fluid at 2000 RPM and pH 4.1.	109

5.35	Scanning Electron Micrograph of an Unexposed Surface of Mild Steel (1018) Sample.	110
5.36	Scanning Electron Micrograph of a Corroded Surface of Mild Steel (1018) after Exposure to Drilling Mud in the Flow Loop at pH 9.5 and 98 °F for 8 hours.	111
5.37	Scanning Electron Micrograph of a Corroded Surface of Mild Steel (1018) after Exposure to Drilling Mud in the Flow Loop at pH 9.5 and 161 °F for 8 hours.	112
5.38	Scanning Electron Micrograph of a Corroded Surface of Mild Steel (1018) after Exposure to Drilling Mud in the Flow Loop at pH 9.5 and 253 °F for 8 hours.	113
5.39	Scanning Electron Micrograph of a Corroded Surface of Mild Steel (1018) after Exposure to Drilling Mud in the Flow Loop at pH 8 and 161 °F for 8 hours.	114
5.40	Scanning Electron Micrograph of a Corroded Surface of Mild Steel (1018) after Exposure to Drilling Mud in the Flow Loop at pH 6 and 161 °F for 8 hours.	115
5.41	Scanning Electron Micrograph of a Corroded Surface of Mild Steel (1018) after Exposure to Drilling Mud in the Flow Loop at pH 4.1 and 161 °F for 8 hours.	116

THESIS ABSTRACT

FULL NAME OF STUDENT : Olawale Surajudeen Shokoya
TITLE OF STUDY : Corrosivity of Water-Base Drilling Fluids
in Deep, Hot Wells
MAJOR FIELD : Petroleum Engineering
DATE OF DEGREE : December, 1994

Corrosive behavior of mild steel type 1018 in a typical drilling fluid used in drilling deep and hot wells was studied. The studies were carried out under simulated flow conditions, temperature, and pressure; which drilling fluid and drill pipe are exposed to while drilling such wells using a dynamic flow loop. Corrosion monitoring and measurements were carried out by weight loss and electrochemical techniques. The electrochemical techniques are: Polarization resistance, Potentiodynamic plots and AC impedance test. They were used to characterize the corrosion behavior of the steel in drilling fluid. Scanning electron microscope was also used to study the general morphology changes of steel samples when exposed to drilling fluid under simulated downhole conditions.

Results show that corrosion rate increases with increase in temperature and decrease in pH. Corrosion rates are low at mildly alkaline to mildly acidic pH range. The drilling fluid generally attacks the grain boundaries of the steel. Diffusion was found to be the rate limiting step for the corrosion reaction. Once diffusion resistance is overcome by increased flow rate or agitation, the corrosiveness of mud increases tremendously. Diffusion resistance led to a capricious and non-linear kinetic behavior. Experiments conducted at high agitation will give a better understanding of mud corrosion reaction kinetics.

MASTER OF SCIENCE DEGREE
KING FAHD UNIVERSITY OF PETROLEUM AND MINERALS
Dhahran, Saudi Arabia
December, 1994

خلاصة الرسالة

اسم الطالب الكامل : اولوالي سراج الدين شكوي
عنوان الدراسة : تآكلية موائع الحفر المائية في الآبار العميقة والحارة
التخصص : هندسة البترول
تاريخ الشهادة : ديسمبر ١٩٩٤ م .

في هذا البحث تمت دراسة تآكل فولاذ نوع ١٠١٨ في موائع حفر مماثلة لتلك المستخدمة في حفر الآبار العميقة والحارة . ولقد أجريت التجارب على جهاز تدفق الموائع الذي يحاكي أنسياب الموائع والحرارة والضغط التي تتعرض لها موائع الحفر وأنبوب الحفر أثناء عملية حفر البئر . لقد تمت ملاحظة وقياس التآكل باستخدام طريقة نقص الوزن وثلاث طرق الكيمياء وهي طريقة مقاومة الاستقطاب وطريقة الرسوم البيانية للجهد الحركي وطريقة اختبار ممانعة التيار الكهربائي المتردد ، كما أستخدم الجهر الالكتروني المسحي لدراسة التغيرات العامة في التشكل التكويني لعينات الفولاذ عند تعرضها لموائع الحفر في ظروف مشابهة لتلك التي في الأعماق .

ولقد أظهرت النتائج أن معدل التآكل يزيد عندما ترتفع الحرارة ويقل الرقم الهيدروجيني . وأن معدلات التآكل تكون بطيئة عندما يتحول مدى الرقم الهيدروجيني للموائع الحفر من القلوي الخفيف إلى الحمضي الخفيف ، وأن موائع الحفر تؤثر على حدود جزيئات الفولاذ وأن أنتشار صفائح الطفل على سطح العينة الذي يعتمد على سرعة أنسياب الموائع تحد من تفاعلات التآكل حيث أنه إذا تم تجاوز مقاومة أنتشار صفائح الطفل بزيادة الأنسياب أو الأرتجاج فإن قابلية الموائع للتآكل سيزداد كثيراً . وأن تواجد مقاومة الأنتشار أدت إلى تفاعلات غير خطية للتآكل . وأن إجراء التجارب عند معدلات إرتجاج عالية سيعطي فهم أفضل لتفاعلات التآكل لموائع الحفر .

درجة الماجستير في العلوم
جامعة الملك فهد للبترول والمعادن
الظهران - المملكة العربية السعودية
ديسمبر ١٩٩٤ م

CHAPTER 1

INTRODUCTION

Drilling fluids are used in the drilling operation primarily for the removal of drill cuttings from the drilled hole. Apart from this, other requirements are expected of the drilling fluid; such as to cool, clean, and lubricate the drill bit and drill string, maintain hole stability, prevent inflow of formation fluids, etc. The success of the operation depends largely on the performance of the drilling fluid circulated down the hole. The drilling fluid must be safe to both the personnel handling it and the environment. It must not corrode or cause excessive wear of drilling equipment. Drilling fluids are sufficiently complex that physical and chemical properties cannot be predicted without continual performance testing. The conditions the fluid is subjected to are constantly changing as drilling progresses deeper downhole.

The corrosiveness of drilling fluids is a deleterious property that has to be prevented and controlled. It has been recognized to be the major cause of drill pipe failures and damage to downhole equipment. It is, therefore, one of the factors considered before the selection of drilling fluid for a drilling operation.

Oil-base drilling fluids are suitable for most drilling operations,

especially where water-base fluids might lead to serious problems. They are also less-corrosive because they are not electrically conductive. However, due to problems of cost, disposal, pollution and environmental restrictions/regulations; oil-base fluids have become less attractive for drilling in all types of formations.

Water-base drilling fluids are cheap, available, and less polluting. Their properties can be easily controlled and maintained. More so, a lot of work has been done to improve the properties of water-base muds in order to make them suitable for most drilling operations. The practice in the drilling industry nowadays is to use lightly treated, low solids, mildly alkaline muds containing no oil instead of the highly treated, heavy weight, high pH muds containing diesel.

One problem that still needs to be tackled, however, is the corrosiveness of water-base muds. They contain a high water fraction which comes in direct contact with the drill pipe and casing. Oxygen and carbon dioxide are entrapped by the high gel structure of these fluids, making them more corrosive; thereby contributing a lot to drill string and downhole equipment corrosion. Corrosion is very difficult to control once it has started. The onset could, however, be prevented. The problem of corrosion are now of prominent importance in the drilling industry because of deeper prospecting for oil and gas, with the resultant encounter of hot and sour formations which aid and promote corrosion.

It is necessary to have an idea of how drilling and downhole conditions affect corrosion in order to mitigate and control the corrosiveness of drilling fluids. It is also important to understand the mechanism and kinetics of the corrosion reaction occurring. Laboratory experiments carried out under simulated downhole conditions of temperature, pressure, contaminants, etc. and drilling conditions of continuous drilling fluid circulation through the drill pipe and the annulus with exposure to high shear at the drill bit; will yield valuable data that can be used in controlling this deleterious property.

The objective of this research, therefore, is to establish the thermal stability, and evaluate the corrosivity of a typical drilling fluid under conditions that simulate deep, hot wells in the presence of mild steel type 1018.

CHAPTER 2

FUNDAMENTALS OF CORROSION

Corrosion can be defined as the destructive attack of a metal by chemical or electrochemical reaction with its environment. Metals naturally exist in a thermodynamically stable state as compounds known as ore. The thermodynamics become unstable by extraction and exposure of the metal to another environment. Corrosion makes the metal to revert to its natural state^[22].

2.1 TYPES OF CORROSION

Corrosion damage occurs by rusting, loss of weight, loss of strength, loss of ductility, and can result in catastrophic failure by cracking or through weakening. Based on the corrosive medium, corrosion can be classified as wet or dry. In general, wet corrosion occurs by an electrochemical mechanism^[30]. Corrosion products are not necessarily observable and metal weight loss need not be appreciable.

The main types of corrosion with respect to outward appearance or altered physical properties are as follows:^[22,30]

- i. **Uniform Corrosion:** Uniform attack is the most common type of corrosion. The entire metal surface area corrodes uniformly as a result of a continuous shift of anodic and cathodic areas due to polarization changes. Of the various types, uniform corrosion is the least damaging.
- ii. **Crevice Corrosion:** This is a localized attack of metals in the hidden parts such as drill pipe joints, drill collars, etc. It is caused by concentration differences of a corrosive medium over the metal surface.
- iii. **Pitting Corrosion:** It often occurs on a crevice, but can also occur on clean metal surfaces. High velocity corrosive medium, such as the circulation of drilling fluid promotes this type of corrosion. Once the pit is formed, the rate of corrosion increases.
- iv. **Erosion-Corrosion:** The combination of erosion and corrosion results in severe attack of metal. Damage appears as a smooth groove on the metal. An example is the wash out of drill pipe which is initiated by pitting in a crevice. Erosion removes protective film from the metal surface and expose it to the corrosive environment.
- v. **Stress Corrosion:** If a metal cracks when subjected to repeated or alternate tensile stress in a corrosive environment, it is said to fail by corrosion fatigue. Stress corrosion cracking also applies to hydrogen embrittlement, sulfide cracking and caustic embrittlement.

- vi. **High-Temperature Corrosion:** Oxidation is the most important high temperature corrosion reaction. This reaction takes place in the presence of oxygen or air. Metals are oxidized when exposed to elevated temperatures in the presence of oxygen. They rely upon oxidation to develop a protective oxide scale to resist corrosion attack. The rate of oxidation increases with increasing temperature.

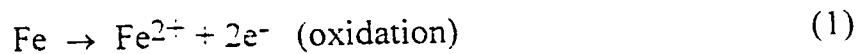
2.2 CORROSION MECHANISM

The electrochemical theory is the theory underlying wet corrosion. For the reaction of a metal and its environment to occur, the Gibbs free energy change, ΔG has to be negative. The more negative the value of ΔG , the greater is the tendency for the metal to corrode. This, however, is not a measure of the reaction rate. A large negative ΔG may or may not be accompanied by a high corrosion rate. In view of the electrochemical mechanism of wet corrosion, anode and cathode areas must be present to form a cell and be in contact with a corrosive medium which will conduct current. The tendency for a metal to corrode can, therefore, be expressed also in terms of the electromotive force (*emf*) existing between the anodic and cathodic areas^[22].

Since *emf* is directly related to ΔG , the greater the *emf* value of a corrosion cell, the greater is the tendency for the corrosion reaction to occur. The current conducted by the corrosion cell in contact with the medium can

be self-induced or impressed on the system from an external source (e.g. as done in instantaneous corrosion measurements). The driving force for the current flow is the potential difference (*emf*) between the electrodes.

The anode is the area where corrosion occurs, the metal ions go into solution in amount chemically equivalent to the reaction at cathodic area. The metal is oxidized and loses electrons, e.g.:



The rate of this reaction is controlled by the cathodic reaction which is usually much slower, hence the rate of corrosion reaction is cathodically controlled.

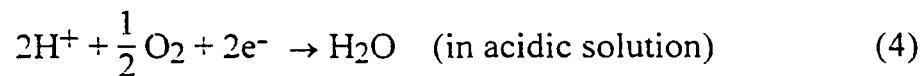
The ion, Fe^{2+} enters the solution and the cathode attracts hydrogen ions which arise from the ionization of water:



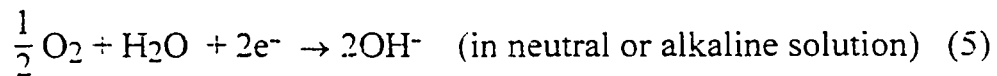
the H^+ ions accept electrons at the cathode to become hydrogen atom (a reduction reaction):



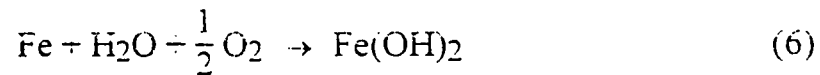
This reaction proceeds rapidly in acids but slowly in alkaline or metal aqueous media. The cathodic reaction can be accelerated by dissolved oxygen according to the following reaction:



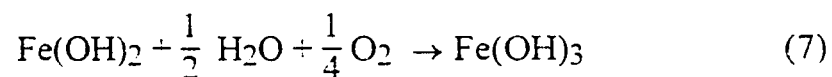
or



Adding (1), (2) and (4), we obtain:



$\text{Fe}(\text{OH})_2$ is the oxide formed on the surface of the metal. Access to dissolved oxygen by the outer surface of this oxide converts it to $\text{Fe}(\text{OH})_3$,



an orange to red-brown colored oxide called RUST^[22].

2.3 CORROSIVE ENVIRONMENTS AND THEIR EFFECT

2.3.1 Dissolved Oxygen

At ordinary and elevated temperatures, dissolved oxygen is always present in drilling fluids. It is necessary for appreciable corrosion of iron. In air-saturated media, the initial corrosion rate is high. This rate reduces with time as the iron oxide film is formed and acts as a barrier to the diffusion of oxygen. The high velocity flow of the medium erodes the oxide film, ensuring continuous supply of oxygen to the metal surface, hence increasing corrosion rate. The presence of oxygen also magnifies the corrosive effect of acid gases - hydrogen sulfide (H_2S) and carbon dioxide (CO_2).

Generally, an increase in oxygen concentration is expected to accelerate corrosion of iron. Temperature and salinity affects oxygen concentration and corrosion. Saline media are more corrosive than non-saline media because of their conductivity,. But at very high salinities, the rate of corrosion is reduced because of the low solubility of oxygen^[22.30].

2.3.2 Temperature

In an open system that allows dissolved oxygen to escape, corrosion rate increases with temperature up to a particular temperature and then falls to a low value. This is caused by the decrease of oxygen solubility in water as temperature increases. This effect eventually overshadows the

accelerating effect of temperature alone. In a closed system, however, corrosion rate continues to increase with temperature until all the oxygen is consumed[22.30].

2.3.3 pH

pH can be defined as the negative logarithm of hydrogen ion concentration. Its effect is dependent on the concentration of dissolved oxygen and the type of acid that controls the pH. In a high alkaline range, corrosion is under anodic control, hence it proceeds at a high rate. For mild alkaline and neutral solutions, some corrosion protection is provided because the corrosion rate is under cathodic control. In the acid range, corrosion is also under anodic control, hence high corrosion rate is expected. The type of acid in solution determines the pH at which corrosion increases rapidly[22.30].

2.3.4 Carbon Dioxide

Carbon dioxide is found entrapped in water at ambient conditions and occurs as a gas kick or slow bleed-in gas while drilling. It can also be found present in formation water, existing as bicarbonate, HCO_3^- or carbonate, CO_3^{2-} . Carbon dioxide dissolves in water to form carbonic acid which lowers the pH, making it corrosive to steel.



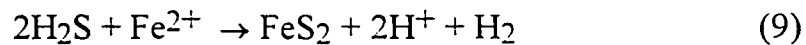
Carbonic acid ionizes to form carbonate ion, CO_3^{2-} which in the presence of divalent cations e.g. calcium ion, Ca^{2+} and magnesium ion, Mg^{2+} , usually precipitates as calcium carbonate, CaCO_3 , magnesium carbonate, MgCO_3 , and iron carbonate, FeCO_3 . The precipitate aggregates to form scale, thus setting up corrosion cells.

The effect of carbon dioxide on corrosion rate is affected by the pH of the medium, the system pressure and temperature. As the pH decreases, bicarbonates converts to carbonic acid and corrosion increases. Conversely, as the pH increases, water tend to become scale-forming and the corrosion rate will decrease. Generally, increased system pressure results in increased solubility while temperature increase normally decreases the solubility of carbon dioxide in water[22.30].

2.3.5 Hydrogen Sulfide

The presence of hydrogen sulfide could be detrimental to steel because it promotes sulfide cracking and hydrogen induced corrosion. During the drilling process, hydrogen sulfide (H_2S) is associated with a gas kick or bleed-in. Another source of H_2S is the action of sulfate-reducing microorganisms on sulfate components of mud additives, and their degradation at high temperatures.

Hydrogen sulfide is relatively non-corrosive in the absence of moisture. In the presence of carbon dioxide, oxygen and water, however, H₂S becomes severely corrosive. It is weakly acidic when dissolved in water. On attack of iron it forms a black precipitate of iron sulfide which deposits on the surface of the metal as a black scale.



The hydrogen released in (9) enters the steel where it can alloy with the steel to embrittle it. It may form molecular hydrogen which tends to blister ductile steel and crack high strength steel. Hydrogen sulfide gas is very poisonous. It is heavier than air and will accumulate at ground level. Personnel should be adequately protected in cases where it is to be encountered[22,30].

2.3.6 Stress Cracking and Hydrogen Embrittlement

When a metal is subjected to cyclic stresses, it eventually fails. Failures of this nature are known as fatigue failures. The number of stress cycle a steel can endure before failure decreases with the applied stress, the steel hardness, and corrosiveness of the environment. Fatigue failure is accelerated by oxygen, carbon dioxide, and hydrogen sulfide.

Hydrogen embrittlement is another form of stress cracking. In the absence of H_2S , hydrogen is collected on the steel surface as a film of atomic hydrogen which penetrates the steel; but in a so small quantity that no harm is done. However, in the presence of H_2S the formation of atomic hydrogen is enhanced, more penetrates into the steel, reduces its ductility, and tends to concentrate in areas of maximum stress. This eventually lead to failure known as sulfide and/or hydrogen induced stress cracking[22,30].

2.4 CORROSION MONITORING

Monitoring the rate of corrosion is very important because it allows for the assessment of the rate of corrosion damages. There are variety of methods for corrosion monitoring and measurement. Of these methods, those commonly used to evaluate the corrosivity of drilling fluids are:

- (1) Weight-loss method. using steel coupons:
- (2) Electrochemical methods: direct current (dc) polarization and alternating current (AC) impedance techniques.

These methods are easily applicable both in the field and in the laboratory. AC impedance polarization, potentiodynamic polarization, and polarization resistance techniques provide rapid, nondestructive means for characterizing not only the corrosion rate, but also the corrosion behavior. It is often desirable to use at least two different types of corrosion monitoring methods to eliminate noise in measurements[29].

2.4.1 Weight-Loss Method

This is the simplest method of corrosion monitoring. Coupons are relatively small specimens of the material of interest. They are exposed to the corrosive medium for a period of time. The specimens take the form of disks, rectangular pieces, or special devices, e.g. U-bends, to check stress corrosion cracking^[29].

One of the simplest approach to coupon evaluation is to determine the mass loss by weighing the coupon before and after exposure to the corrosive medium. This method can provide an accurate estimation of uniform corrosion, and allows for visual, X-ray, and Scanning Electron Microscope (SEM) examination of specimens to determine the type of attack. However, in cases where pitting, cracking or embrittlement occurs it might not be very accurate. The cost of setting up and running a coupon test program is relatively low. The laboratory experiment should, however, be set up to represent and simulate the actual field conditions that is being investigated.

Corrosion rate is usually measured as loss in mass per unit surface area of original specimen for a particular exposure period, thus:

$$\text{Weight Loss} = \frac{W_i - W_f}{A_i}, (\text{mg/cm}^2) \quad (10)$$

where

W_i = mass of coupon before exposure, mg

W_f = mass of coupon after exposure, mg

A_i = surface area of coupon before exposure, cm^2

This can be expressed in milli-inches (mils) per year (mpy)^[28] as follows:

$$\text{Corrosion rate} = 18.2 * \frac{\text{weight loss (mg / cm}^2\text{)}}{\text{time (days)}} * k$$

or

$$\text{Corrosion rate} = 437 * \frac{\text{weight loss (mg / cm}^2\text{)}}{\text{time (hours)}} * k \quad (11)$$

$k = 1.0$ for carbon steel (density correction factor)

$= 0.976 - 1.027$ for stainless steels.

The corrosion rate in mpy expresses the depth of surface in thousands of an inch, which would be removed in a year, assuming that the corrosion had occurred evenly over the entire surface.

Principle of Polarization:

The mining and alloying process disturbs a metal's equilibrium that exist in the ore state. Before any factor that helps to bring the metal back to equilibrium can be appreciated, we need to know the equilibrium state of the metal. When a net current flow to or from the surface of a metal, the metal is no longer in equilibrium. The measured potential of such a metal is altered to an extent which is dependent on the magnitude of the current and its

direction. The extent of potential change caused by net current flow to or from the surface of the metal is called **polarization**[22].

The measured potential of a corroding metal is the equilibrium potential of both polarized anodes and cathodes existing on the surface of the metal and known as the corrosion potential, E_{CORR} which corresponds to a corrosion current, I_{CORR} . Figure 2.1 shows an hypothetical cathodic and anodic polarization (Tafel) plot.

By Faraday's law, the corrosion rate of anodic areas on a metal surface is proportional to I_{CORR} , hence the corrosion rate per unit area can be expressed as a current density. The causes of electrode polarization are concentration polarization, activation polarization, and ohmic potential drop. Concentration polarization refers to electrochemical reactions which are controlled by the diffusion in the electrolyte. Activation polarization in an electrochemical process is caused by a slow reaction at the electrode, i.e. the reaction requires an activation energy in order to occur. Polarization measurements include an ohmic potential (iR) drop through a portion of the electrolyte surrounding the electrode, through a metal-reaction product film on the surface, or both. Its contribution to polarization is equal to iR , where i is the current density and R is the resistance of the film and/or surface of length, l and specific conductivity, κ . Concentration polarization decreases with agitation whereas activation and ohmic drop are not affected significantly[25].

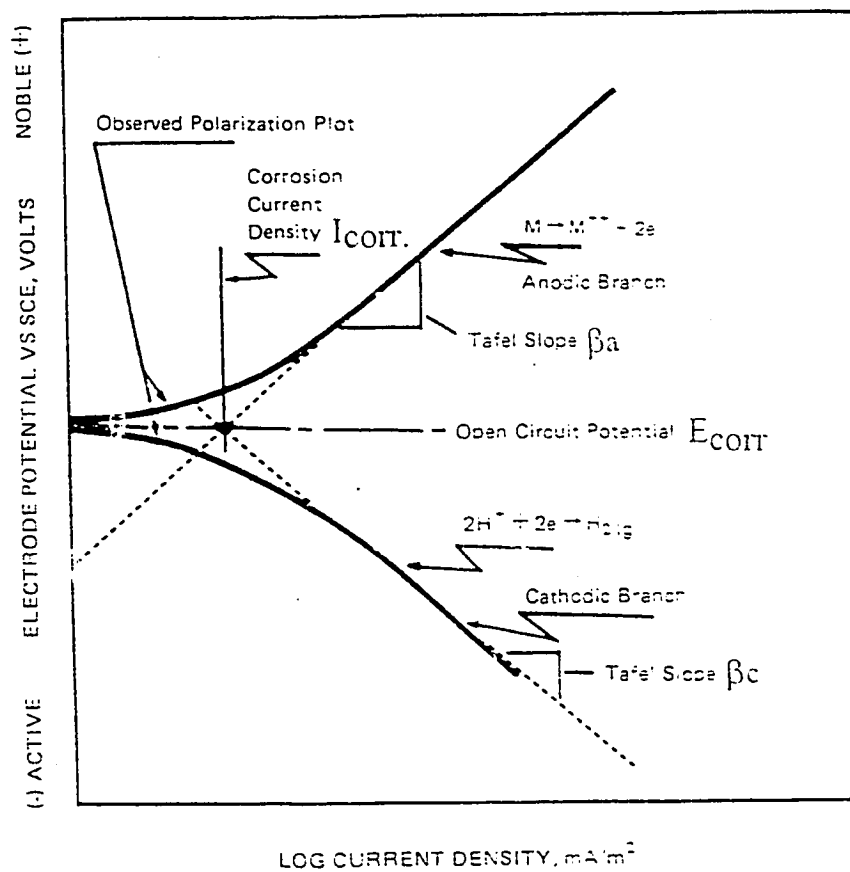


Figure 2.1: Hypothetical Cathodic and Anodic Polarization Plot Showing the Extrapolation of Tafel Slopes to the Corrosion Potential to Obtain Corrosion Current Density (from [28]).

Electrode polarization limit the magnitude of current produced by a cell and hence affects the corrosion rate. The extent of polarization depends on the nature of the metal, the electrolyte and the exposed area of the metal. If the anodic area of a corroding metal is very small, there may be considerable anodic polarization accompanying corrosion, even though the unit area of the bare anode polarizes only slightly at a given current density. Consequently, the anode-cathode area ratio is important in determining corrosion rate. Tafel equation ($E = a + \beta \log I$) expresses polarization behavior. The anodic and cathodic Tafel slopes are utilized in the Stern and Geary equation^[22] to calculate the corrosion current.

$$I_{\text{corr.}} = \frac{I_{\text{applied}}}{2.3\Delta E} \frac{\beta_c \beta_a}{\beta_c + \beta_a} \quad (12)$$

where

β_c = Tafel slope for the cathodic reaction

β_a = Tafel slope for the anodic reaction

$\frac{I_{\text{applied}}}{\Delta E}$ = Polarization slope in the region near $E_{\text{corr.}}$

for which ΔE is linear with I_{applied} .

Under conditions of slight polarization, for which ΔE is not more than about 10 mV, the anode-cathode area ratio, which need not be known, remains essentially constant and conditions at the surface of the corroding metal are largely undisturbed. This equation has been used successfully for

determining the corrosion rates of various metals in several aqueous environments at ordinary or elevated temperatures. It has an advantage in calculating instantaneous corrosion rates for many metals in a wide variety of environments and under various conditions of velocity and temperature. It can also be used to evaluate inhibitors and protective coatings, as well as for detecting changes of corrosion with time. The equation is, however, not applicable for calculating corrosion rates in the presence of interfering oxidation-reduction systems that are not involved directly in the corrosion reaction. Also, if an ohmic drop is involved in the measurement, a calibration is required^[22,25].

2.4.2 Polarization Resistance

This is a direct current (dc) electrochemical method of evaluating corrosion. As opposed to the coupon method which provides information on remaining mass of metal, polarization resistance provides an estimate of the corrosion rate. It is based on the concept that corrosion rate of a probe is inversely proportional to its polarization resistance, i.e. the slope of the potential-current response in the vicinity of the corrosion potential, E_{corr} ^[29].

An electronic power supply polarizes the specimen about 10 mV from the E_{corr} of the system. This slight shift of the specimen's potential is called *linear polarization*^[23]. The current necessary to produce such a small

polarization is proportional to the original, undisturbed corrosion current of the specimen. This method has two important limitations:

- (1) The corroding environment needs to be an electrolyte with a reasonably low resistivity. High resistivity electrolytes give erroneously low corrosion rates,
- (2) It provides no information on localized corrosion and type of attack.

The method has the advantage of providing an instantaneous estimate of corrosion rate. It is best suited for determining periods when substantial corrosion rate changes occur, and for continuous monitoring of corrosion, especially in a flow process. It is necessary to employ a probe which carries electrodes made of the specimen of material under investigation, and installed in an area where the evaluation of corrosion is desired[23,29].

The Petrolite corrosion meter uses the Polarization Admittance Instantaneous Rate (PAIR) principle (polarization resistance). It measures the current required to shift the potential of a test electrode by 10 mV. From the Stern-Geary equation (12), I_{corr} can be expressed as follows:

$$I_{\text{corr}} = \frac{\Delta I}{\Delta E} \frac{\beta_c \beta_a}{\beta_c + \beta_a} \quad (13).$$

The probe carries three electrodes - test, reference, and auxiliary - that establish electrical contact with the corrosive medium. The corrosion meter

has an adjustable current source, an ammeter, and a voltmeter. It compares the potential of the test electrode with the natural potential of the reference electrode. The auxiliary electrode supplies the current necessary for the test electrode's 10 mV shift, and the reference electrode is unaffected by the measurement process. All three electrodes are made of the same material.

The corrosion rate is related to the required polarization current (ΔI) and electrode potential shift ($\Delta E = 10 \text{ mV}$) by the following equation:

$$\text{corrosion rate} = K \frac{\Delta I}{\Delta E} \quad (14).$$

The PAIR constant, K includes several factors such as the equivalent weight of the metal-to-metal ion, density of the metal, exposed area of electrode, Tafel factor, voltage shift, and meter factor^[23].

2.4.3 Potentiodynamic Polarization Diagrams

This method of dc electrochemical corrosion measurement employs a potentiostat and x-y recorder data acquisition system, to obtain a current density-potential response to a potentiodynamic polarization sweep at a certain rate in the cathodic and anodic modes, i.e. making the metal act as either a cathode or anode separately, but not simultaneously. The potentiodynamic polarization measurements are valuable in rapidly

predicting how a material will behave when exposed to a particular environment. This is an artificial method for corroding the sample, and it is analogous to elevated temperature studies of corrosion; where temperature is the driving force^[32]. Here voltage drives the electrochemical reaction.

This method is advantageous because it helps to understand better, how the specimen behaves in the corrosive medium. Analysis of the resulting polarization diagram will provide information about the corrosion behavior of the metal and the rate of corrosion. The results of polarization-current density analyses can be used to identify the potential for the occurrence of localized corrosion. It can also be used to determine the effectiveness of inhibitors^[29].

The electrochemical cell is set up with three electrodes: the working electrode (test specimen), a standard reference electrode placed close to the working electrode, and a counter (auxiliary) electrode; all placed in the corroding medium and connected to the potentiostat. It requires a skilled personnel to interpret the results obtained from a potentiodynamic polarization measurement. Corrosion rate is obtained by applying Faraday's law^[32]:

$$W = \frac{QM}{nF} \quad (15)$$

where

W = weight of electroactive species, g

Q = quantity of electric charge, coulombs

M = molecular weight of electroactive species, g

n = number of electrons involved in the reaction

F = the Faraday, 96487 coulombs

with equivalent weight, $m = M/n$ and $Q = It$;

$$\frac{W}{t} = \frac{I m}{F} \quad (\text{g/s}).$$

We can express this corrosion rate in mpy by dividing the right hand side by the electrode area (cm^2) and density (g/cm^3). Converting seconds to years and centimeters to mils, we have:

$$\text{corrosion rate (mpy)} = \frac{0.13 * I_{\text{corr}} * m}{\rho} \quad (16)$$

where

I_{corr} = corrosion current density, I/A ($\mu\text{A}/\text{cm}^2$).

2.4.4 AC Impedance Polarization

The AC impedance approach to electrochemical measurement of corrosion permits the resistive and capacitive elements of the electrochemical corrosion reaction to be separated and analyzed

independently. The method is particularly attractive in the case of highly resistive corrosive media[29].

Electrochemical impedance measurements provides a rapid, nondestructive means for characterizing not only the corrosion rate, but also the corrosion mechanism of metals in a variety of environments. A cause-and-effect relationship is assumed to exist between applied electrochemical potential and the corresponding electrochemical current. For an electrochemical impedance to be defined correctly, it is necessary to apply a perturbing AC signal of low amplitude over the dc potential such that the response may define a linearity range which depends on the polarization point. The low limit of the perturbing signal is determined by the signal-to-noise ratio which can be accepted by the measuring instrument (typically 1mHz). The high limit is defined by the onset of non-linear distortion (typically 40-50 kHz)[29,31].

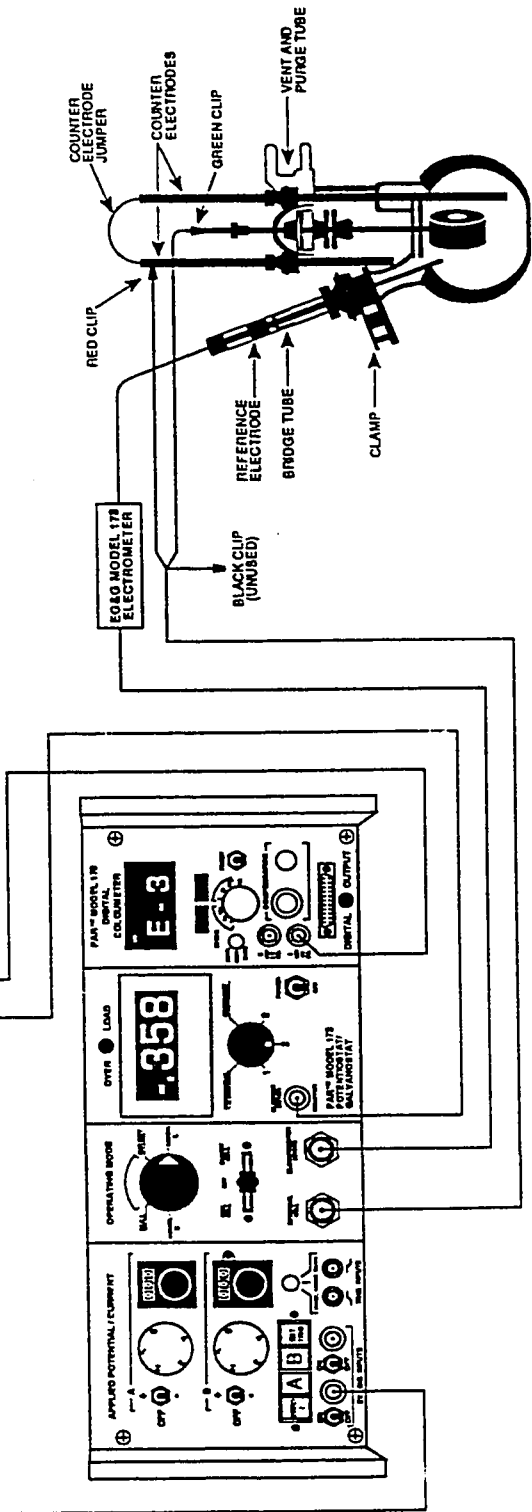
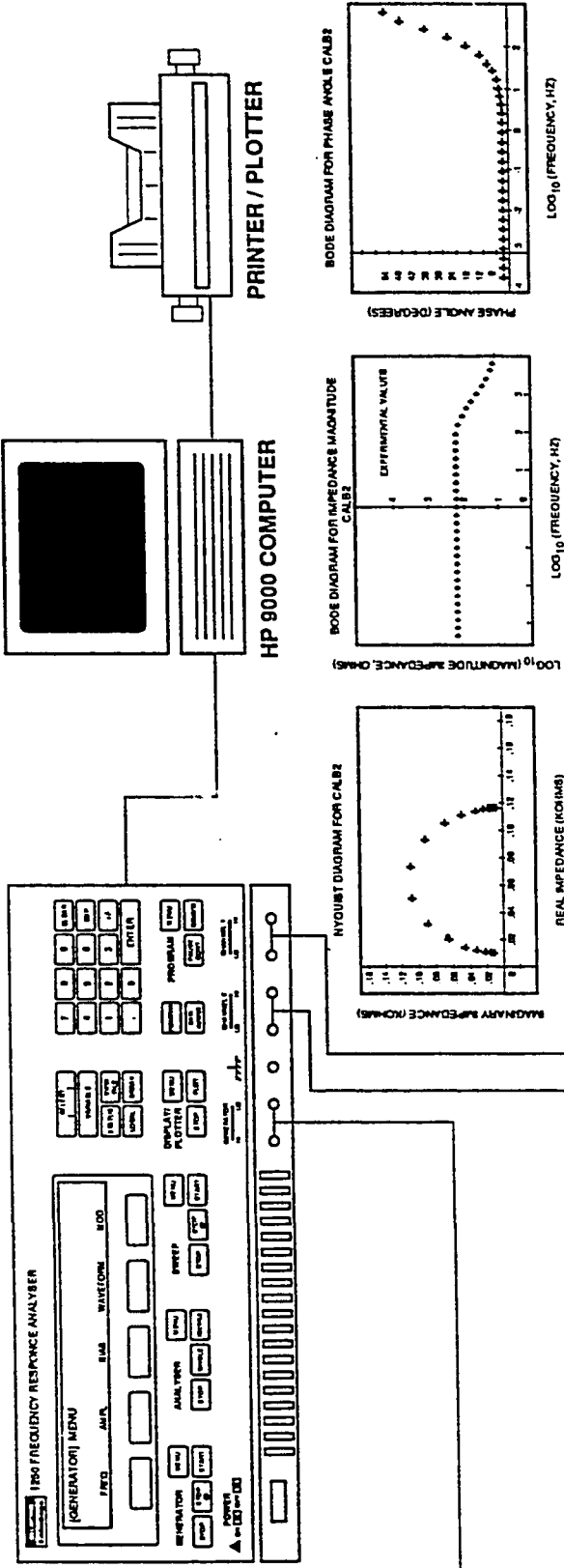
Impedance measurements must be made over a wide range of frequencies in order to attain the high frequency limit of the impedance equal to the electrolyte resistance. To do this, it is necessary to employ a rather sophisticated AC frequency generator and response analyzer system. A digital frequency response analyzer analyzes the three electrode corrosion cell's response to the perturbing (polarization) signal. This is correlated with two synchronous reference signals, one in phase with the response and the other 90° out of phase. The real and imaginary parts of the impedance are thus obtained and plotted. An impedance versus frequency plot is also made to obtain an impedance spectra. Analysis of these plots is used to

extract information useful for characterizing the corrosion rate and mechanism. The data is reduced from a set of hundreds of spectra to several meaningful parameters which will allow the recognition of patterns. Figure 2.2 shows a typical AC impedance measurement set-up. This method is very powerful in that more precise corrosion rates (compared to other techniques) can be obtained along with the description of the corrosion characteristics and mechanism[24,26,29].

The basis of impedance data analysis is the construction of 'equivalent circuits' for the electrochemical interface existing between the corrosive medium and the metal surface. The electrical elements in the circuit will have the same impedance behavior as that measured for the system. The simplest equivalent circuit is made up of the electrolyte resistance, the electrochemical double layer capacitance, and the charge transfer resistance. The charge transfer resistance is equivalent to the polarization resistance of the interface and inversely proportional to the corrosion rate[31]. Polarization about the dc determined equilibrium corrosion potential by an AC signal of amplitude, ΔE and frequency, f (i.e. $\Delta E \sin ft$) results in a flow of current, $\Delta I(\sin ft + \theta)$.

The impedance, $Z (= \frac{\Delta E}{\Delta I})$ has a phase angle, θ which corresponds to the difference between the applied potential and the resultant current. From a complex plane plot of negative imaginary impedance versus the real impedance (Nyquist diagram), it is possible to deduce the mechanism of the process[31].

DATA ACQUISITION SYSTEM



K47 CORROSION CELL

Figure 2.2: IMPEDANCE TECHNIQUE FOR CORROSION MEASUREMENTS

2.5 FACTORS AFFECTING REPRODUCIBILITY OF CORROSION RATE MEASUREMENTS

The complex nature of the mechanism of corrosion and the diversity of environmental conditions that may be encountered; culminates in several important factors which determine the reproducibility of experimental results. These factors may be divided into two categories: those involving the metal surface and those associated with the environment.

The factors concerning the metal surface are: cleanliness, presence and nature of surface films, presence of more than one phase in the metal, the preparation of the surface for a test, and the polarization characteristics of the metal. The composition of the corrosive environment, its homogeneity, the presence of foreign matter e.g. dirt, and the freedom to access for air are of importance from the environmental stand point. In fact, anything that may be of importance to the electrochemical nature of corrosion will influence the amount and nature of the corrosive attack.

Great care must be taken in the preparation and exposure of the specimens used for corrosion measurements, either in the laboratory or in the field, in order to obtain reproducible results. However, even when the greatest possible care is taken, it is not to be expected that absolute reproducibility will be achieved. There are many factors beyond the control of the experimenter, statistical control is however, often achieved. Consequently, the absolute error of measurement can be reduced by increasing the number of identical specimens tested.

The type of attack that occurs can greatly influence the reproducibility of the results. If the attack is uniform, the reproducibility will, in general, be much greater than if the attack is localized to a few points on the metal surface.

CHAPTER 3

LITERATURE REVIEW

The adverse impact of drill string corrosion and corrosivity of water-base muds came into limelight in the late 1960s. With deeper prospecting for oil, hot and sour gas wells are encountered; and these in the presence or absence of oxygen causes corrosion.

It has been generally observed that corrosion sets in at the early stages of putting well tubulars on service under sour and harsh conditions. Corrosive environments significantly affect the corrosion fatigue performance of well tubulars. Even the high strength steels used for deep drilling are not spared as they are attacked by sour gases from sulfur and carbon based mud additives or from the natural gas constituents of the reservoir. Another source of tubular corrosion is acid stimulation. When hydrochloric and hydrofluoric acids (HCl and HF) are used for matrix treatment of reservoirs, the acids aid and speed up the corrosive reactions occurring on the steel tubulars. It has been found that treatment of drilling fluid has offered the best corrosion control with minimum cost. The study of causes and mitigation of drilling fluid corrosion under various conditions has been carried out by quite a few researchers.

Simpson and Barbee^[1], in 1967, investigated the causes of brittle

cracking and failures of high strength tubular goods that have been exposed to water base packer muds, the sources of sulfide deposits and iron carbonate corrosion products found on tubings; even from wells where there is no known sulfide in produced fluids. Lignosulfonate mud, a common mud type thought to be non-corrosive was found to degrade at temperatures above 300 °F to form carbon dioxide (CO₂) and hydrogen sulfide (H₂S). Bacterial action on lignosulfonate mud causes a breakdown of organic additives to form organic acids, CO₂ and soluble sulfide.

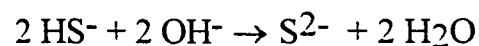
Electrochemical reduction of sulfur-oxide present in lignosulfonate was found to be the cause of iron sulfide deposit on drill pipe coupons placed in solution containing it; at pH of 8.1, free of bacteria and aged for 16 hours at 200 °F. The authors concluded that electrochemical reduction of sulfur-containing organic mud additives is the cause of sulfide formed in water-base packer fluids when bacterial or high-temperature degradation seems unlikely. Several case histories of tubing and casing failures are cited in situations where such electrochemical reactions are thought to have occurred.

In 1972, Zitter^[2] studied the corrosion of casings exposed to sour gases. He observed that higher corrosion rates were indicated by tubulars at early stages. Protective surface film grows thicker with temperature increase. The author proposed a reaction mechanism from the detection of calcium chloride and calcium carbonate in the surface films by X-ray diffraction studies. Although he had only few data available for judging the effect of

time on corrosion, he concluded that after the initially high corrosion depth there is no further significant increase.

Bush^[3], in 1974, identified the primary causes of drilling fluid corrosion as oxygen, hydrogen sulfide, and carbon dioxide (with oxygen as the major problem because of its constant presence and pitting characteristics). He recommended the removal of dissolved oxygen with oxygen scavenger (e.g. sodium sulfite) and hydrogen sulfide with sulfide scavenger (zinc oxide, or other metal compounds). He also suggested the neutralization of acid forming gases with alkaline materials to achieve drilling fluid corrosion control.

Carney and Jones^[4], also in 1974 focused on the various problems caused by hydrogen sulfide, even in small quantities during drilling and completion. They discussed the advantages and disadvantages of using compounds of copper, zinc, iron, hydrogen peroxide and chelates for scavenging hydrogen sulfide; they concluded that raising the mud pH (alkalinity) will cause the hydrogen sulfide to produce sulfide ions which do not contribute to corrosion of drill pipe.



Even if the sulfide ions (S^{2-}) are not available, no H_2S gas can be formed. They also cautioned that the pH must be maintained high because S^{2-} are dangerous at low pH.

Mauzy^[5], in 1974 gave some precautionary measures to be taken to avoid sulfide stress cracking of drill pipes. Most important of these are the avoidance of creating H₂S in the drilling fluid by sulfate reducing organisms and using sulfur based drilling fluid additives. He also gave some suggestions on how to avoid these problems.

Azar and Luminus^[6], in 1975, carried out experimental study of the effect of drilling fluid pH on the corrosion fatigue performance of grades D and E drill pipe material. He discovered that drilling fluid pH is not a valid measurement for corrosion control. The drill pipe materials were found to have better corrosion-fatigue life expectancy at pH of 8.0 than at 9.0, and only one percent less than at 10.0.

Woodroof et al.^[7] studied the corrosion inhibition of HCl-HF acid mixtures with the addition of mutual solvents (ethylene glycol monobutyl ether) at high temperatures and pressure. Their study showed that increasing test temperatures results in increasing corrosion rates. Also, increasing the yield strength of test coupons leads to increase in corrosion rates.

In 1978, **Smith et al.** ^[8], conducted weight loss measurements and determined the effect of various parameters on the rate of corrosion. They noted the importance of testing at high pressure and temperature, and under dynamic conditions or at least with agitation. They found out the following: (a) corrosion rate increases with acid concentration, (b) more severe corrosion occurs at elevated temperatures, (c) at lower acid concentration, increasing pressure reduces the rate of corrosion more effectively than with

higher acid concentration, and (d) that test data should be compared using both static and dynamic/agitated test procedures.

Ray et al.^[9], in 1979, acknowledged the success of using a combination of sodium hydroxide (NaOH) and zinc compounds for treating drilling fluids to contain the influx of H₂S. They, however, have to search for alternate sulfide scavenger because of the disadvantages inherent in the above. Their search indicated that iron oxide is an effective scavenger for H₂S at bottomhole temperatures and pressures, and even in high H₂S concentrations.

Also in 1979, **Azar**^[10], conducted corrosion fatigue tests on grade E material, using fresh water non-dispersed bentonite, and dispersed lignosulfonate muds containing oxygen (O₂), CO₂ and chlorides. His study showed a decrease in the life expectancy of drill pipe material as the concentration of O₂, CO₂, and chlorides dissolved in the mud increases.

Samuels and Gupta^[11], in 1983, reviewed the corrosion chemistry of carbon steel; which is the most commonly used material in drilling operations. They discussed the effect of dissolved H₂S, CO₂ and O₂ as well as pH on carbon steel corrosion in aqueous solutions. The importance of knowing the type of corrosion occurring and study of the exposed coupon's surface by scanning electron microscopy (SEM) was stressed. They studied the behavior of iron oxide as H₂S and O₂ scavenger.

They found that general (weight loss) corrosion rates of carbon steel are high at pH of 6-9 at all sulfide levels and that corrosion rate increases dramatically with increase in sulfide concentration. Electrochemical and SEM evaluation enabled the authors to identify localized corrosion on the metal. The metal experienced severe pitting attack even at a pH of 14 and 200 ppm of soluble sulfides. The pit grew at a rate of 10 inches per year while the corrosion rate determined by weight loss was within acceptable limits of 10 mpy.

The authors concluded that pitting corrosion which is not frequently detected by conventional field test methods is a major cause of drill pipe failure in H₂S environment. At pH values greater than 12, severe pitting was observed, irrespective of sulfide levels and contrary to generally accepted theories. Ironite sponge (a specially formulated iron oxide) was found to completely eliminate pitting tendencies of carbon steel in solutions containing sulfide ions at pH of 8 and above. The sponge reduces general corrosion rate by the reduction of sulfide ions in solution.

Moussa^[12], in 1983, measured corrosion rate under simulated bottomhole conditions by using a flow loop and roller oven. He used the weight loss method to determine the corrosion rate of flat coupons of mild steel (1018) for temperatures ranging from ambient to 500 °F. He found that corrosion rate increases as temperature increases at low pH, but decreases as pH increases, even at high temperatures. He also discovered that corrosion rate varies with the equipment used to simulate the bottomhole condition. The rolling technique yields lower rates than those

measured in the hot end of the flow loop at the same temperature, and almost equal to the rates measured at the cold end.

Using statistical analysis, **Okoye et al.**[13], determined the relationships of corrosion variables using data obtained under simulated bottomhole conditions. Their regression analyses showed similar conclusion as those of **Moussa**[12], that the corrosion rate due to mud increases with temperature if $1/pH$ is high, and decreases as pH increases, even at higher temperatures. Furthermore, corrosion rate was found to increase with mud weight increase, decrease in pH, and increase in temperature. With increase in pressure, rate of corrosion increases, however, no trend was obtained at constant temperature. All the above results were obtained at 95% confidence level.

Gilbert and Engen[14], studied the corrosion phenomenon observed in Khuff gas wells. Their study indicated that acid attack, caused by HCl stimulation of these wells is the possible cause of corrosion. Although the level of corrosion observed during the time of their study was considered acceptable, they called for additional study because an increase of water production will likely increase the corrosivity of the downhole equipment.

Al-Marhoun and Rahman[15] also studied the corrosive behavior of drilling fluids under simulated bottomhole conditions, using both the dynamic flow loop and the roller oven. They used the Polarization Admittance Instantaneous Rate (PAIR) technique to measure corrosion rate. Their study was conducted by aging water-base drilling fluids in the roller

oven for 24 hours and in a dynamic flow loop at a shear rate of 5000 s^{-1} for 6 hours. Both tests were conducted at temperatures between ambient and 347°F .

The results obtained using weight loss technique for the roller oven samples and PAIR in the flow loop showed an increase in corrosion rate with temperature increase. They attributed this to the increase of electrochemical activity, and the release of oxygen; associated with the degradation of mud components as a result of temperature increase. They noted that very severe corrosion can be obtained at temperatures above 248°F .

Revisiting Khuff gas formation, **Kasnick and Engen**^[16] analyzed the result of the investigation into the cause(s) of scale deposits and underlying corrosion in tubing strings. They concluded that exposure of the tubing string to HCl aids corrosion and scale formation.

Abdalla^[17], measured the weight loss of high alloy steel coupons after 12 hours and 6 hours exposure to various acid mixtures at 200°F in order to determine the optimum acid formulation that would reduce corrosion inherent upon acid stimulation. He found that 10-20 gallons/ft inhibited, 15% HCl is the best formulation for stimulating tight gas bearing formations at high pressure and temperature without corroding the completion equipment.

Ciaraldi et al.[18], carried out corrosion tests on aluminum drill pipe alloy 2014-T6 in a water-base, low solids, non-dispersed drilling mud. Their electrochemical tests (cyclic polarization and galvanic coupling to steel), were carried out in stirred drilling fluid and aimed at determining the parameter that has the greatest effect on corrosion behavior at either ambient temperature or 160 °F. Cyclic polarization tests showed that temperature contributed most significantly to corrosion. Raising the temperature from ambient to 160 °F increased the equilibrium potential by approximately 100 mV. Aeration (oxygen) decreases the equilibrium potential by approximately 70 mV and increase in chloride concentration from 3,000 to 10,000 ppm increase the equilibrium potential by 45 mV. Hence, corrosion of aluminum is no problem at 160 °F and high chloride levels; in the presence of oxygen. Galvanic Coupling tests indicate low corrosion rates. The coupling effectively shifted the potential of aluminum to the positive direction, hence reducing the corrosion rate, although not as significant as expected.

Al-Marhoun and Rahman[19], in 1990 studied the effects of composition, contaminants, and temperature on the corrosion behavior of drilling fluids. The mud composition used has a broad range of clay, polymer, dispersant, and weighting (barite) materials. Contaminants are mainly lime and gypsum. The study was carried out at temperatures between ambient and 446 °F. Both the dynamic flow loop and the roller oven were used, with corrosion rate measured with PAIR and weight loss techniques respectively. They were only able to measure corrosion in the loop up to 347 °F due to the design limitations of the corrosion cell. Results

of their study showed that corrosion rate increases with temperature increase for all the mud formulations tested. The values obtained from the weight-loss method, although generally lower than that from PAIR, are very comparable.

They concluded that drilling fluid prepared from cellulose ethers or lignosulfonates are not effective in preventing corrosion at temperatures above 248°F. Copolymers of vinylsulfonate-vinylamide (VSVA) and styrene sulfonate maleic acid anhydrite (SSMA) are very effective in controlling corrosion at high temperature and high electrolyte contamination. Finally, they suggested that the rate of corrosion can be reduced if attapulgitc is used instead of bentonite in drilling fluids. They also found that the measurement obtained from the PAIR method is more accurate than the weight-loss measurement, because it includes the localized corrosion tendencies.

It is observed from the literature that practically no work has been done to understand the corrosion behavior, and corrosion reaction mechanism of drill pipe materials exposed to drilling fluids. Only few of the studies were carried out under conditions simulating mud circulation experienced while drilling. Among these few, electrochemical evaluation of corrosion was not carried out extensively.

TABLE I: LITERATURE REVIEW SUMMARY

Investigator & Year	Method(s)	Study Parameters	Corrosion Medium	Remarks/Conclusions
Simpson & Barbee (1967)	Discussion, Laboratory tests	Temperature, Bacterial action, Electrochemical reaction	Water-Base Lignosulfonate mud	Water-base lignosulfonate mud degrades at temperatures above 300 °F to produce CO ₂ and H ₂ S. Bacterial action on lignosulfonate and organic additives results in the production of organic acids, soluble sulfides and CO ₂ . Electrochemical reduction of sulfur containing organic additives is the cause of sulfide formed in water-base packer fluids without bacterial action or high temperature degradation.
Zitter (1972)	Field (sour gas well)	Time	Carbon-dioxide, hydrogen sulfide	High corrosion rates indicated by tubulars at early stages. Protective surface film grows thicker with temperature. Proposed a reaction mechanism from the detection of calcium chloride and calcium carbonate in surface films examined by x-ray diffraction.
Bush (1974)	Field tests, drill string coupons	Inhibitors	Oxygen, hydrogen sulfide, & carbon-dioxide	Removal of dissolved oxygen with sulfite, precipitation of sulfite ions with zinc or other metal compounds, & neutralization of carbon-dioxide with alkaline materials can mitigate drill string fluid corrosion problems.
Carney & Jones (1974)	Discussion	Inhibitors, pH	Hydrogen sulfide	By properly maintaining an alkaline mud & monitoring sulfides, corrosion problems caused by hydrogen sulfide can be controlled.
Mauzy (1974)	Discussion	Inhibitors, Time, Temperature, & pH	Hydrogen sulfide	Creation of hydrogen sulfide in the drilling fluid by the action of sulfate reducing organisms on sulfur components of drilling fluids should be avoided.

Investigator & Year	Method(s)	Study Parameters		Corrosion Medium	Remarks/Conclusions
		Corrosion Fatigue	pH		
Azar & Luminus (1975)	Corrosion Fatigue			Gases, pH level	In drilling fluid environment, various dissolved gases and fluid pH dictate the corrosion fatigue endurance of drill pipe.
Woodroof <i>et al.</i> (1975)	Weight loss	Inhibitors, Temperature, Pressure, Coupon yield strength		HCl-HF acids/mutual solvents mixture	Increase in pressure has no significant effect on corrosion rate. Increase in temperature & increased yield strength of material resulted in increased corrosion rate for the inhibited HCl-HF/mutual solvent system.
Smith <i>et al.</i> (1978)	Weight loss	Inhibitor concentration, Temperature, Exposure time, Agitation, steel type & Chemical additives		Acid (HCl)	It is important to test at high pressure & temperature under dynamic flow or at least agitated conditions. Corrosion rate increases with acid concentration & temperature increase. Some surfactants can reduce inhibitor effectiveness.
Ray <i>et al.</i> (1979)	Discussion	Sulfide scavenger, pH		Hydrogen sulfide	Iron oxide is an effective scavenger for hydrogen sulfide, even at high hydrogen sulfide concentrations at bottom-hole temperatures & pressure.
Azar (1979)	Fatigue	Chloride concentration		Oxygen, carbon-dioxide, chlorides	Drill pipe life expectancy decreases as the concentration of oxygen, carbon-dioxide, & chlorides increases.
Samuels & Gupta (1983)	Discussion, Weight Loss, Electrochemical, SEM	pH, Scavenger		Hydrogen sulfide, Oxygen	It is important to know the type of corrosion occurring by examining the surface of exposed coupons by SEM. Corrosion rate of carbon steel is higher at pH 6 to 9. It increases with increase in sulfide concentration. Severe pitting accompanied the corrosion at pH 12 and above. Ironite sponge is effective for scavenging hydrogen sulfide and oxygen.

Investigator & Year	Study Parameters		Corrosion Medium	Remarks/Conclusions
	Method(s)	Parameters		
Moussa (1983)	Weight loss using flow loop & roller oven	Temperature, pH	Oxygen	Corrosion rate increases with increase in temperature at low pH. It decreases at high temperatures as pH increases. Corrosion rate varies with the equipment used to simulate bottom-hole conditions.
Okoye <i>et al.</i> (1988)	General (statistical analyses)	Temperature, Pressure, pH, Viscosity, Density	Hydrogen sulfide, carbon-dioxide, & oxygen	Corrosion rate increases as temperature increases if /pH is high. It decreases as pH increases even at high temperatures. Corrosion rate increases with increase in mud density & pressure. No trend was observed at constant temperature for pressure effect.
Gilbert & Engen (1988)	Field Tests	Inhibitors	Hydrochloric acid, chlorides	Corrosion & scaling observed in Khuff gas wells was attributed to HCl acid used in stimulating the formation
Al-Marhoum & Rahman (1988)	Electrochemical, Weight loss, using flow loop & roller oven	Temperature, 24 hrs. aging in roller oven & 6 hrs. in flow loop	Oxygen	Corrosion rate increases with temperature increase. This is due to increased electrochemical activity & release of oxygen from the degradation of mud components.
Kasnick & Engen (1988)	Field Tests	Scale formation	Hydrogen sulfide, carbon-dioxide	Drilling fluids exposed to hydrogen sulfide carbon-dioxide gases, and HCl together with extreme temperatures & high pressures are probably the main cause of corrosion/scaling in Saudi Arabian Khuff gas wells.
Abdalla (1989)	Weight loss	Temperature, Inhibitors, Pressure	Hydrochloric acid, hydrogen sulfide	Optimum acid formulation that would reduce corrosion inherent upon acid stimulation was found to be 10-20 gal/ft inhibited, 15% HCl.

Investigator & Year	Method(s)		Study Parameters	Corrosion Medium	Remarks/Conclusions
Ciaraldi <i>et al.</i> (1990)	Electrochemical	Chloride concentration, Temperature	Oxygen	Increasing temperature indicated higher corrosion rates. Increase in chloride concentration did not significantly affect corrosion rate.	
Al-Marhoum & Rahman (1990)	Electrochemical, & weight loss, using dynamic flow loop & roller oven	Composition, Contaminants, Temperature	Oxygen	Increase in temperature results in increased corrosion rates for all mud composition/formulations. Weight loss & electrochemical rates are comparable, although weight loss rates are generally lower. Drilling fluid prepared from cellulose ethers or lignosulfonates are not effective in preventing corrosion at temperatures above 248 °F. VSVA & SSMA are however, very effective in controlling corrosion at high temperature & high electrolyte contamination. Using attapulgite instead of bentonite in drilling fluids can reduce the rate of corrosion.	

CHAPTER 4

EXPERIMENTAL SET-UP AND PROCEDURE

4.1 EXPERIMENTAL SET-UP

4.1.1 Mud Formulation

A typical water-base mud used in drilling deep wells in hostile formations was used for this research. It consists of the following components and concentrations:

Base Mud I

Fresh water	-	1 bbl
Bentonite	-	10 ppb
Lime	-	0.2 ppb
Hydroxy Ethyl Cellulose (HEC)	-	0.5 ppb

Base Mud II

Base Mud I	-	0.2 bbl
Fresh water	-	0.4 bbl
Dextrid	-	2 ppb
XC-Polymer	-	0.5 ppb
Calcium carbonate	-	2 ppb

Mud Sample

Base Mud II	-	0.8 bbl
Fresh water	-	0.2 bbl
Thermathin	-	3 ppb
Bentonite	-	5 ppb
Lime	-	0.25 ppb

4.1.2 Equipment

Laboratory test procedures used in simulating the conditions encountered by the mud during circulation from the surface, through the drill pipe and the annulus include equipment such as dynamic flow loop, high pressure-high temperature (HPHT) viscometer, and roller oven. All these equipment were used in this study.

4.1.2a *Dynamic Flow Loop*

A dynamic flow loop available at the Petroleum Engineering Department of King Fahd University of Petroleum and Minerals was reconstructed with major changes in design as part of this work. It was used to simulate drilling fluid circulation under downhole conditions existing within the drill pipe, the drill bit, and the annulus as well as the temperatures and pressure encountered. The loop is made up of stainless steel tubes of 3/8 inch and 1/2 inch outside diameters with total length of 89 m. Its schematic is shown in Figure 4.1. The flow loop consists of the following major components and sections:

LEGEND

- 1 - Mud Reservoir with Mixer
- 2 - Feed Pump
- 3 - Mud Pump
- 4 - Cooling Bath
- 5 - Heater
- 6 - Capillary Viscometers
- 7 - Test Section
- 8 - Heater Control & Temperature Measurement Panel
- 9 - Pressure Flow Control & Measurement Panel Including Corrosion Meter.

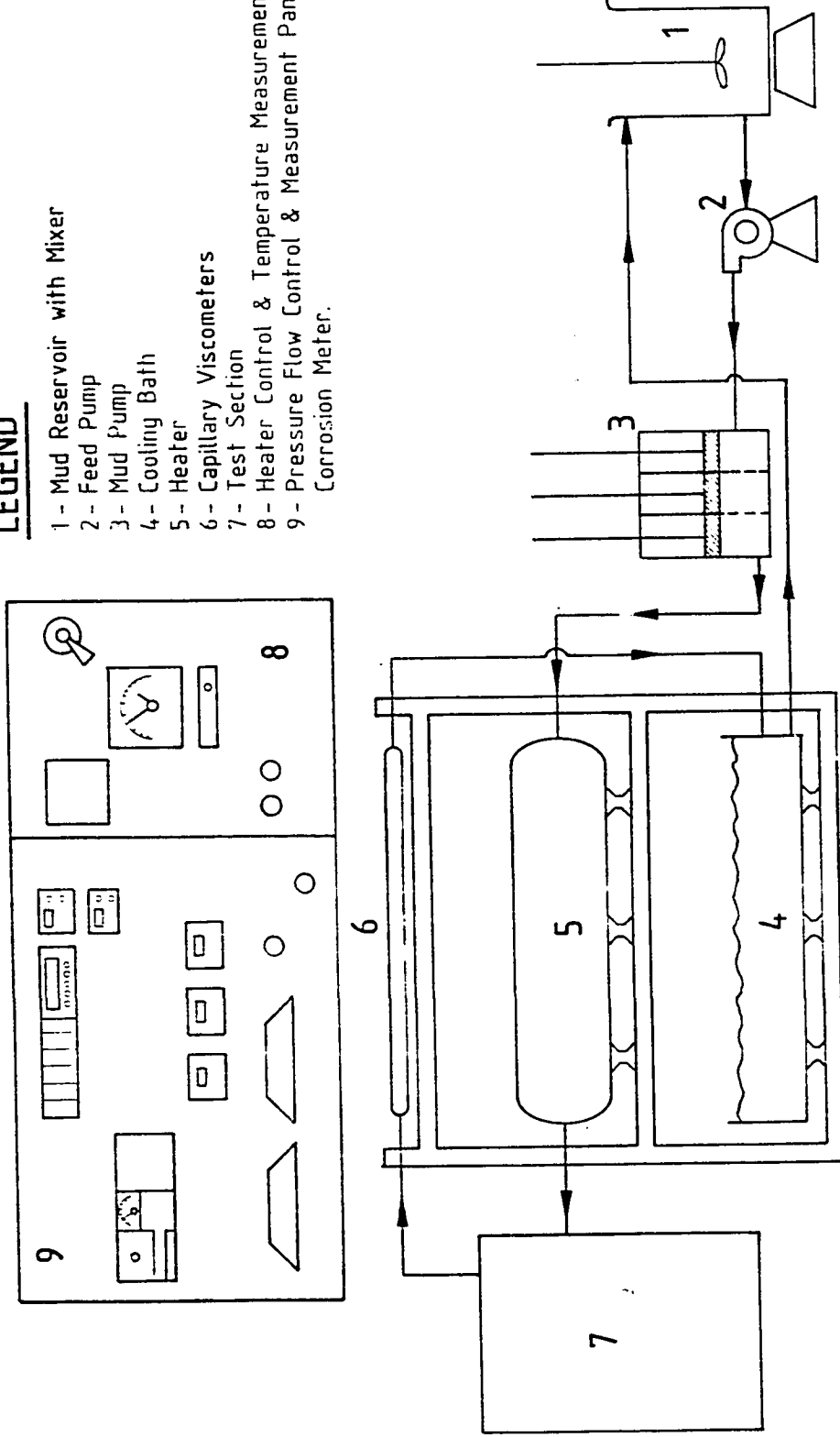


Figure 4.1 : Schematic Diagram of the Dynamic Flow Loop.

(i) Pumping Unit

The pump used to force the mud through the loop is a variable drive triplex piston pump. It is capable of delivering 20 gal/min. at 6000 psi pressure. The pump's delivery side is made of stainless steel, while the pistons are made of ceramic to prevent the problems of erosion and corrosion capable of being caused by high density, high solids content drilling fluid. The pump is equipped with a feed pump at the suction side to give the pump a sufficient head and to further homogenize the drilling fluid. The delivery pressure of the pump is monitored by a pressure gauge and pressure transducer installed on the positive side of the pump.

(ii) Mud Reservoir

A stainless steel cylindrical tank is used as the mud pit. The feed pump takes its suction from this tank, and the mud eventually returns to the tank after circulation through the loop to form a continuous flow system. It is equipped with a heavy duty stirrer to homogenize the mud and prevent the settling of solids. A pH probe and thermocouple is incorporated on the tank to monitor the pH and temperature of the mud respectively.

(iii) Heating and Cooling Section

To raise the mud to the desired temperature of test, it is flowed through a cylindrical tank filled with silicone oil which is heated by a thermostated immersion heater having a capacity of 18.8 kW.

Before returning to the reservoir, the mud is cooled down to ambient temperature by passing it through a cooling bath filled with water. The heating oil temperature is monitored and controlled by a thermocouple immersed in it, and connected to the heater control panel. Temperature of the flowing mud is also monitored at different points by thermocouples connected to the heater control panel.

(iv) Test Section

The test section (Fig. 4.2) consists of two major parts. The first part is the combination of a shear valve, a dynamic filtration cell, and corrosion cells. It is made up of two sections- the cold and hot sections. These simulates the temperature regimes experienced by the mud while being circulated through the hole. By applying shear through the shear valve, the shear rate experienced by the mud at the drill bit is simulated. It also helps to break up gels formed by the mud.

The electrochemical corrosion cell is a high pressure stainless steel cell in which instantaneous corrosion measuring probe is immersed (Fig. 4.3a). This probe is hooked up to the Petrolite corrosion data acquisition system for corrosion rate measurements by polarization resistance.

The linear corrosion cell (Fig. 4.3b) is a thick-walled stainless steel tube. It can carry up to six rectangular flat coupons installed on Teflon coupon carriers, designed to fit into the cell. Corrosion rate is determined by weight loss of the coupons. This set-up allows for a comparison of the

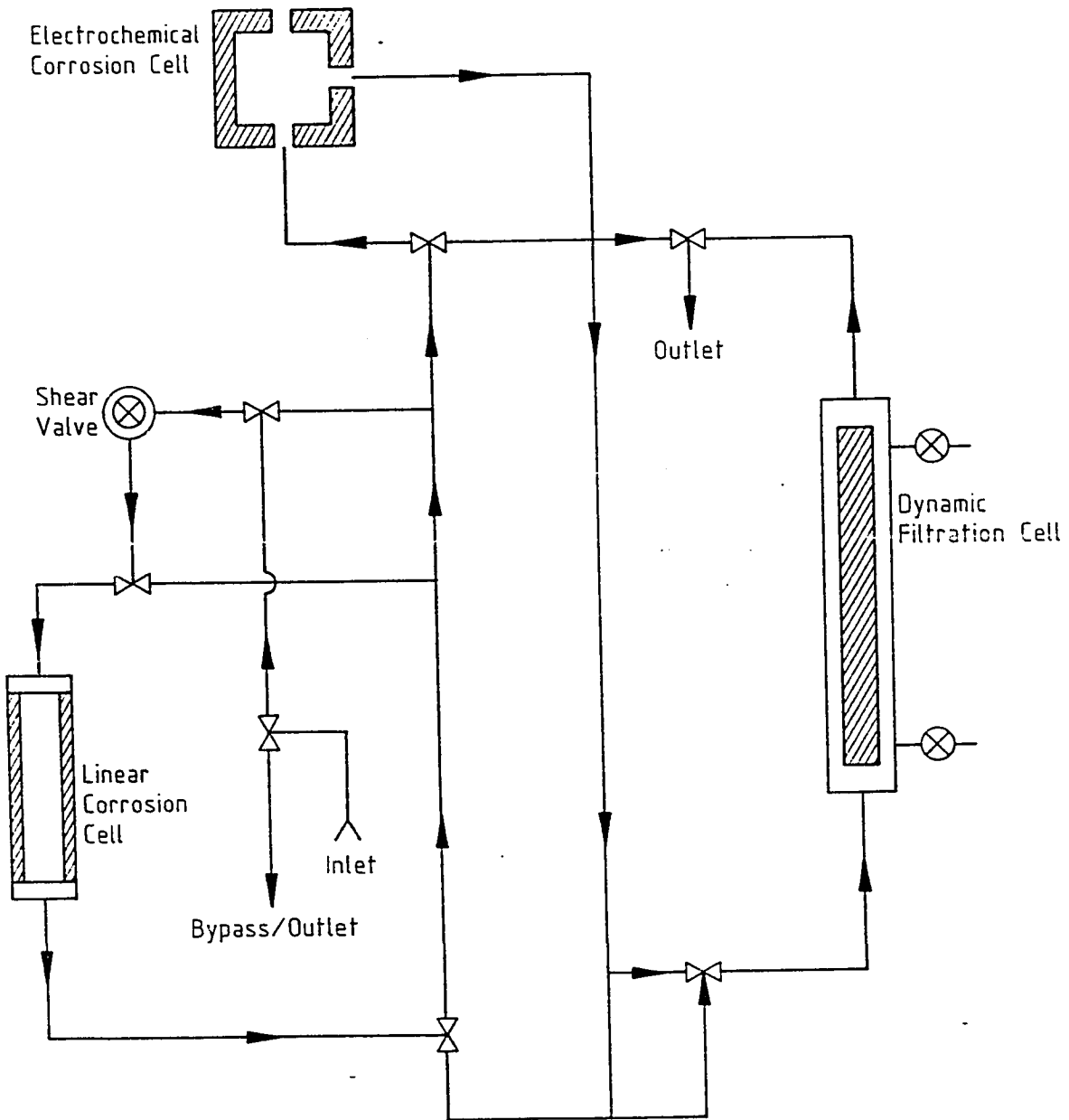


Figure 4.2 : Schematic Diagram of the Test Section.

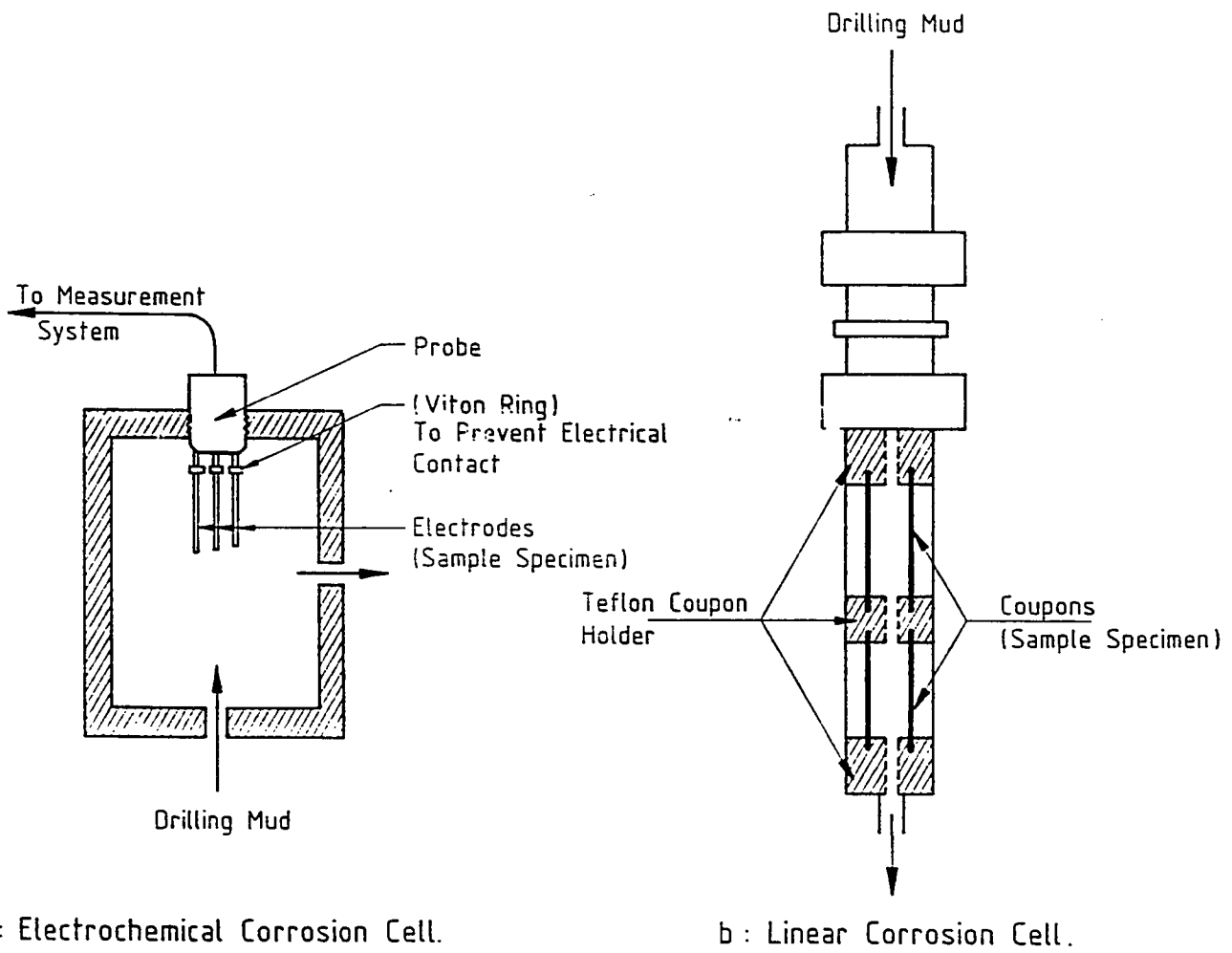


Figure 4.3 : Flow Loop Corrosion Cells.

electrochemical and weight loss measurements.

The second part of the test section consists of three capillary viscometers made up of 1/4 inch, 3/8 inch, and 1/2 inch outside diameter stainless steel tubes. Absolute and differential pressure transducers installed at the end of these viscometers enable the measurement of the viscosity of the circulated drilling fluid.

4.1.2b *HPHT Viscometer*

The FANN-70 HPHT Viscometer was used to study the thermal stability of the test mud immediately after preparation, and after aging in the roller oven. The viscometer (Fig. 4.4) is a direct indicating coaxial cylinder viscometer that measures drilling fluid rheological properties at high pressures and elevated temperatures. It is made up of the control console, the remote test station and the test cell. The control console contains all controls, displays, power supply, the pressurization pump, and test cell preparation station. The remote test station contains the magnetic torsion sensor, the magnetic cell drive, and the cell heaters and cooling systems. It also contains a cylindrical safety shield which is designed to protect the operator in case of a cell failure at high pressure. The test station is designed such that measurements cannot be made unless the safety shield is closed. The test cell is designed to withstand 20,000 psi pressure at 500°F. It includes a torsion assembly hooked onto a bob with a magnetic rotor.

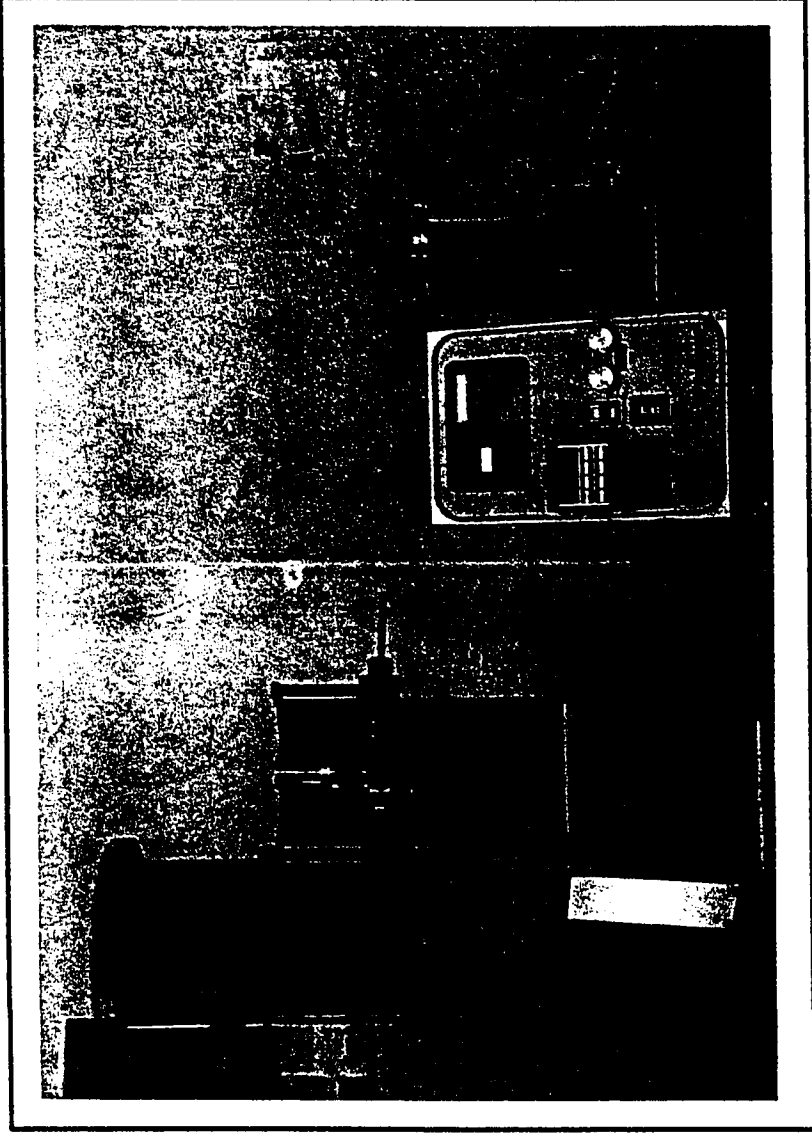


Figure 4.4: FANN-70 High Pressure-High Temperature Viscometer.

4.1.2c *Roller Oven*

The roller oven was used to simulate the heating and rotational action of the drilling mud in the annulus, as well as the effect of aging on corrosion and thermal stability of the mud.

The oven (Fig. 4.5) has 5 rollers which carries up to 16; 500 ml capacity test cells at a time. The cells are rolled at an approximate speed of 50 rpm. They are designed to withstand high temperature and pressure as well as highly corrosive mud. Steel coupons can be placed inside the cells to study corrosion of drilling fluid by weight loss method. The oven can be operated at a maximum temperature of 550°F.

4.1.2d *Princeton Applied Research Model 350A Corrosion Measurement System*

This is a direct current (dc) potentiostat. It is a microprocessor based instrument which can be used for different dc corrosion measurement techniques such as potentiodynamic, polarization resistance, Tafel plot, pitting scan, etc. The potentiostat requires a three electrode electrochemical cell. A potential sweep can be applied at user specified rate on both the cathodic and anodic sides of the corrosion potential of the cell. The corresponding current density is measured by the equipment. The equipment is equipped with an x-y recorder/plotter that can generate potential-current density plot in real-time.

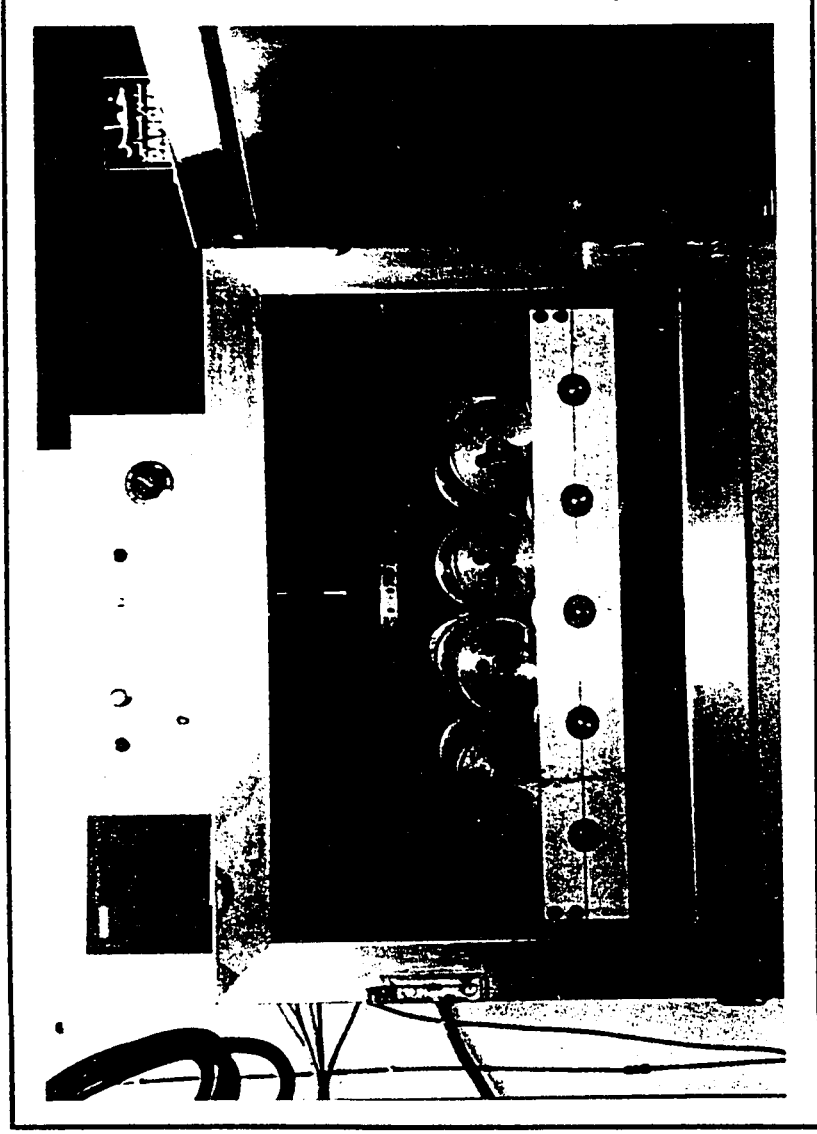


Figure 4.5: Baroid Roller Oven with 500 ml Aging Cells.

4.1.2e *Princeton Applied Research (PAR) Model 173 Potentiostat and Solartron-Schlumberger 1250 Frequency Response Analyzer*

These equipment provides a state-of-the-art electrochemical impedance measurement. The potentiostat with plug-in coulometer model 179 measures the corrosion potential of the cell and applies a specified dc voltage on the test specimen. The frequency response analyzer (FRA) applies an alternating current (AC) on this dc voltage to generate the impedance response of the system. The FRA can be programmed to sweep from a minimum frequency to a maximum frequency, in a number of steps, in the required frequency range. The impedance response is analyzed and separated into real and imaginary parts and stored by the equipment. The stored data can be retrieved by an attached computer and plotted for further analysis.

4.2 PROCEDURE

4.2.1 Mud Preparation

The test mud was prepared by adding and mixing the components in the order listed in 4.1.1. After the addition and mixture of all components, the mud was allowed to age for at least 24 hours to allow for complete hydration of the clay (bentonite). After this period, the pH and density of the mud were measured and recorded. The mud is now ready for the different tests carried out.

To prepare mud sample with pH different from the above, 5% HCl was added to the mud after complete hydration of the bentonite. Enough quantity of HCl was added to bring the mud to the desired pH value.

4.2.2 Preparation of Corrosion Coupons

The steel coupons used for corrosion study by weight loss were prepared as follows, prior to exposure and after the test:

Before Test

- i) All rough edges on the surface of coupons were smoothed.
- ii) The coupons were then dipped into trichloroethylene to degrease their surfaces.
- iii) They were etched in a 5% HCl solution,
- iv) Neutralized in a saturated solution of sodium bi-carbonate, and
- v) Cleaned under tap water by scrubbing with nylon brush, and rinsed with acetone.
- vi) They were dried in a vacuum oven and then weighed.

After Test

- i) On removal of the coupons from the test sample, they were immersed in a saturated solution of sodium bi-carbonate.
- ii) The mud and corrosion products were cleaned off the coupons' surface by scrubbing with nylon brush under tap water.
- iii) They were rinsed with acetone, oven dried and weighed.

4.2.3 HPHT Viscometer

With all parts of the test cell cleaned, and the mechanical zero of the equipment set, 165 ml of mud sample was placed in the test cell; 140 ml directly into cell and 25 ml through a port opening. It was lowered into the hot well of the remote test station, ready for testing.

The dial reading at different rpm settings were measured for the freshly prepared mud at 3000 psi for 200°F, 250°F, 300°F, and 400°F temperatures to determine the thermal stability of the mud. After aging the mud in the roller oven for 5, 10, 15, and 20 days at the above temperatures, the mud was tested again in the viscometer at the same pressure to determine the effect of aging on the thermal stability of the mud. These tests are necessary prior to the test in the flow loop in order to forestall any unforeseen circumstance(s).

4.2.4 Roller Oven

Stainless steel aging cells of 500 ml capacity were cleaned and filled with the mud sample. Three cylindrical corrosion test coupons, 9.35 mm in diameter and 27.8 mm in length; made of 1018 cold-rolled mild steel were weighed and placed in each cell containing mud sample. The coupons were placed in such a way that they have no electrical contact with the cell.

The cells were capped, the stem valve was installed and through it the cell was pressurized with nitrogen to prevent evaporation of water, and

eventual solidification of the mud. The applied pressure depends on the vapor pressure of water at the test temperature. The cells were then placed on rollers in the oven. The oven was maintained at the test temperature for 30 minutes prior to placement of the test cells in order to make sure that samples attain the test temperature as soon as they are placed in the oven.

After the attainment of the exposure period, the test cell was removed from the oven and allowed to cool down to room temperature. Pressure was bled off the cell by slowly opening the stem valve. When all pressure has been released, the cap was removed, the coupons were removed and cleaned, and the mud in the cells not containing corrosion coupons were tested in the viscometer. The coupons were weighed and the difference in the weight from the initial weight was recorded as the loss in mass. The average mass losses of three exposed coupons were recorded for each cell. Four (4) set of cells were placed in the oven at the same time for a particular temperature, each for different exposure time. After 20 days when the last cell is removed, new coupons were put in place for tests at other temperatures.

4.2.5 Flow Loop

With the thermal stability of the test mud already established at the temperatures of interest, the mud was flowed through the dynamic flow loop at suitable temperatures. Figures 4.6a, 4.6b and 4.6c show the set-up of the flow loop. Four rectangular flat coupons of approximate dimensions: 20 mm x 10 mm x 1.5 mm were installed in the linear corrosion cells on the cold and hot sections of the loop. These were removed after the completion of the



Figure 4.6a: Experimental Set-Up of the Dynamic Flow Loop showing the Test Section, the Heating and Cooling System, and the Heater Control Panel.

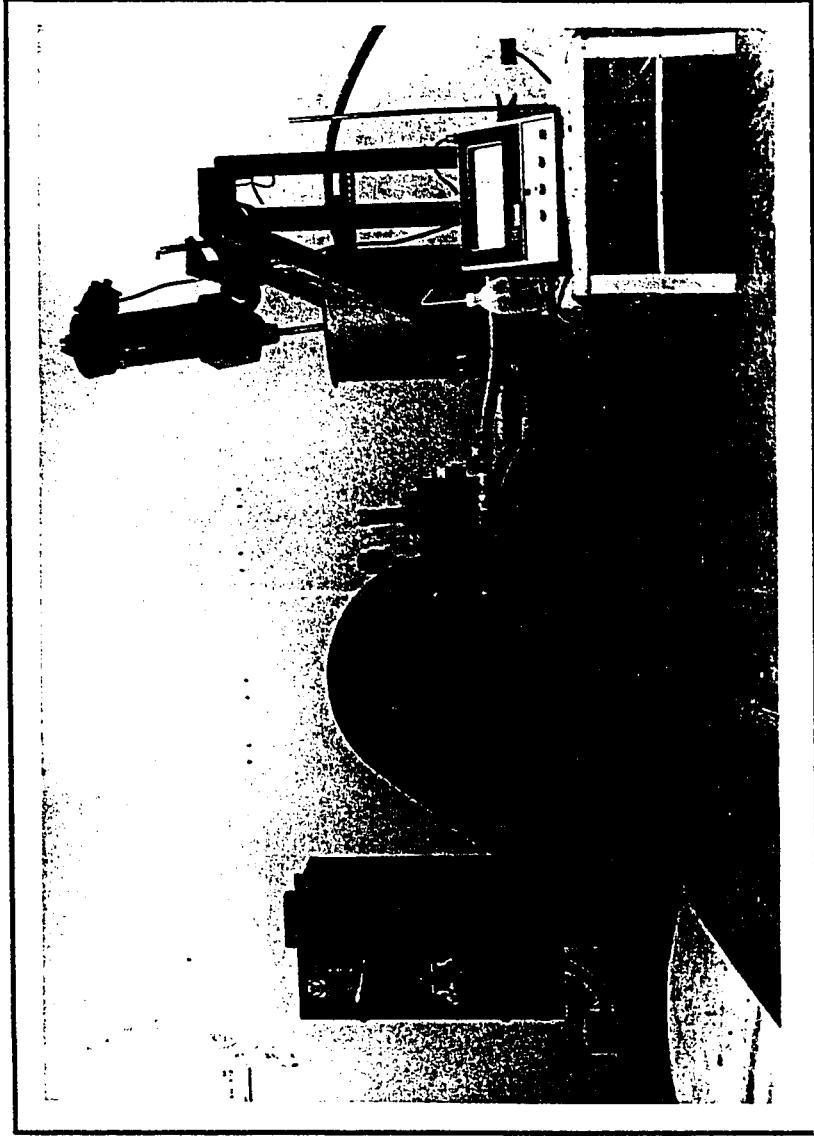


Figure 4.6b: Experimental Set-Up of the Dynamic Flow Loop showing the Pumping Unit, the Mud Reservoir, Mixer and pH Meter.

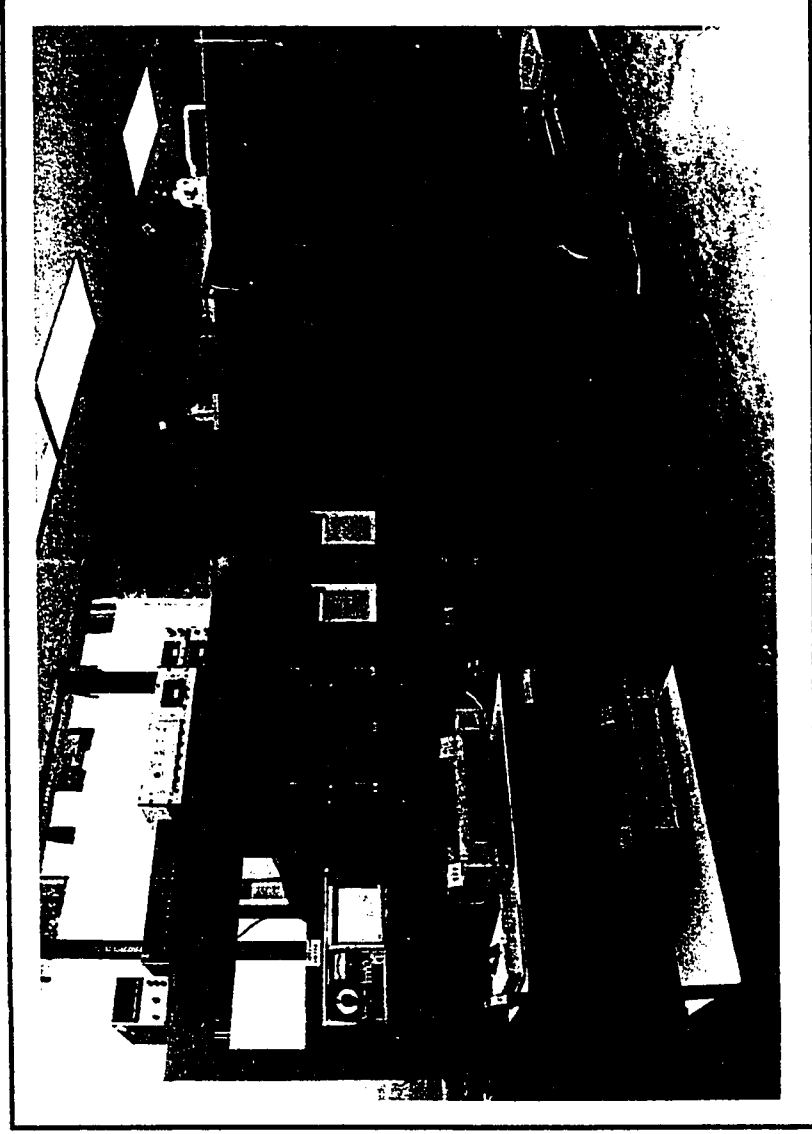


Figure 4.6c: Experimental Set-Up of the Dynamic Flow Loop showing the Control Panel with Petrolite Corrosion Meter, other Measuring Instruments and Recorders.

test, cleaned and weighed. An average mass loss of the coupons was recorded as an indication of the corrosion rate. The coupons were scanned by an electron microscope to determine their surface characteristics after exposure.

Electrochemical measurements were obtained only after the flow process becomes stable. This is determined by the stability of the operating temperature and pressure. Instantaneous corrosion rates were measured using the PAIR method, and recorded at 3000 psi pressure and ambient temperature (98 °F), 105 °F, 196 °F, and 253 °F for 8 hours of flow at mud pH of 9.5. The pH of the mud was reduced to 8.1, 6.0, and 4.1 by adding 5% HCl solution to the mud. For each pH, corrosion rates were obtained at 161 °F and 3000 psi. After each run, the loop was cleaned by flowing water through it to prevent plugging of the tubes and valves.

4.2.6 Potentiodynamic Polarization Tests

A cylindrical test specimen of mild steel (1018), 12.7 mm in length and 9.4 mm in diameter was used for these tests. The test specimen was polished to 600-grit finish with emery paper before each test. After polishing, the specimen was rinsed with distilled water, degreased with acetone and air-dried.

The polished sample was installed on a rotating cylinder electrode (RCE) as the working electrode. The counter electrode is a piece of platinum

wire, while the reference electrode used is the saturated calomel electrode (SCE). The three electrodes were placed in a glass cell containing the mud sample and connected to the dc potentiostat (Fig. 4.7). The SCE was connected remotely via a salt bridge containing saturated sodium chloride solution to prevent its contamination. Before tests were carried out, this arrangement was tested for ohmic drop effect and found to be non significant.

At static and ambient conditions, a potential sweep from 250 mV below the corrosion potential, E_{CORR} (i.e. in the cathodic region) to 1.2 V above E_{CORR} (anodic region) was applied to the system at 5 mV/s rate. This was done for mud pH of 10.9 (original mud), 8.0, 6.0, 5.1, and 4.1. From the potentiodynamic plots obtained, the corrosion behavior of the steel sample in the mud was determined. Corrosion current density were determined by drawing the Tafel slopes for each curve and corrosion rate calculated from equation (16) as a function of pH.

Hydrodynamic test was carried out at pH 10.9 and 4.1 for different rotation speed of the RCE. This equipment is ideal for the control of mass transfer characteristics of an electrochemical process^[27]. By rotation, the effect of diffusion (concentration polarization) is eliminated. Potential sweep was applied to the system from E_{CORR} to 2.5 V in the anodic direction at 5 mV/s rate for 0, 100, 500, 800, 1000, 1500, and 2000 rpm's. From the potentiodynamic plots obtained, a potential of 500 mV where the corrosion reaction was thought to be in equilibrium was chosen for AC impedance tests. Limiting current densities were determined for each mud sample at the different rpm's for use in the study of system kinetics.

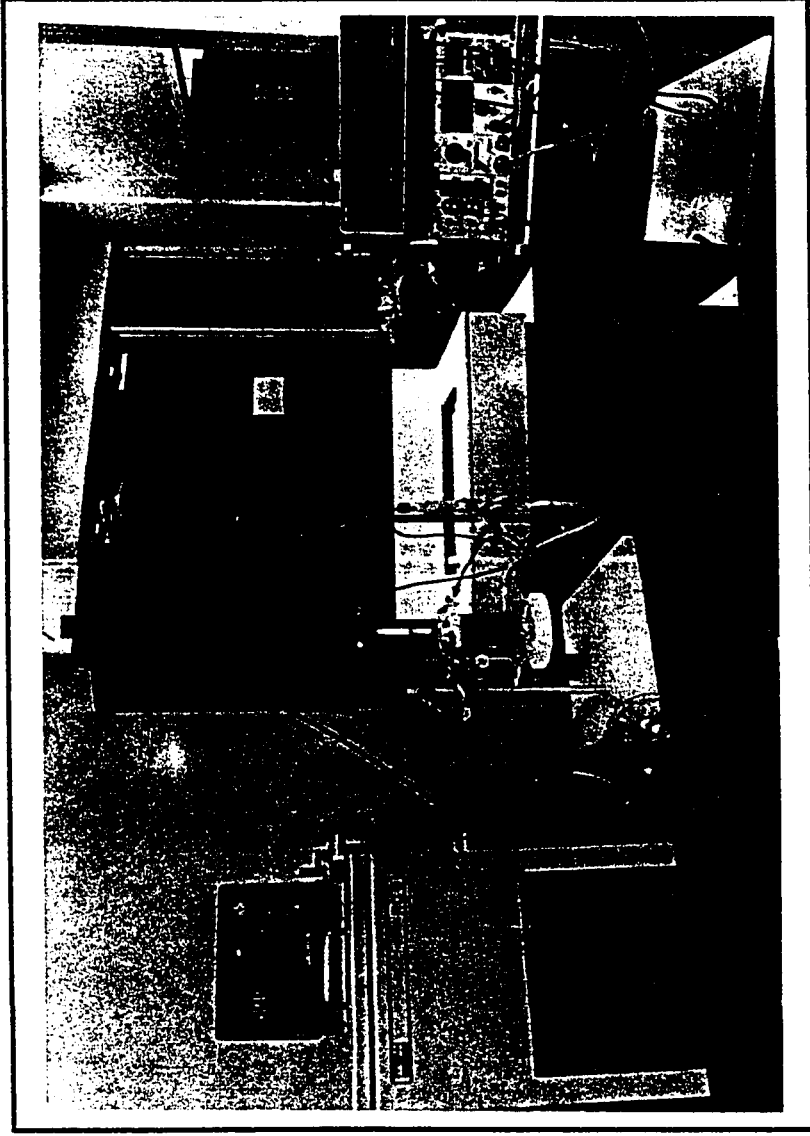


Figure 4.7: Experimental Set-Up of Potentiodynamic and AC Impedance Tests.

4.2.7 AC Impedance Tests

The same test specimen used for potentiodynamic polarization tests was prepared as described in 4.2.6 prior to each test. These tests were carried out at ambient conditions and RCE rotation speeds of 0, 500, 1000, and 2000 rpm's. The three electrode cell was connected to the PAR 173 potentiostat and the FRA. A perturbing sinusoidal AC signal of 5 mV amplitude was superimposed on a dc potential of 500 mV (anodic) over the frequency range of 50 kHz to 1 mHz, taking 4 steps per decade. Impedance spectra were obtained and plotted for mud pH of 10.9 and 4.1. Shown in figure 4.7 above is the potentiostat and FRA used for these tests.

4.2.8 Scanning Electron Microscope (SEM) Investigation

Surface of steel samples exposed to mud in the flow loop under different conditions were examined under the SEM to determine morphological changes. An unexposed sample was first observed to serve as a basis for comparison for exposed samples. The sample was mounted on the sample holder and made conductive with aluminium adhesive tape. The sample holder was then mounted on the Jeol JSM 840 SEM and its micrograph was taken at 500X magnification using 20 kV accelerating voltage.

Properly cleaned exposed samples were similarly mounted on the SEM and examined first at 250X magnification to observe the corrosion damage. A typically corroded part of the surface was further examined at 500X magnification and its micrograph taken to reveal the physical nature of the corrosion that occurred.

CHAPTER 5

RESULTS AND DISCUSSION

Tests were carried out on a typical water-base mud used in the field for drilling deep wells in hot formations. The only component missing from the field mud is the weighting material, barite. Barite was not included in the test mud because it is an inert material, therefore it will not contribute to the mud components reaction which are thought to influence corrosivity. Furthermore, a high density mud is not desirable for tests carried out with the flow loop because of the possible erosion of fittings, valves and pump. More so, there is the possibility of plugging the lines which might lead to disastrous consequences.

Analysis and interpretation of the experimental data are presented below. The experimental data are tabulated in the Appendices.

5.1 Thermal Stability of Mud

The ability of a drilling mud to withstand progressively increasing temperature while going downhole and decreasing temperature on coming back to the surface is termed as its thermal stability. Apart from the temperature regimes, the duration of time the mud is exposed to a particular

temperature is another factor affecting its stability. The indicator for determining thermal stability is the mud's rheological properties. The formulae for calculation of these properties are given in Appendix A. Figures 5.1 through 5.13 shows the results obtained for our mud formulation.

Consistency curves shown in figures 5.1 to 5.4 were obtained at temperatures of 200 °F, 250 °F, 300 °F, and 400 °F and time ranging from the day of mud preparation to 20 days. The curves show measurements obtained at 3000 psi after hot-roll aging at the above temperatures and time in the roller oven. All rheological properties are determined from these curves. Figure 5.5 shows a comparison of consistency curves obtained at ambient conditions and that obtained at elevated pressure and temperature (3000 psi, 200 °F) just after mud preparation. It shows the importance of obtaining the consistency curves at conditions of temperature and pressure simulating downhole conditions. The measurements made at ambient conditions give erroneous rheological properties which will lead to wrong conclusions on the mud's thermal stability.

Under simulated downhole conditions of temperature and pressure, it was found that effective and plastic viscosities decrease with increase in temperature and aging (Figs. 5.6 to 5.9). This is due to the aggregation of clay platelets at high temperature. The polymer constituent of the mud flocculates the aggregated platelets, thereby enabling them to move freely in the suspension^[21]. At 300 °F, there is an increase in the effective viscosity for 10 and 15 days aging and then a decrease at 400 °F. Similar behavior

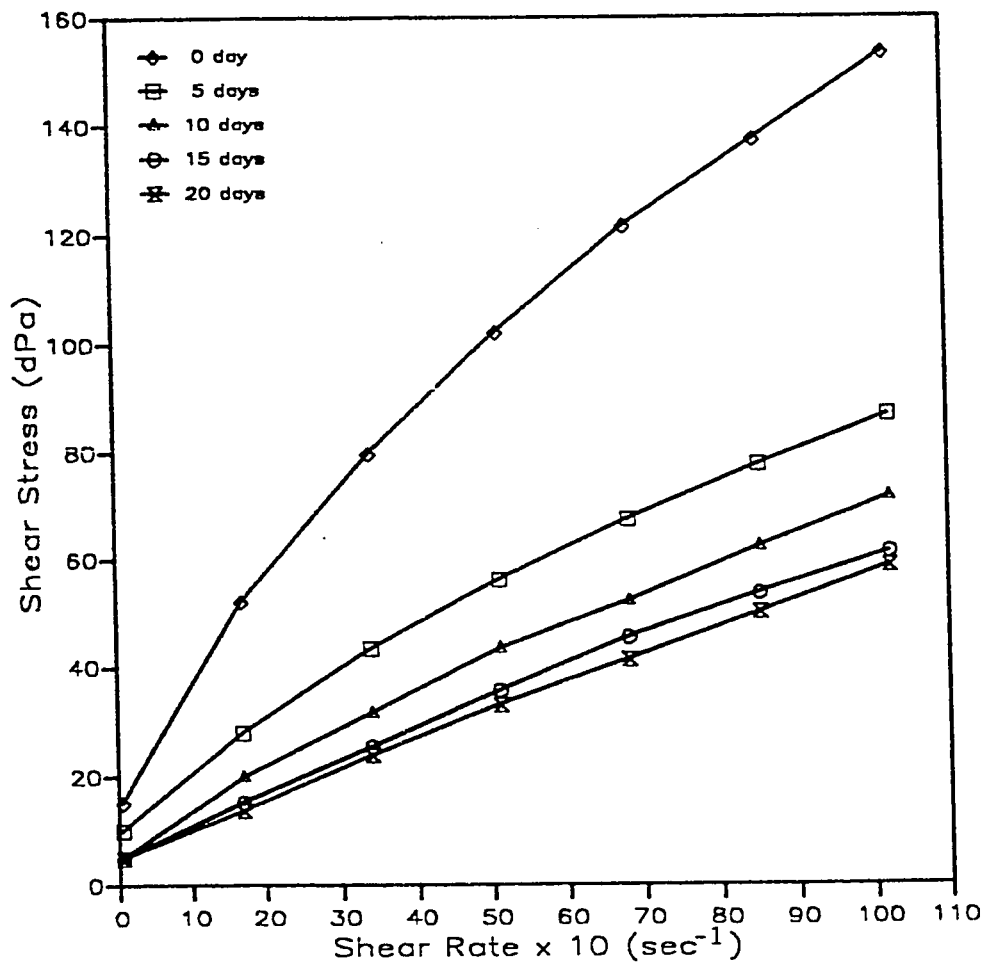


Figure 5.1: Consistency Curve Obtained at 3000 psi After Aging In Roller Oven at 200° F.

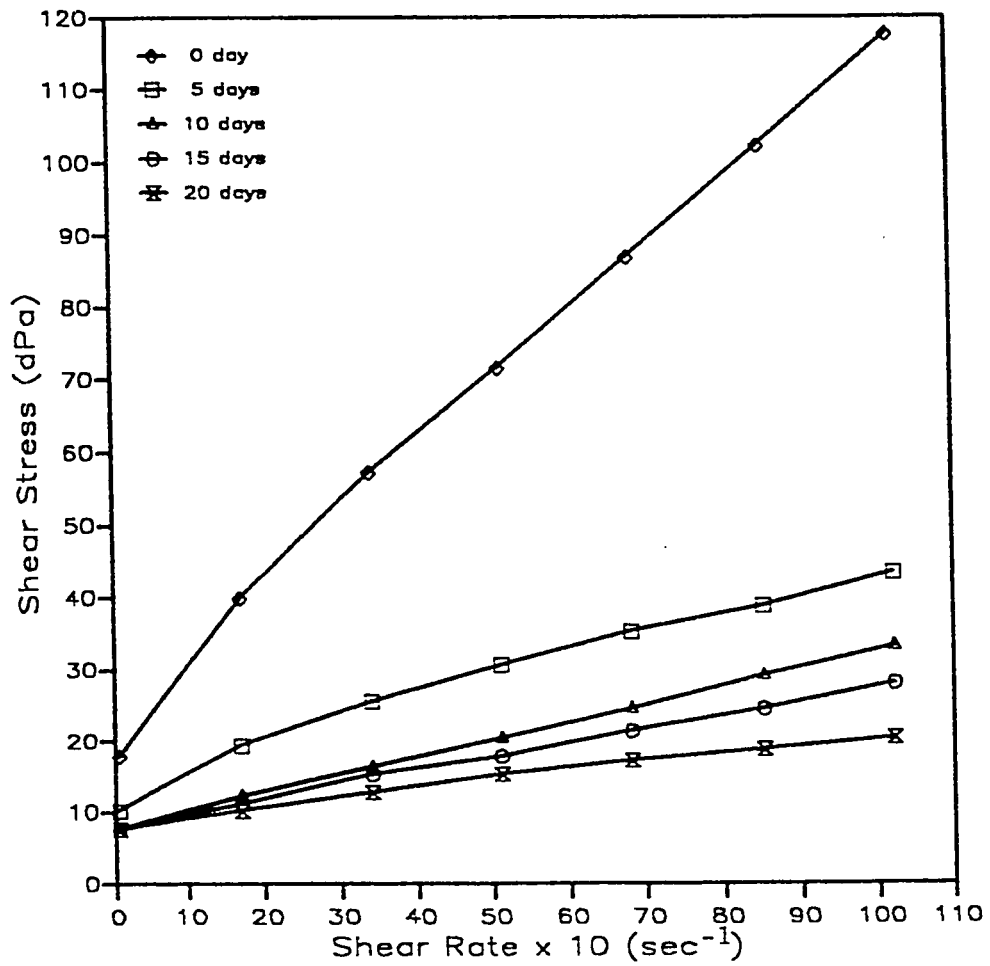


Figure 5.2: Consistency Curve Obtained at 3000 psi After Aging In Roller Oven at 250 °F.

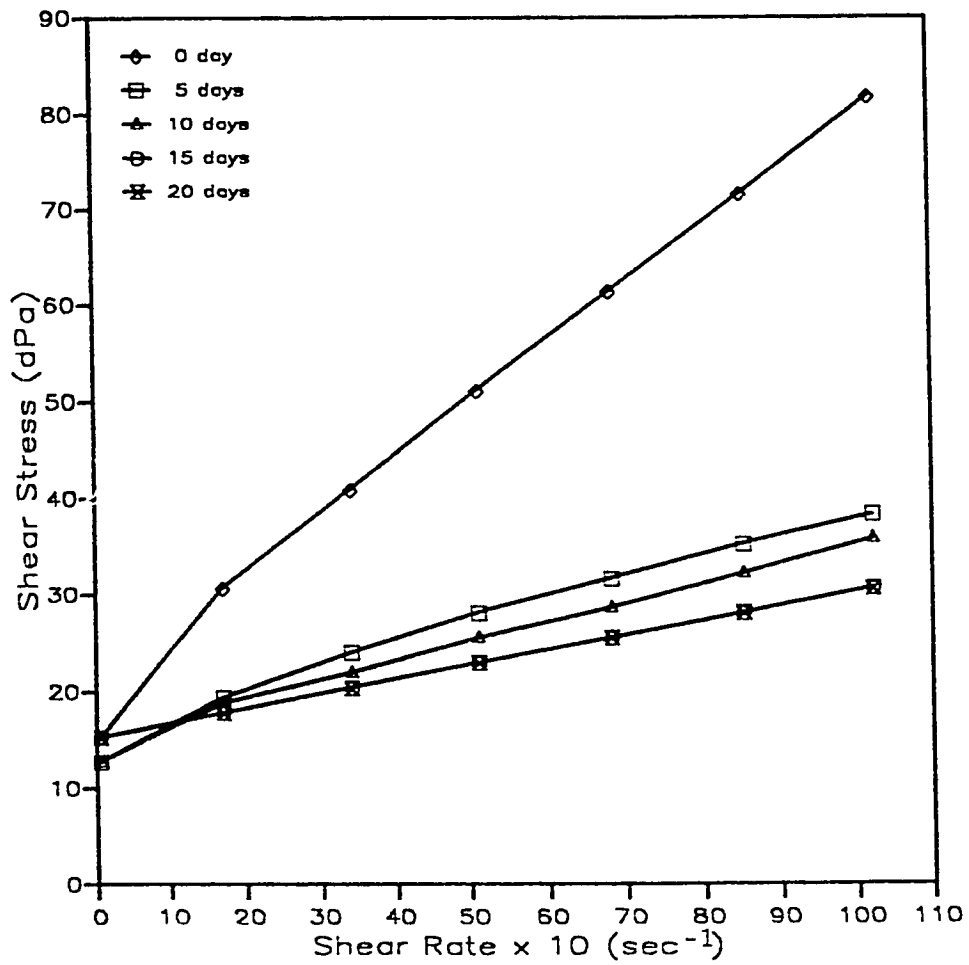


Figure 5.3: Consistency Curve Obtained at 3000 psi After Aging in Roller Oven at 300 °F.

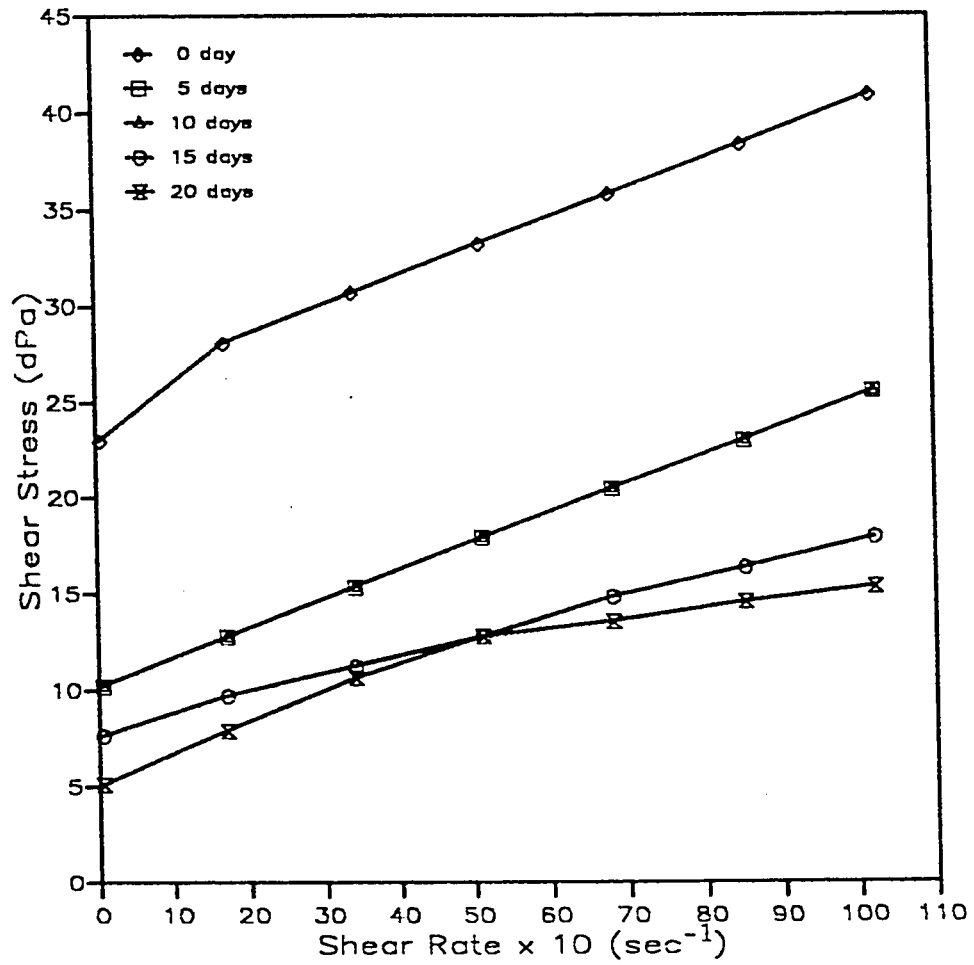


Figure 5.4: Consistency Curve Obtained at 3000 psi After Aging In Roller Oven at 400 °F.

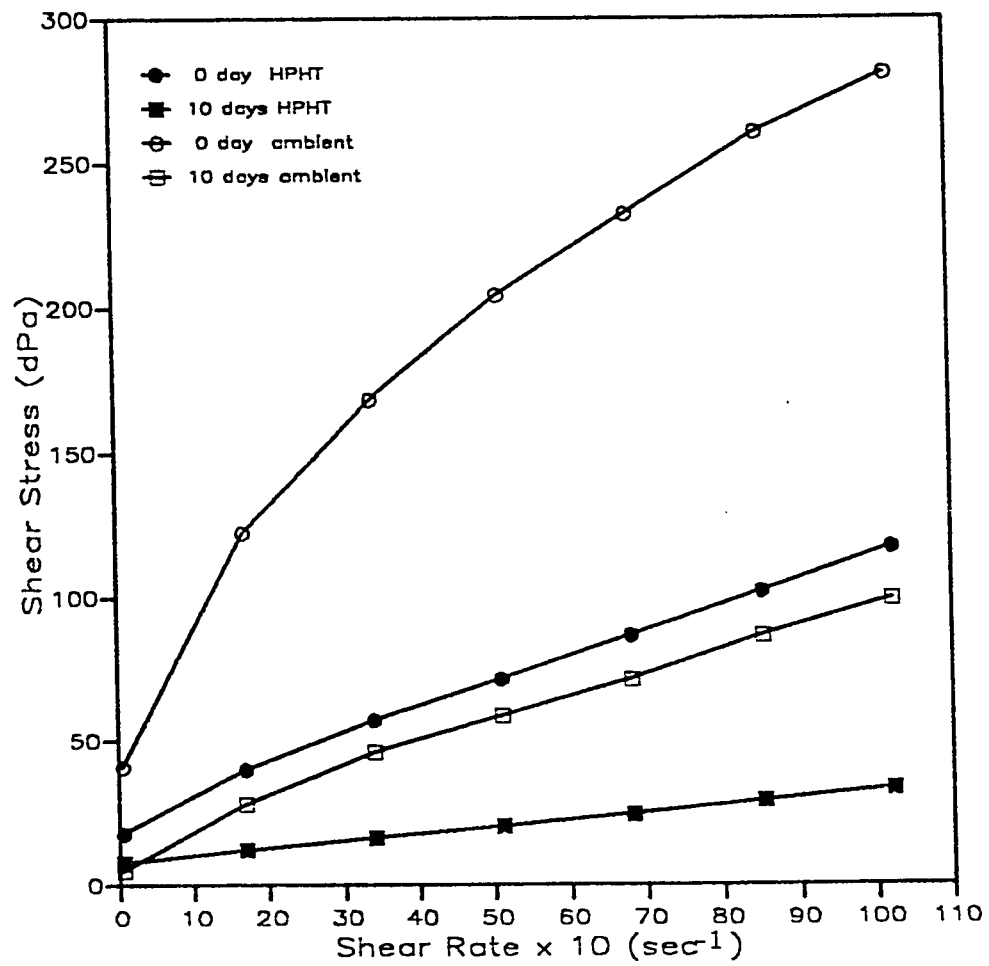


Figure 5.5: Comparison of Consistency Curves Obtained Under Downhole (250 °F, 3000 psi) and Surface Conditions.

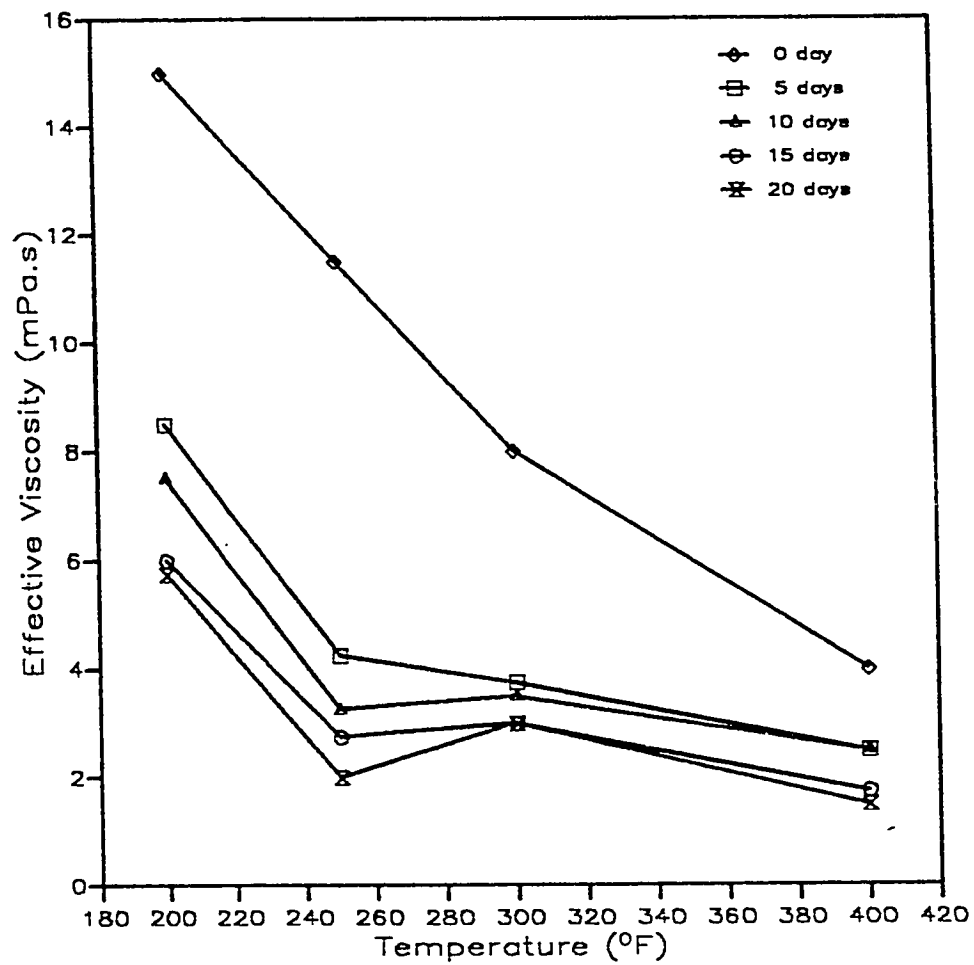


Figure 5.6: Effect of Temperature on Effective Viscosity Measured at 1022 sec^{-1} Shear Rate.

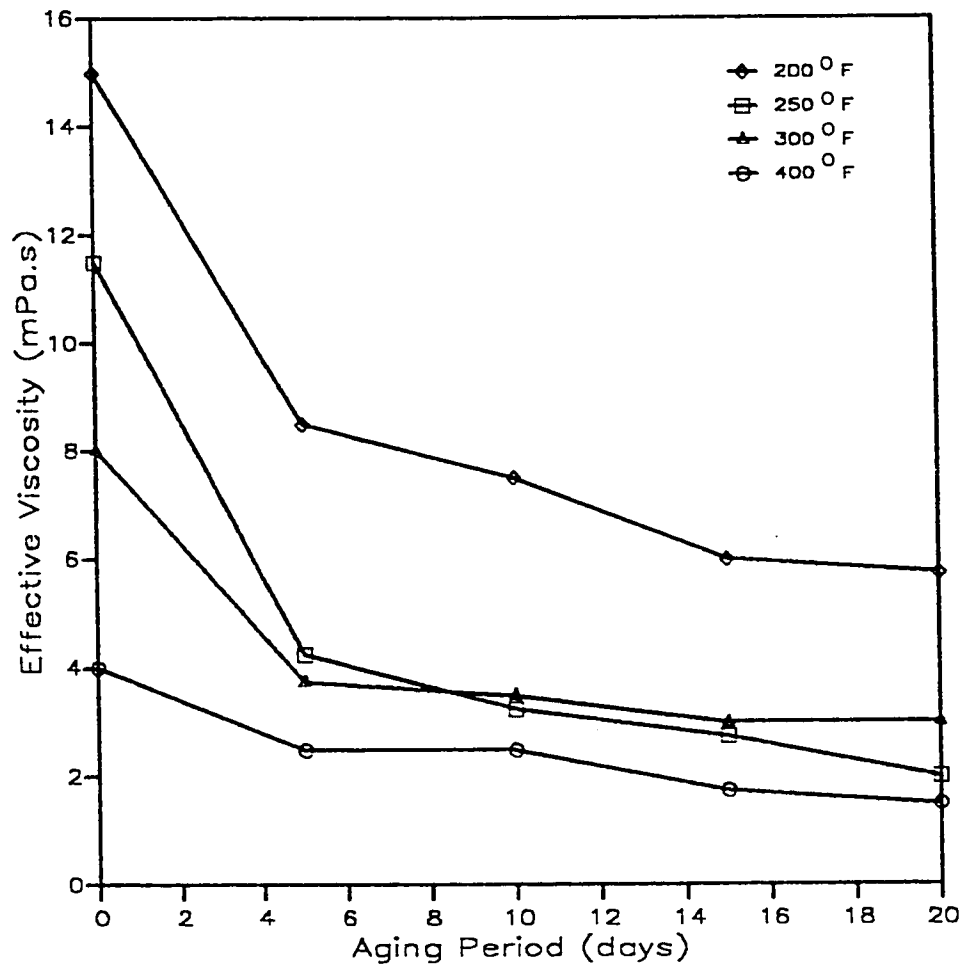


Figure 5.7: Effect of Aging on Effective Viscosity Measured at 1022 sec^{-1} Shear Rate.

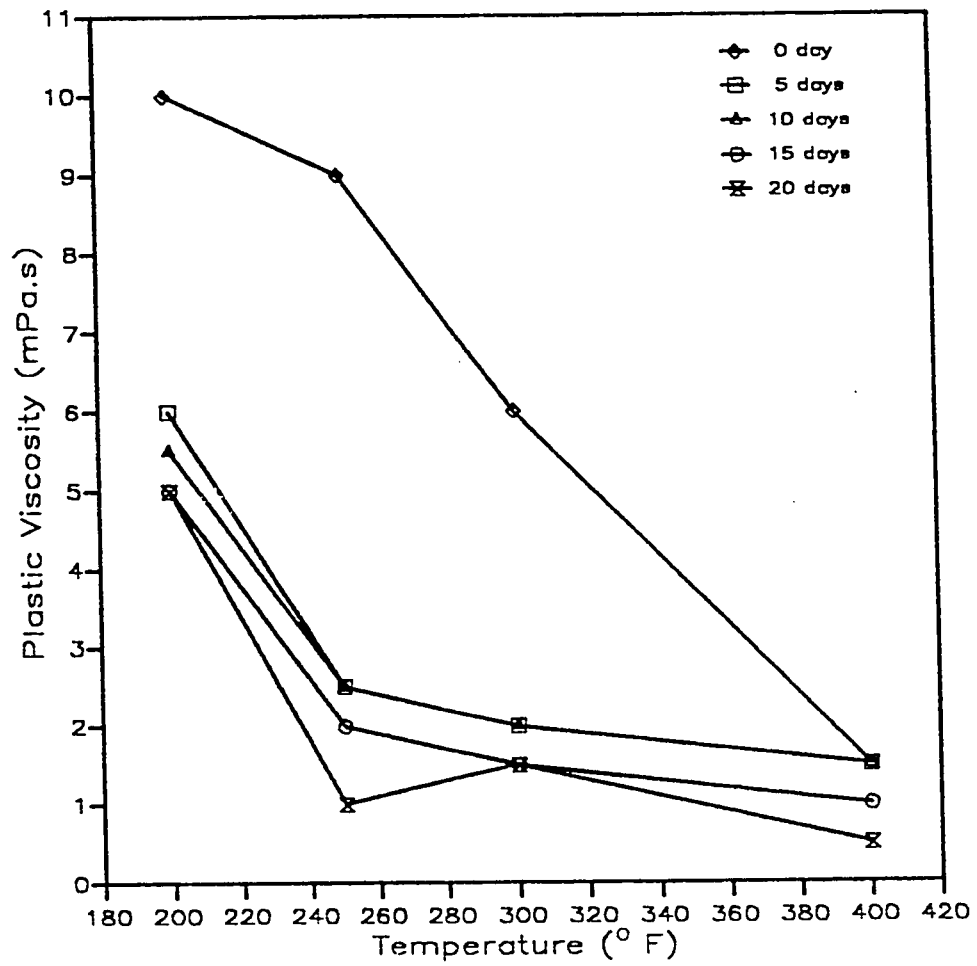


Figure 5.8: Effect of Temperature on Plastic Viscosity.

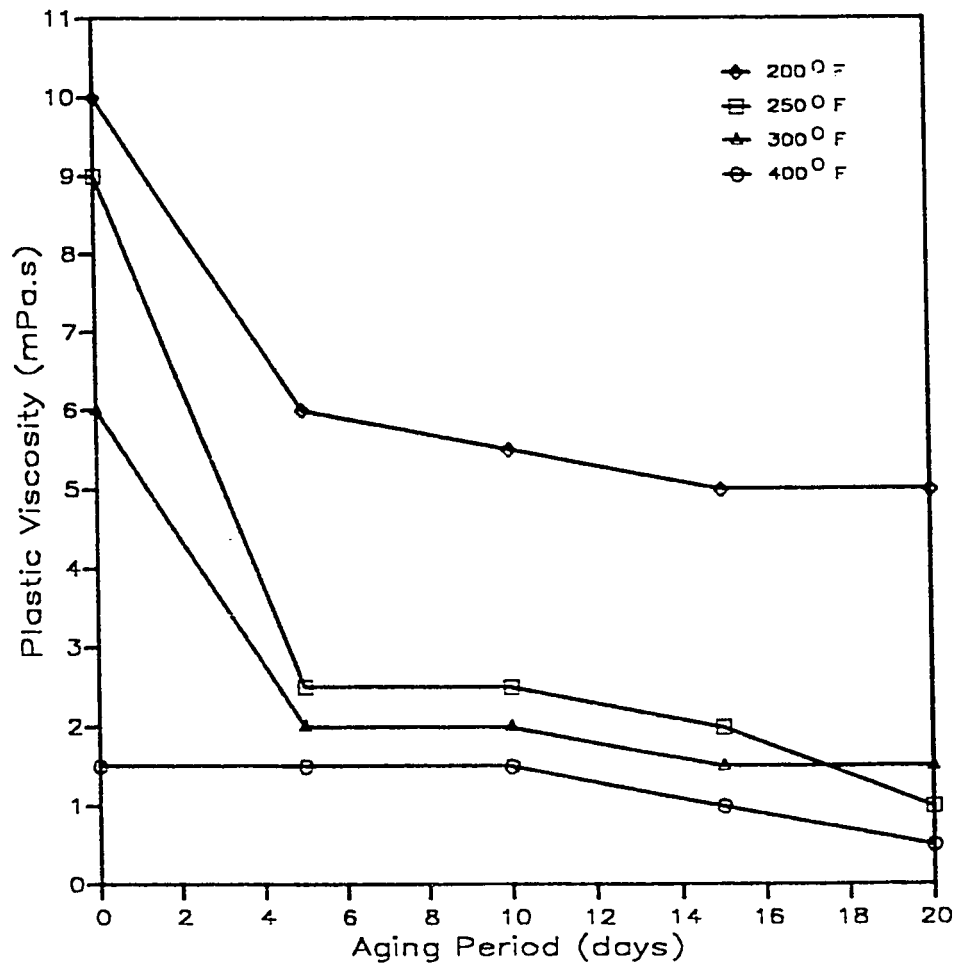


Figure 5.9: Effect of Aging on Plastic Viscosity.

was observed for the plastic viscosity for 20 days aging period. The increase in viscosity at this point could be attributed to the degradation of the polymer constituents of the mud and consequent dehydration of clay platelets. The capability of the polymer in flocculating clay platelets decreases; the platelets approach one another closely due to an increase in interparticle attractive forces, resulting in increased viscosity. Further increase in temperature causes the aggregation of the platelets and hence flocculation, resulting in low viscosities^[21]. Because of the increase in the degree of dispersion with aging under agitated conditions, and the tendency of the interparticle attractive forces to increase with temperature increase (deflocculation)^[20], it is observed that the effect of aging diminishes with increase in aging period and temperature.

The yield strength (Figs. 5.10 and 5.11) shows a trend similar to the plastic viscosity. It also decreases with increase in temperature and aging. Considering the fact that our mud is a fully deflocculated suspension (presence of thermathin), this is expected. The increase experienced at 300 °F is due to the increase in interparticle forces above the boiling point of water^[20].

The gel strength (Figs. 5.12 and 5.13) increases initially with increase in temperature due to the increased flocculation of the clay platelets. It decreases between 300 °F and 400 °F because of increased aggregation of platelets with temperature increase. This reduces the number of platelet units that can build up gel structure, and the surface area available for particle interaction. The behavior at day zero is due to the highly deflocculated state of the mud as opposed to what was explained above. The decrease of gel

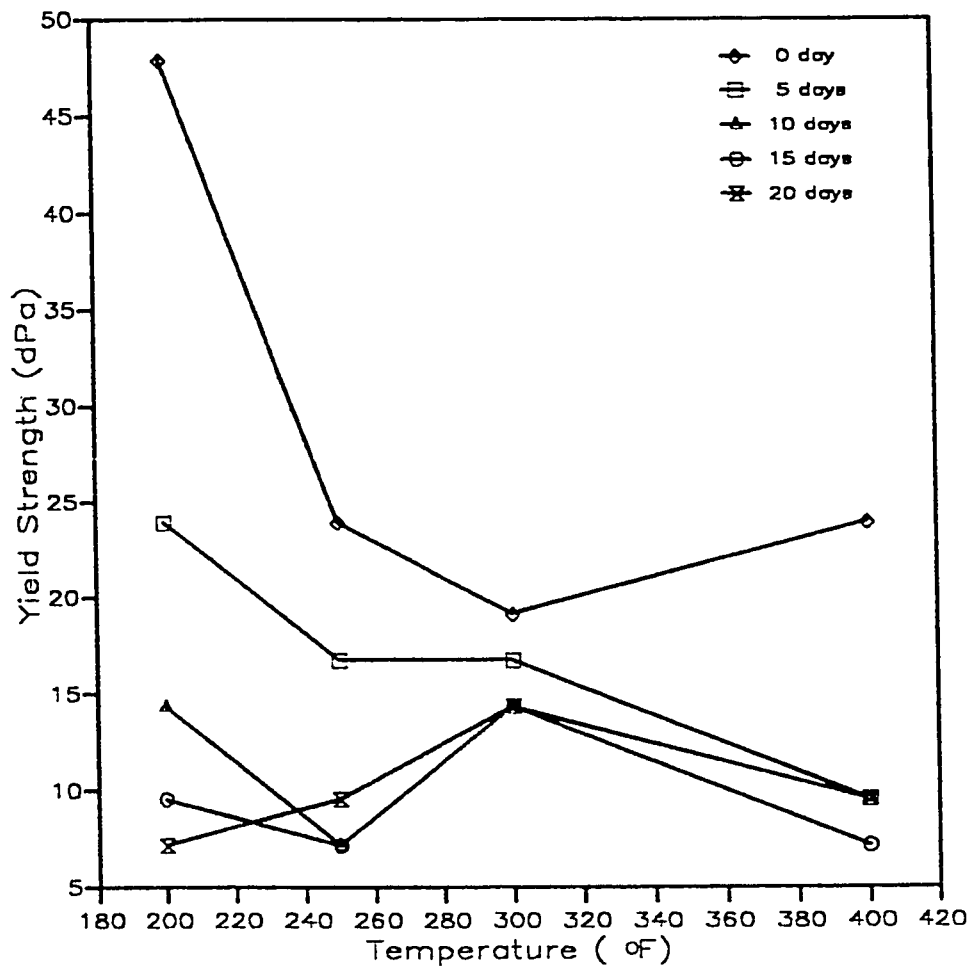


Figure 5.10: Effect of Temperature on Yield Strength.

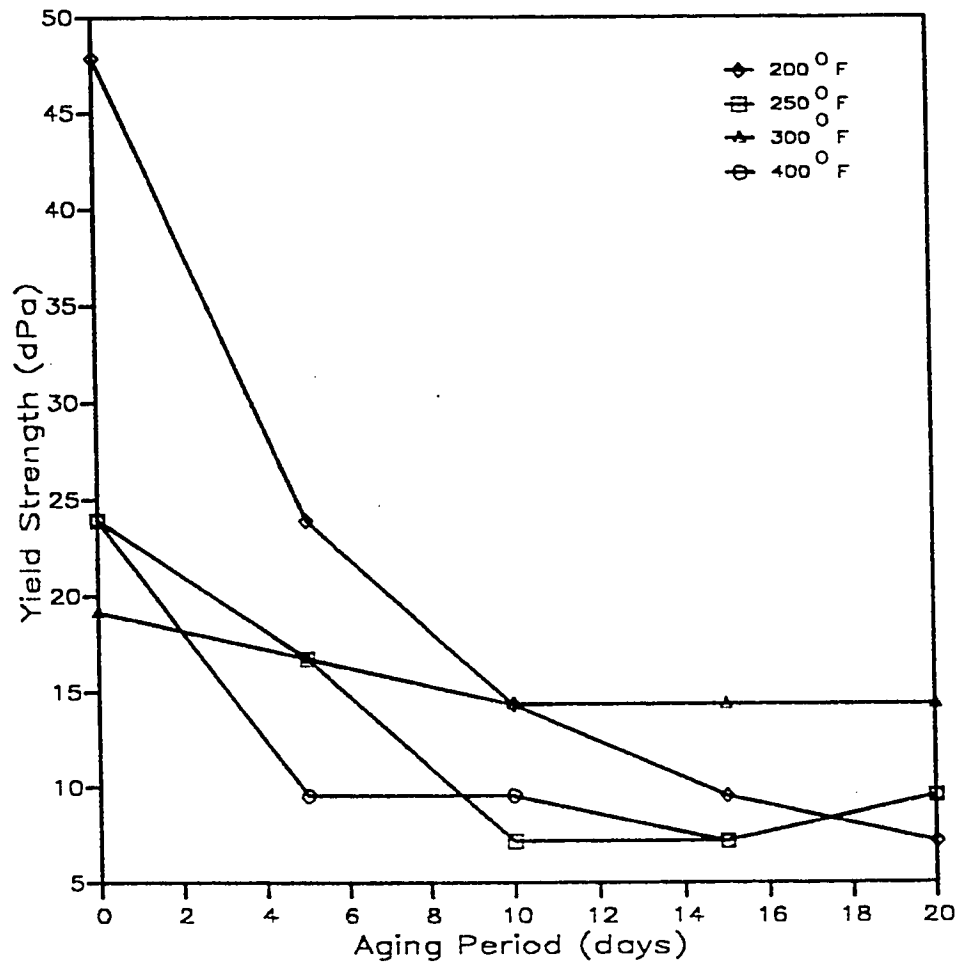


Figure 5.11: Effect of Aging on Yield Strength.

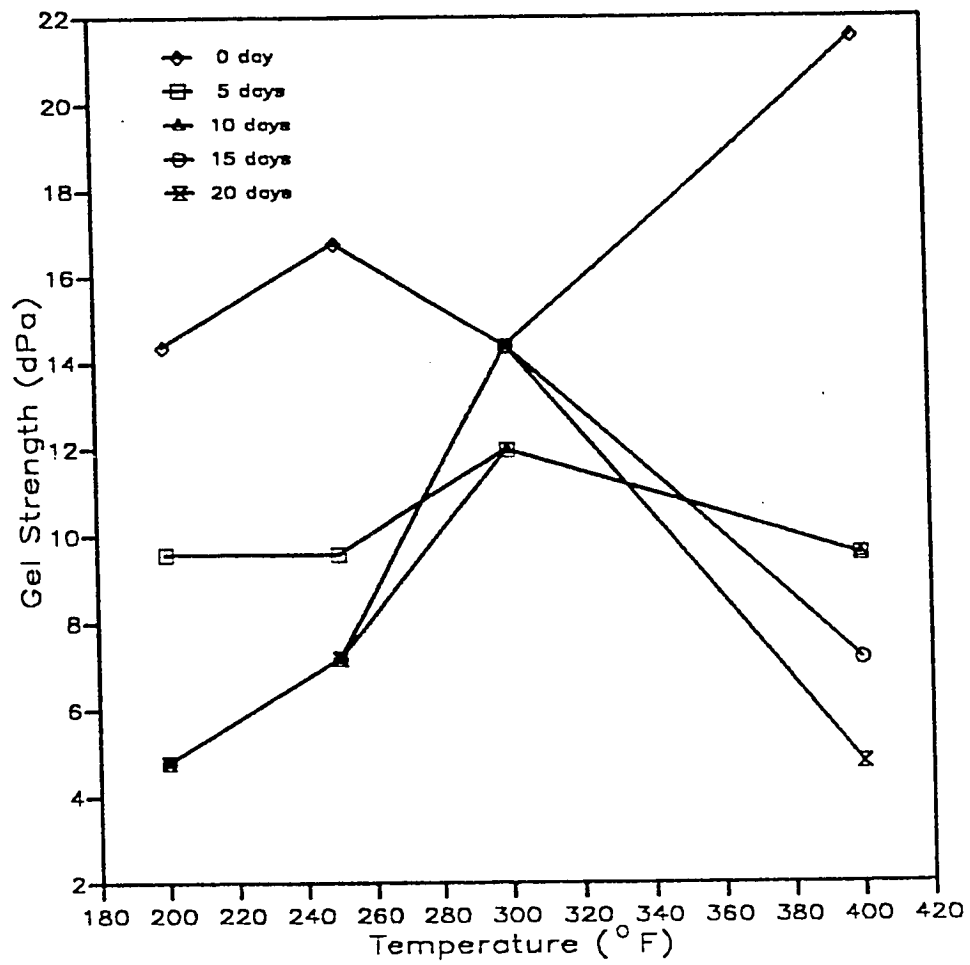


Figure 5.12: Effect of Temperature on Gel Strength.

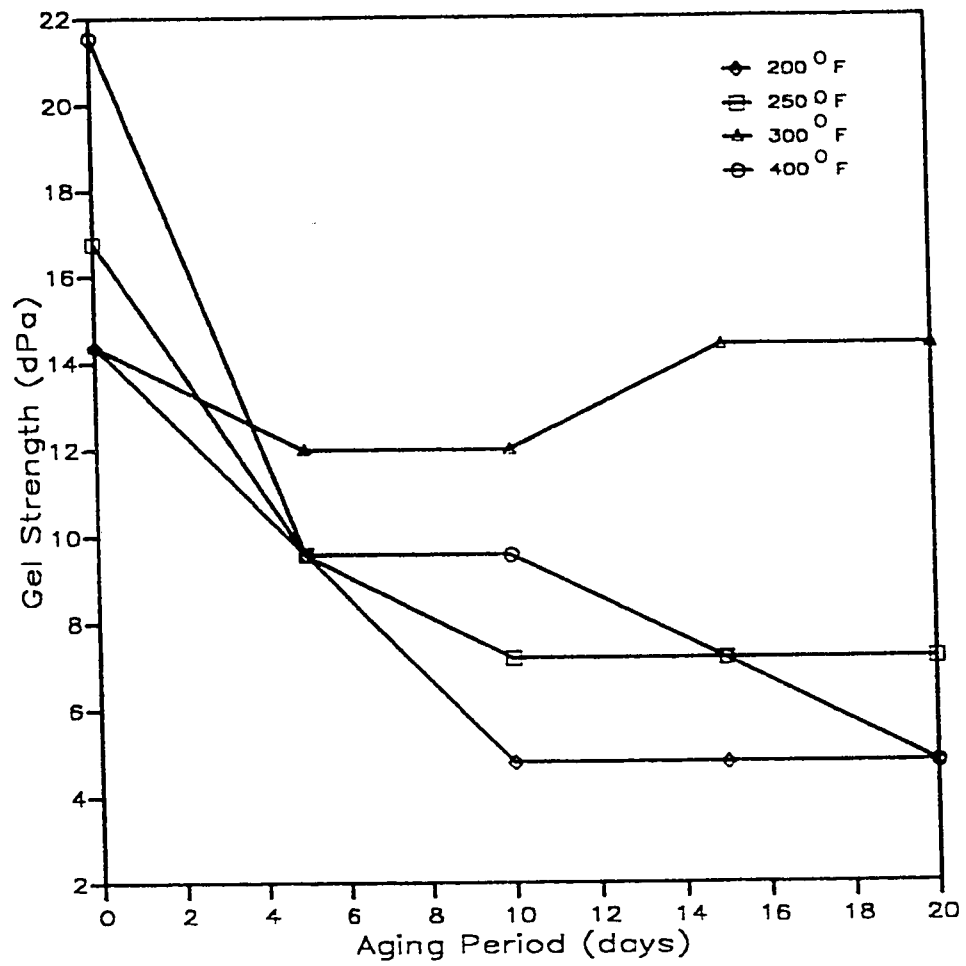


Figure 5.13: Effect of Aging on Gel Strength.

strength with aging is caused by the high degree of dispersion experienced with continuous agitation while aging.

Based on the observed behavior of the mud's rheological properties, we can say that the mud is stable up to 400 °F, the degradation experienced at 300 °F notwithstanding. The mud can therefore, be tested in the flow loop for temperatures up to 400 °F.

5.2 Effect of Temperature and Exposure Time on Mud Corrosivity

Visual inspection of steel coupons exposed to mud for different temperatures and time in the roller oven shows no sign of pitting. The surface of the coupons were smooth, indicating that uniform type of corrosion occurred. Weight loss were calculated by using equation (10).

Figures 5.14 and 5.15 show the effect of temperature and exposure time on weight loss of steel coupons exposed to drilling mud in the roller oven. Weight loss and thus corrosion rates of test coupons increase with increase in temperature. Weight loss increases with increase in exposure time, however, the increase is not very significant; but a shift is noticed at different temperatures. Weight loss increase with temperature increase is inversely related to the change in mud pH during the exposure period at test temperatures (Figs. 5.16 and 5.17). The oxygen trapped within the mud enhances the effect of temperature on corrosion. Corrosion rate is, however, expected to be reduced as oxide film is formed on the surface of coupon and

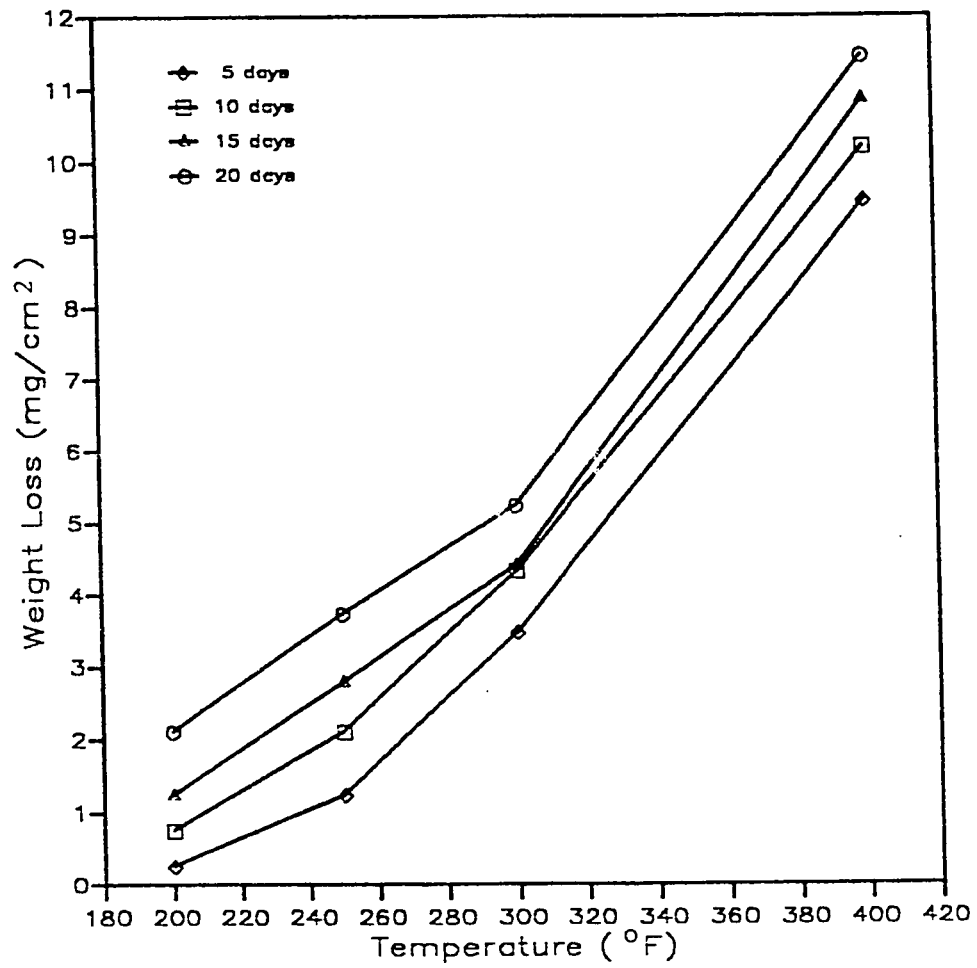


Figure 5.14: Effect of Temperature on Weight Loss Measured Using the Roller Oven at Mud pH of 10.9.

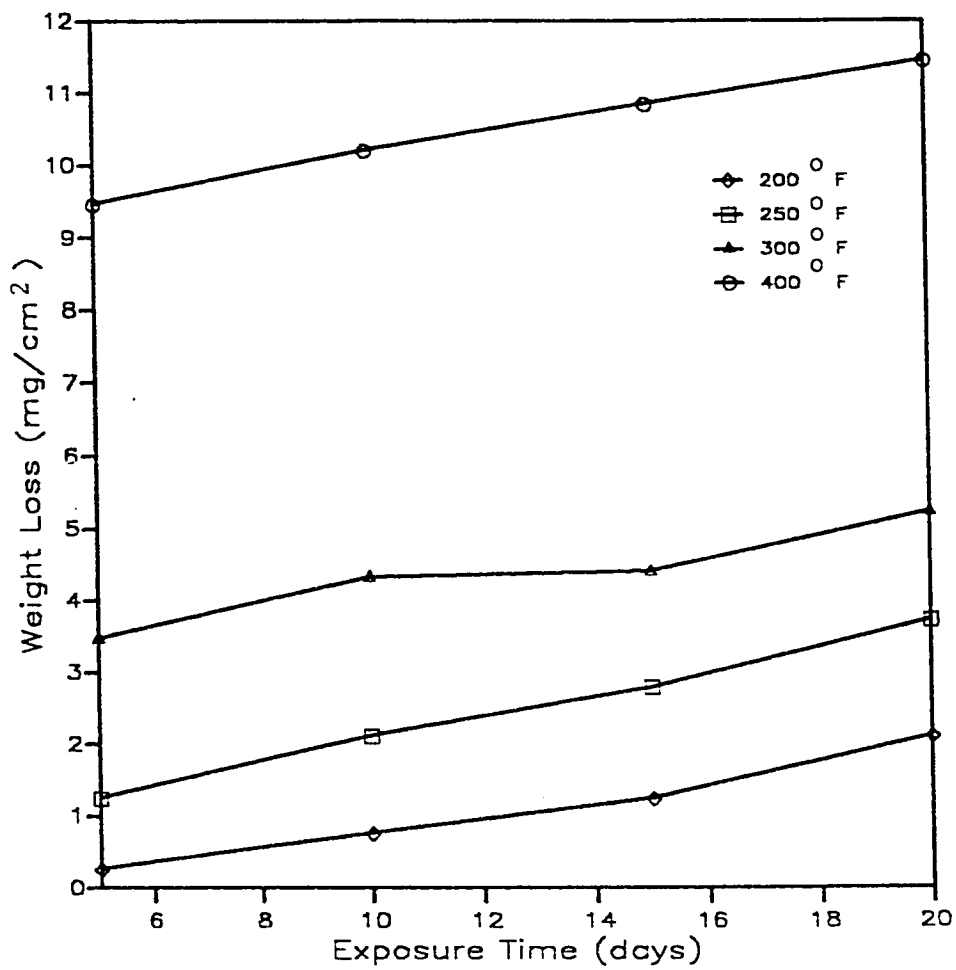


Figure 5.15: Effect of Exposure Time on Weight Loss Measured Using the Roller Oven at Mud pH of 10.9.

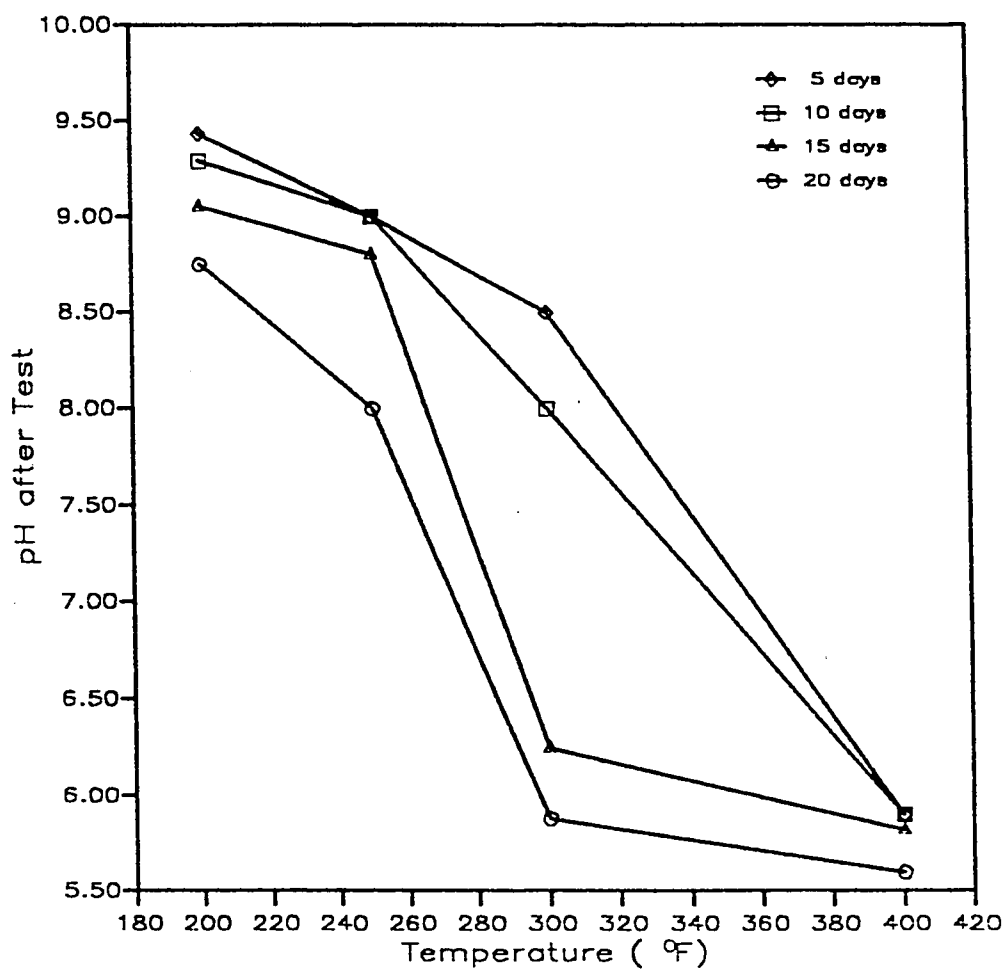


Figure 5.16: Effect of Temperature and Corrosion on Mud pH Under Roller Oven Conditions.

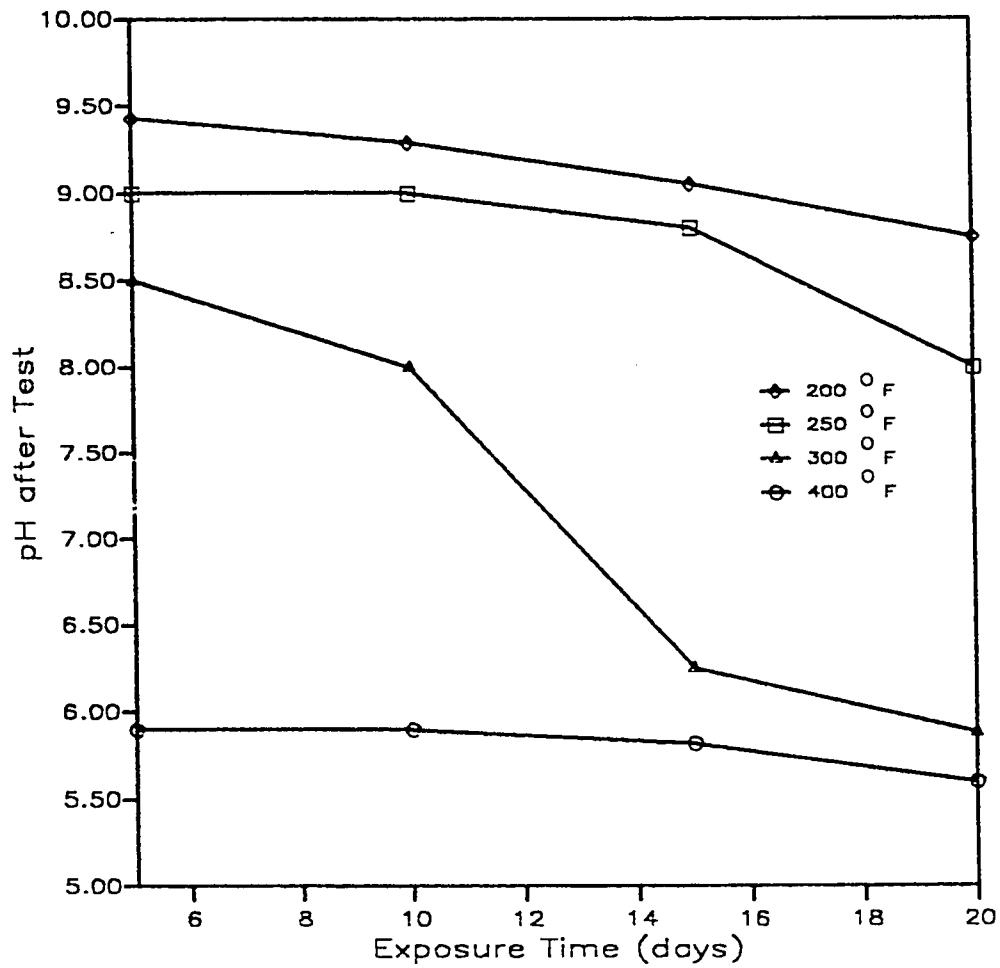


Figure 5.17: Effect of Exposure Time on Mud pH Under Roller Oven Conditions In the presence of Corroded Samples.

as the dissolved oxygen is consumed^[22,30]. The degradation of polymeric compounds contained in the mud at high temperature releases oxygen from the compounds and restores the level of oxygen in solution^[21]. The decrease of pH towards the acidic region due to the chemical reaction of the mud components plus corrosion reaction products as temperature increases overshadows this expectation. At any pH, hydrogen ions are available to react with and dissolve the oxide film. As the pH decreases, there is increased hydrogen evolution and greater accessibility of oxygen to the metal surface, thereby increasing weight loss with temperature increase.

The increase in weight loss with time can be attributed to the fact that more time is available for the reactions to occur, chemical and corrosion reaction products lead to decrease in pH with time and thus increase in weight loss. The corrosion rate equation (11) is not valid for my calculations from weight loss measurements because of the procedure followed in carrying out the roller oven tests. Electrochemical methods are thus used to monitor corrosion rate.

Results obtained from coupons exposed in the flow loop are shown in Figures 5.18 and 5.19. No particular trend of corrosion rate with temperature could be deduced from these results. One factor that is obvious, however, is that the flow rate which inadvertently varied during the experiment has an effect on the corrosion rate obtained. Due to this limitation in the system, we decided to use more advanced electrochemical techniques; along with the rotating cylinder electrode (RCE) which has well established hydrodynamic characteristics, to confirm this effect.

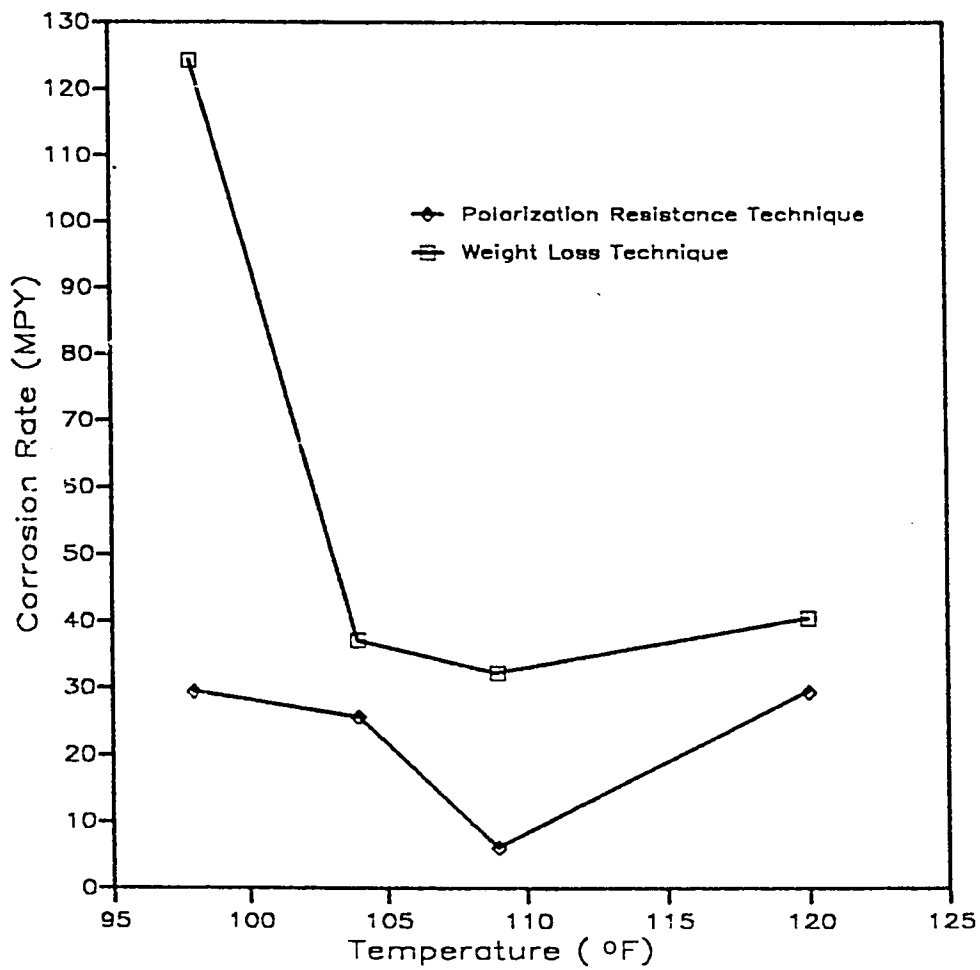


Figure 5.18: Effect of Temperature on Corrosion Rate Measured at the COLD Section of Flow Loop. Mud pH = 9.5

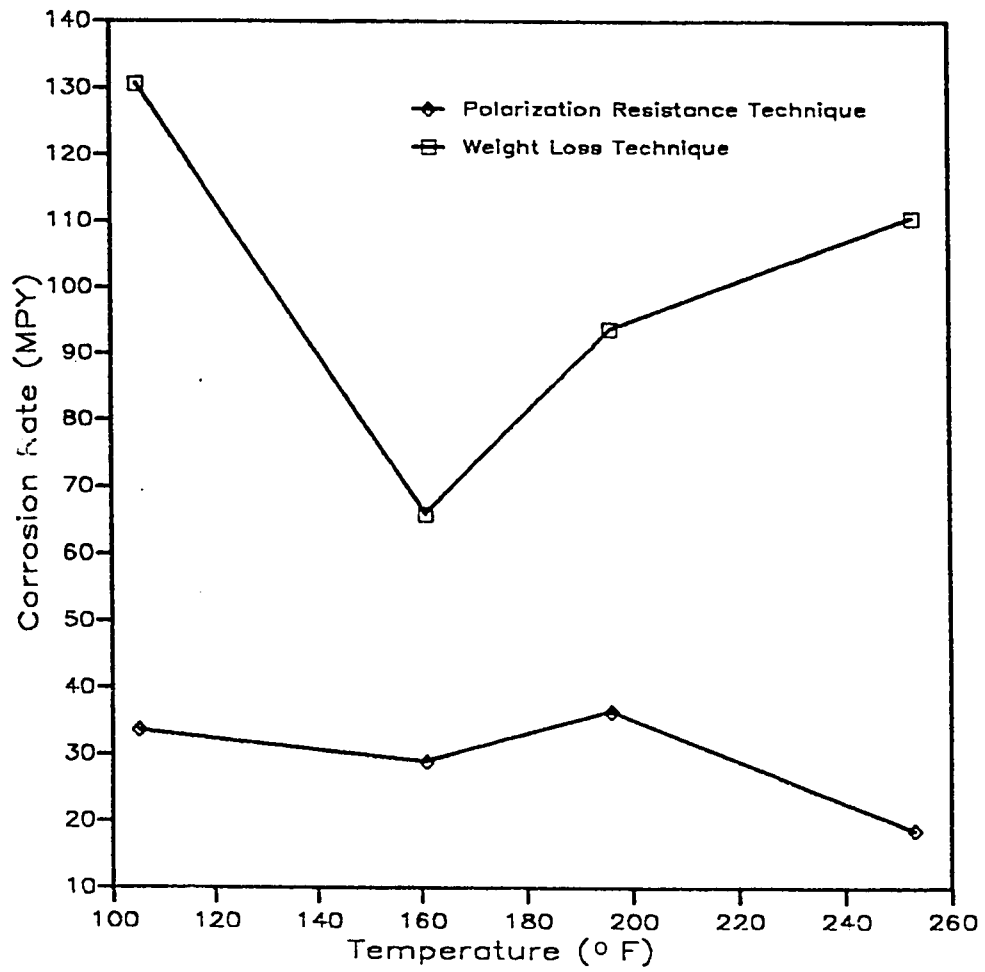


Figure 5.19: Effect of Temperature on Corrosion Rate Measured at the HOT Section of Flow Loop. Mud pH = 9.5

In the cold section of the loop, corrosion rate is highest at 98 °F for which flow rate is about 61 cm³/s and lowest at 109 °F which corresponds to flow rate of 22.4 cm³/s (Tables B8 and B12). Corrosion rate increases as the flow rate increases to 51 cm³/s at 120 °F. Similar behavior was observed at the hot section (Tables B9 and B13).

Increased flow rate reduces mass transfer resistance existing between the bulk of the liquid and the metal surface by eroding the protective film formed on the surface, thereby promoting the diffusion of corroding species in the mud to the metal surface thus enhancing further corrosion. These results also show that weight loss determined corrosion rates are higher in magnitude than instantaneous polarization resistance measurements. This could be due to the type of corrosion attack that occurred on the coupons, resulting in appreciable weight loss.

Careful observation of the experimental data in Appendix B shows that corrosion rates measured by weight loss of coupons exposed in the flow loop for only 8 hours is comparable in magnitude to those of coupons exposed for up to 10 days in the roller oven under similar conditions of temperature and pH. This observation indicates the importance of conducting tests on drilling fluid under flow conditions experienced in practice.

5.3 Effect of pH and Exposure Time on Mud Corrosivity

Figures 5.20 and 5.21 show the effect of pH and exposure time on the corrosiveness of drilling mud. Roller oven tests indicate an increase in weight loss with increased acidity. No significant effect of pH was noticed after 5 and 10 days of metal's exposure. From 15 days, however, weight loss and thus corrosion rate increases sharply with pH decrease. Weight loss is significantly affected by pH and exposure time.

Result of tests carried out in the flow loop (Figs. 5.22 and 5.23) show a decrease in corrosion rate from pH 9.5 to 6.0. A sudden increase of corrosion rate was observed from pH 6.0 to 4.1. Similar trend was obtained for both the cold and hot sections of the loop with weight loss and polarization resistance measurements. This behavior could be due to the protection of the metal surface at mild alkaline and neutral pH. Cathodic reaction (hydrogen formation) proceeds slowly in this region and controls the corrosion process. As observed for the effect of temperature in Figures 5.18 and 5.19, corrosion rate measured by weight loss are higher than polarization resistance measurements.

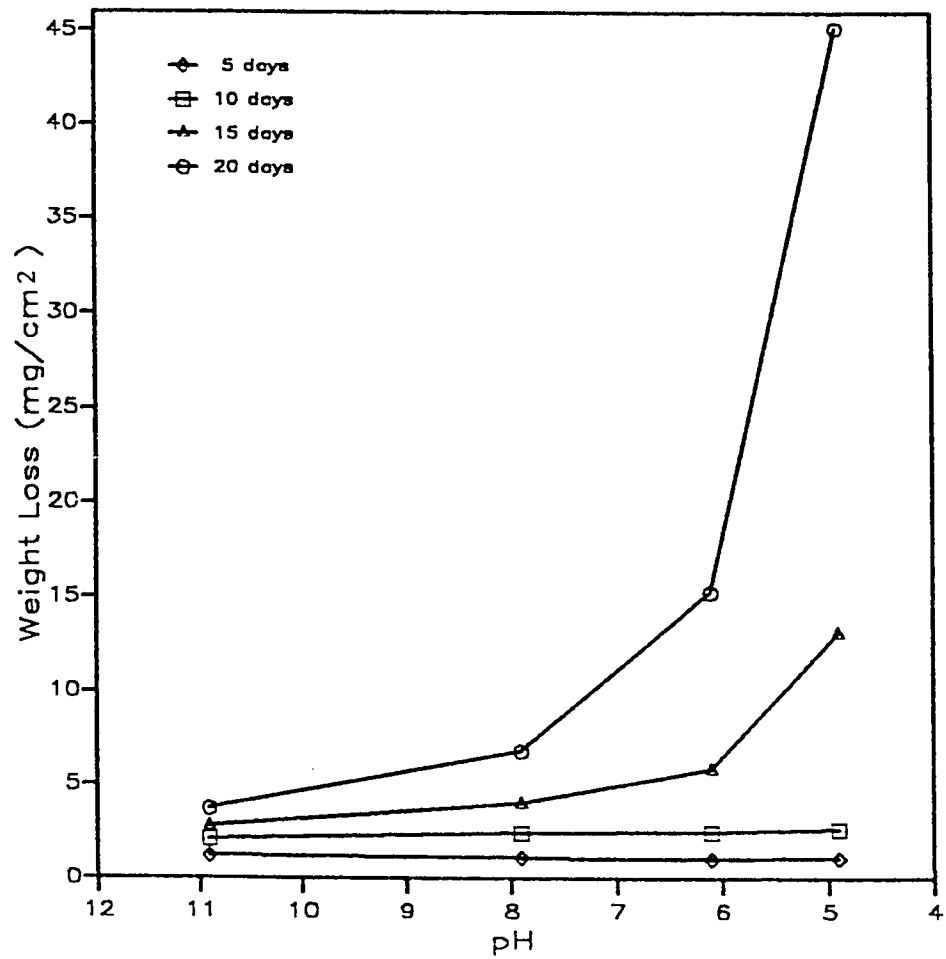


Figure 5.20: Effect of pH on Weight Loss of Coupons Exposed at 250 °F for 20 days in the Roller Oven.

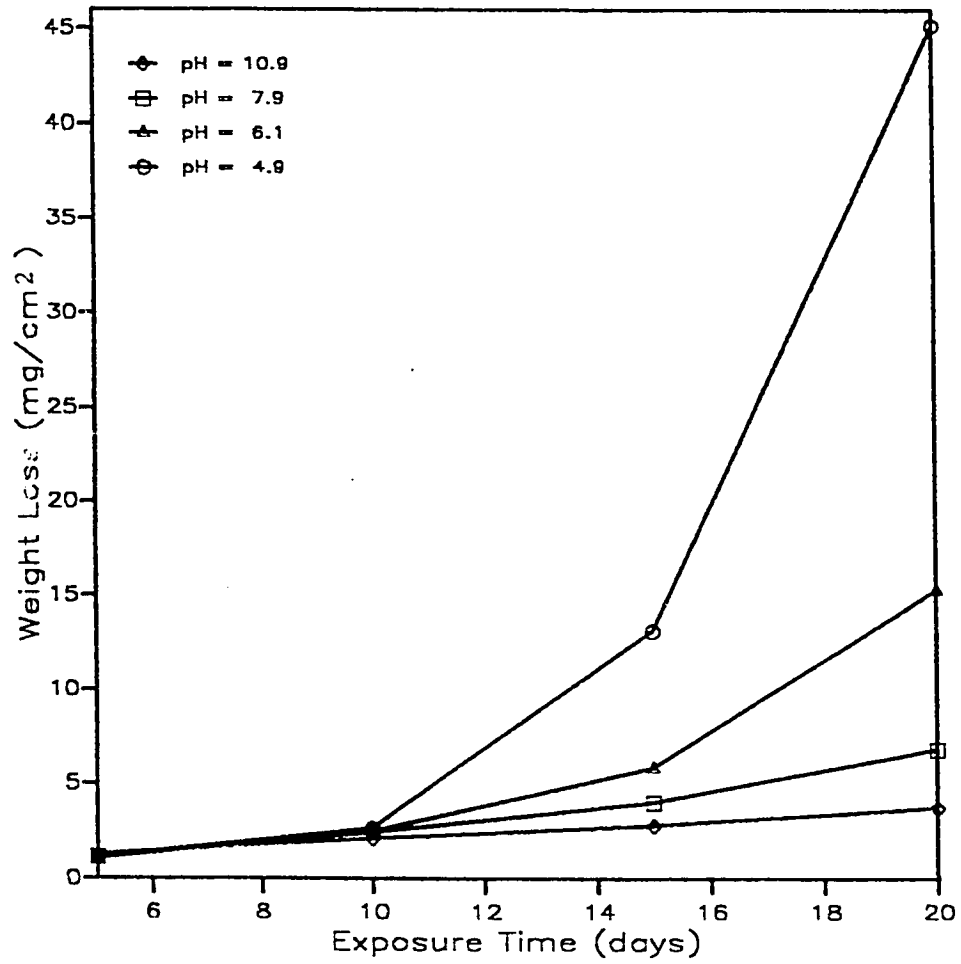


Figure 5.21: Effect of Exposure Time on Weight Loss of Coupons Exposed at 250 °F in the Roller Oven.

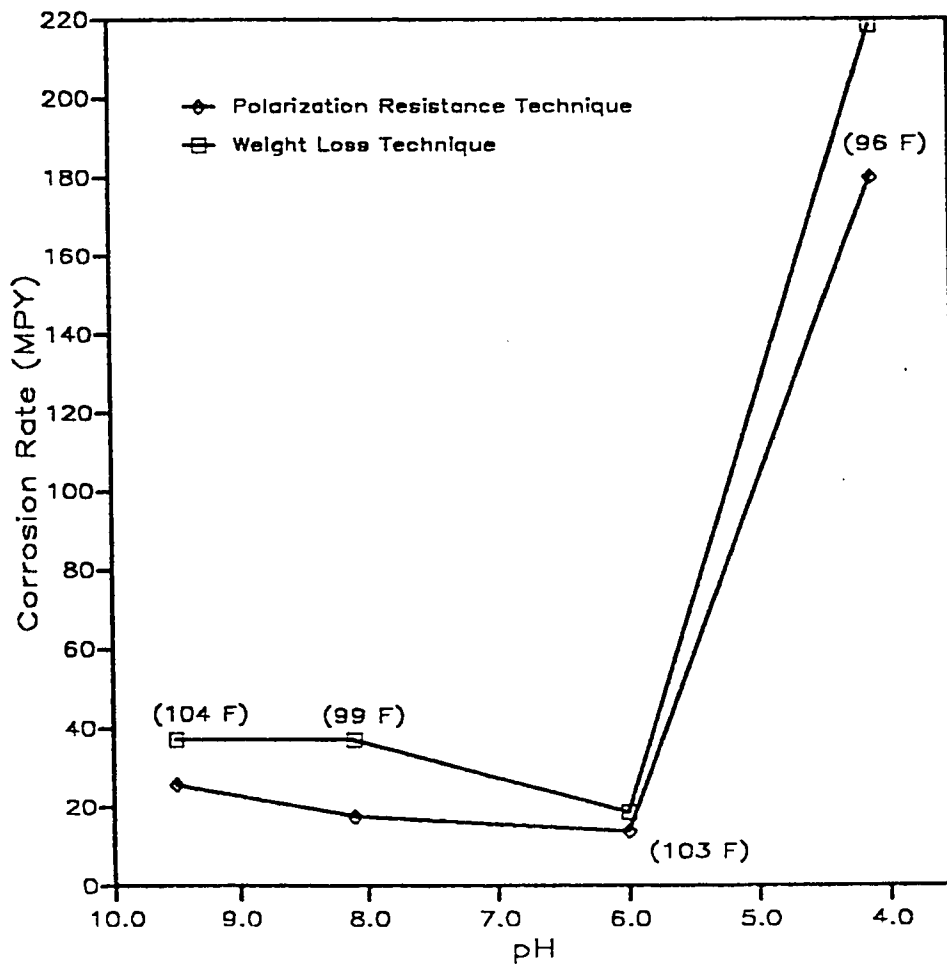


Figure 5.22: Effect of pH on Corrosion Rate Measured at the COLD Section of Flow Loop.

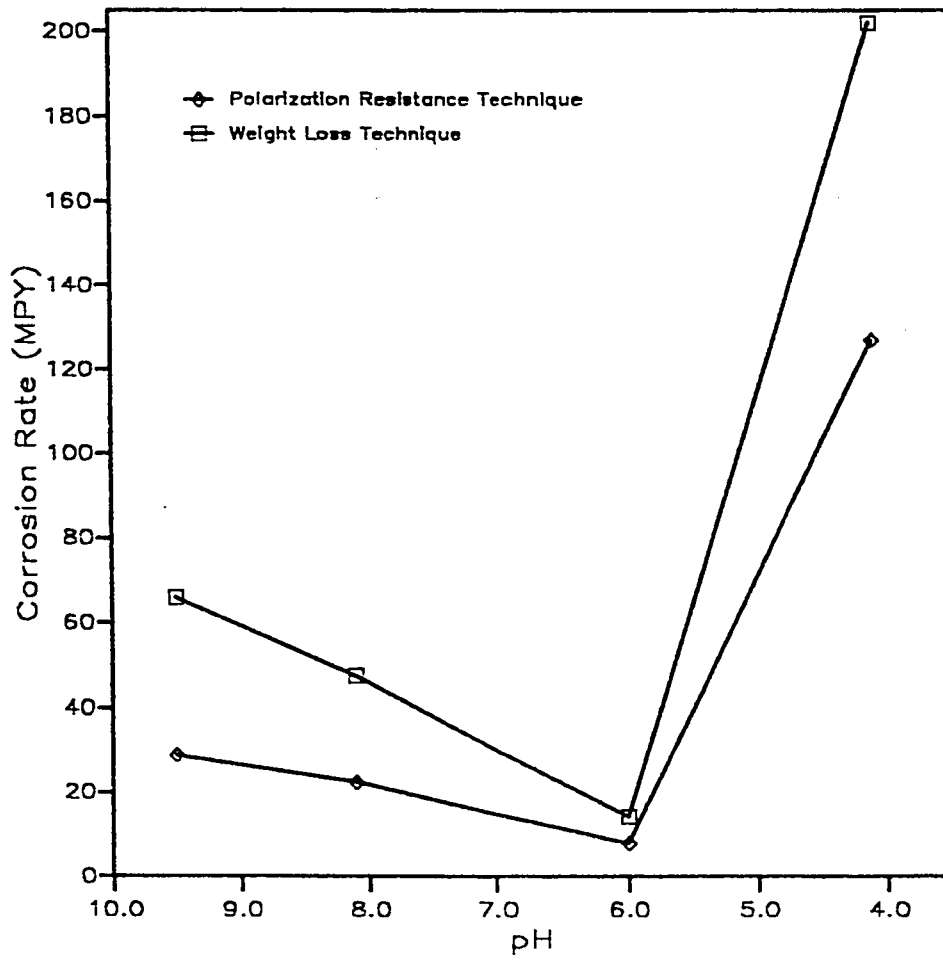


Figure 5.23: Effect of pH on Corrosion Rate Measured at the HOT Section of Flow Loop. Mud Temperature = 161 °F.

5.4 Potentiodynamic Polarization Results

Figures 5.24 and 5.25 show the results obtained from potentiodynamic Tafel plots under static and ambient conditions by applying a 5 mV/s potential sweep on the working electrode (steel sample), immersed in the drilling fluid. In Figure 5.24, a shift of corrosion potential, E_{CORR} to more active potentials with decrease in pH is observed. There is an anodic current shift of about 40 mA from pH 10.9 to 4.1, and increase in corrosion current density, I_{CORR} with decrease in pH. This indicates higher corrosion tendency of the steel sample with increase in mud's acidity. At pH 8.0, 6.0, and 5.1, there is evidence of passivation (formation of oxide layer) which protracts for more than 200 mV range. This behavior depicts that at this pH range, the corrosion product is stable and adherent and thus give some immunity to the steel from the corrosive mud medium.

Figure 5.25 shows a slight decrease in corrosion rate from 8.05 mpy at pH 10.9 to 7.41 mpy at pH 8.0. Thereafter, the mud becomes more corrosive; resulting in a sharp increase in rate from 7.92 mpy at pH 6.0 to 57.69 mpy at pH 4.1. This result is similar to what was observed in Figures 5.22 and 5.23 for the flow loop tests. It may, therefore, be desirable to consider operating the drilling fluid at pH range 8 to 6, considering the low corrosion rate and the inherent passivation offered within the system.

Several anodic potentiodynamic polarization curves were obtained at different speeds of the rotating cylinder electrode (RCE) for mud pH of 4.1 and 10.9. Two set of plots showing dependence of corrosion current density

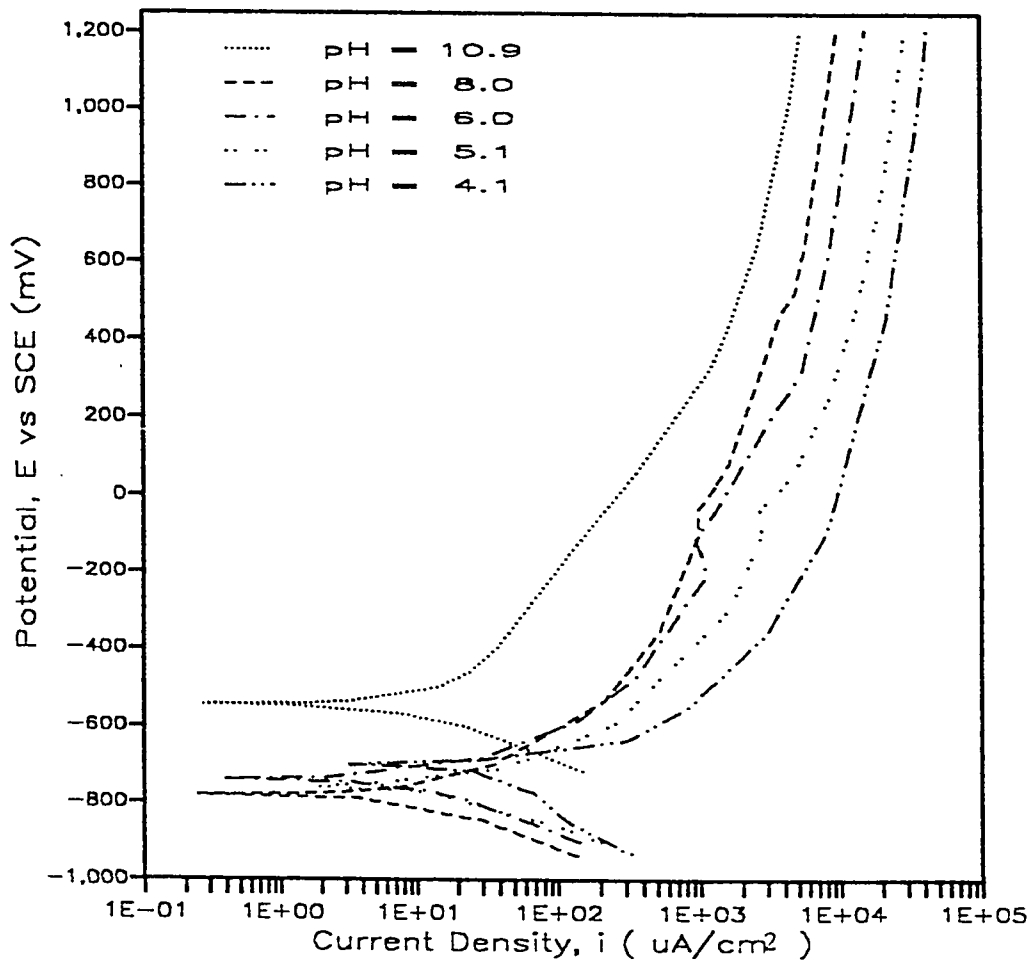


Figure 5.24: Potentiodynamic Polarization Diagram Obtained Under Static and Ambient Conditions.

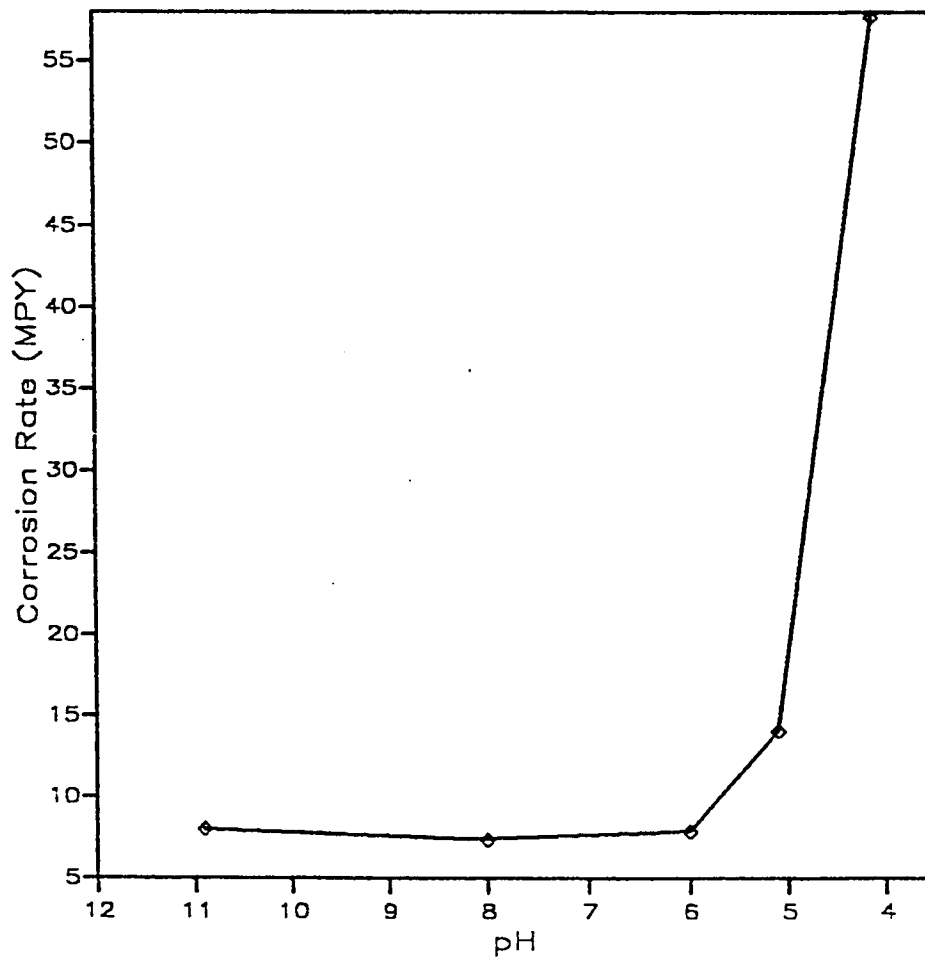


Figure 5.25: Effect of pH on Corrosion Rate Measured Under Static and Ambient Conditions by Potentiodynamic Polarization.

on rate of agitation are shown in Figures 5.26 and 5.27. These curves show a tendency towards a limiting current density, i_{lim} , a region of equilibrium corrosion reaction; characterized by constant current density with potential increase. This region is not very well pronounced in these figures. In addition, at rotation speeds of the RCE greater than 500 rpm, the experimental determination of i_{lim} becomes more difficult because the current plateaus are even less obvious and not very well defined. This observed behavior is due to excessive rise of current with polarization at these speeds because of the change in energy required to detach mud gels that formed on the working electrode at lower rpm's.

A plot of limiting current density obtained at a chosen equilibrium potential of 500 mV versus square root of angular velocity shown in Figure 5.28 is non-linear. This confirms the undefined and capricious nature of the mud formulation in terms of electrode kinetics. It shows that diffusion activities are far from the limiting range. Thus, increased agitation or high flow rate experienced in practice will tremendously affect the mud corrosivity^[27].

5.5 AC Impedance Results

Figure 5.29 shows AC impedance spectra at different rpm's for mud with pH of 10.9. The corresponding spectra at pH 4.1 is shown in Figure 5.30. Figure 5.29 illustrates the effect of agitation on impedance spectra. A big shift of solution ohmic resistance (R_{SO}) is observed. This suggests that

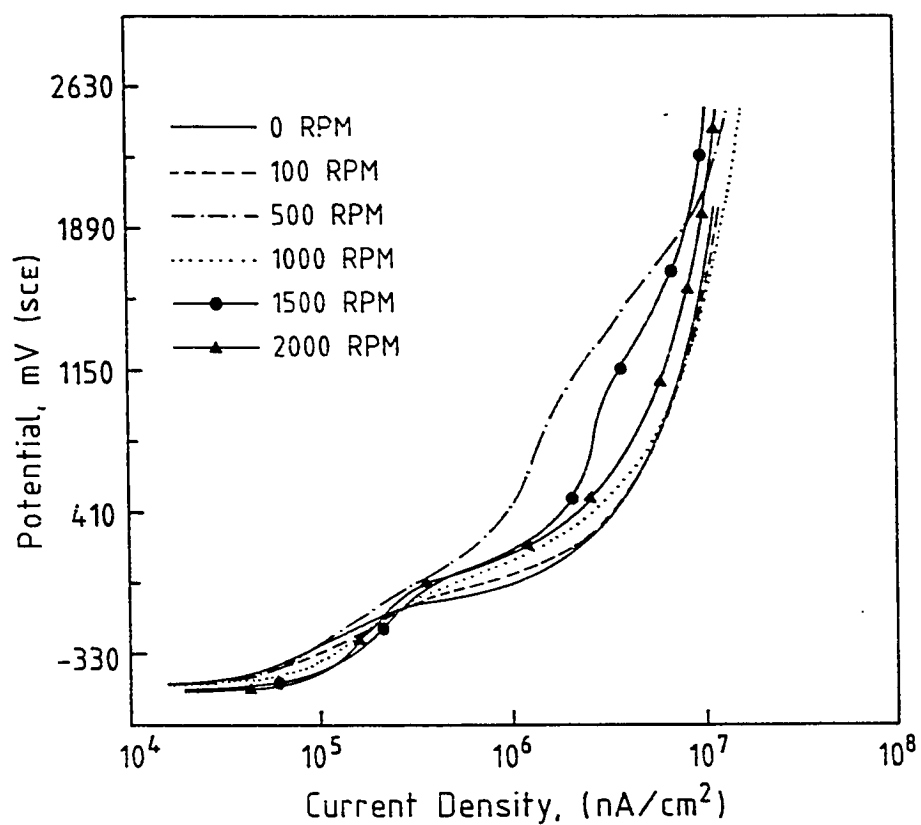


Figure 5.26: Potentiodynamic Curves in the Anodic Region at Different Rotation Speed of the RCE to Show the Effect of Diffusion. Mud pH = 10.9.

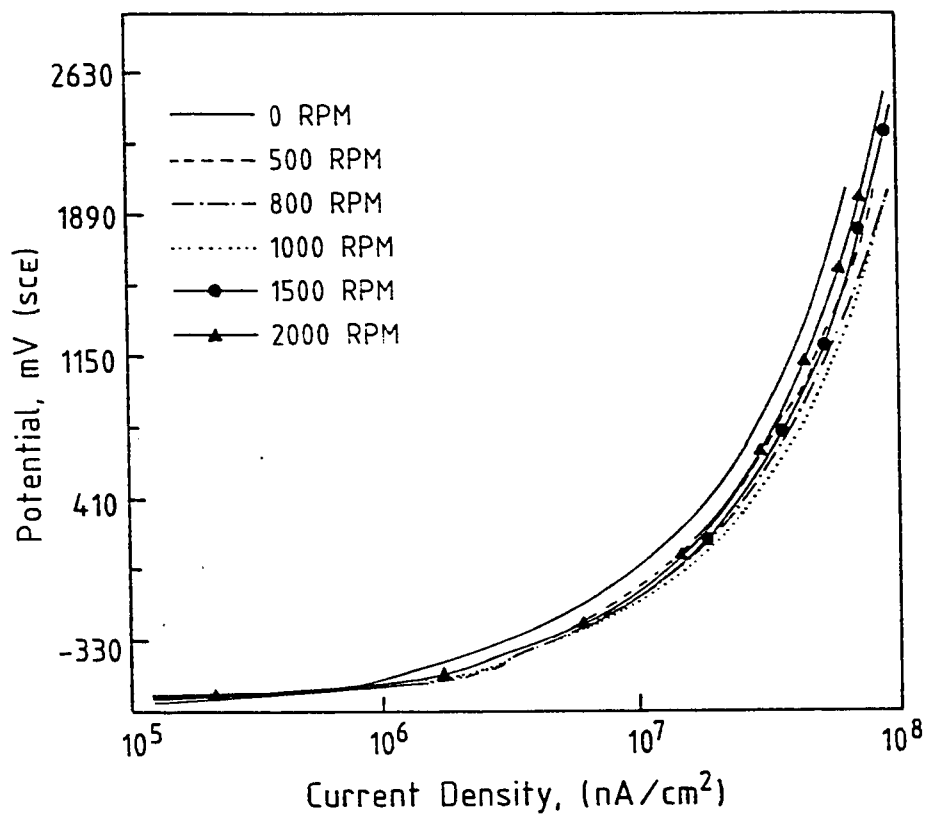


Figure 5.27: Potentiodynamic Curves in the Anodic Region at Different Rotation Speed of the RCE to Show the Effect of Diffusion. Mud pH = 4.1.

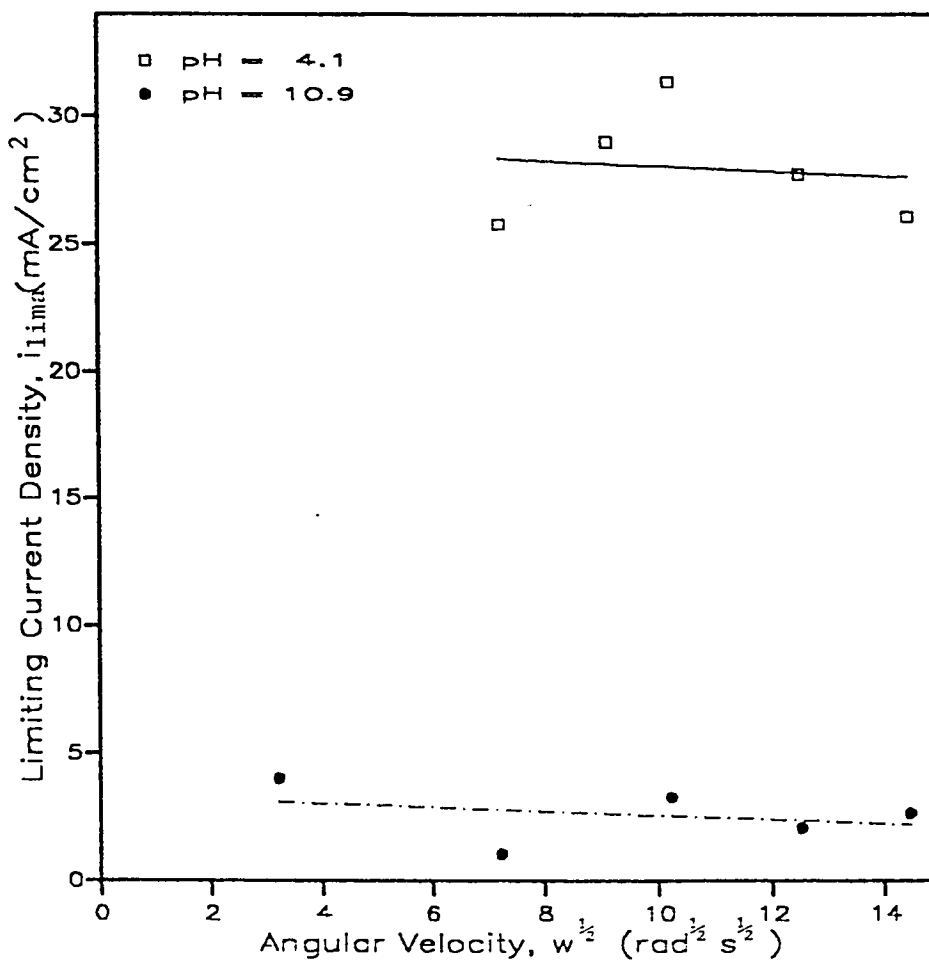
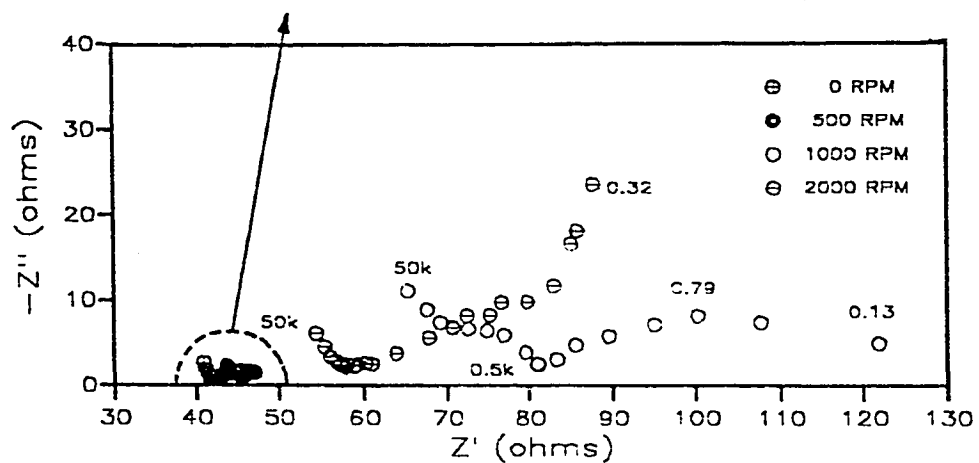
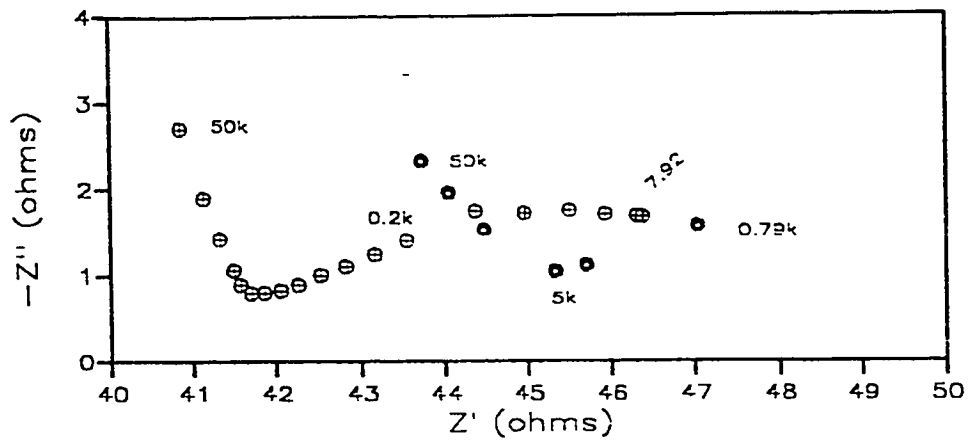


Figure 5.28: Anodic Limiting Current Density vs Square Root of Angular Velocity for Mud pH 4.1 and 10.9.



(numbers are frequencies in Hz)

Figure 5.29: Impedance Spectra of Mild Steel (1018) in Water-Based Drilling Fluid at 500 mV (vs SCE) and pH 10.9

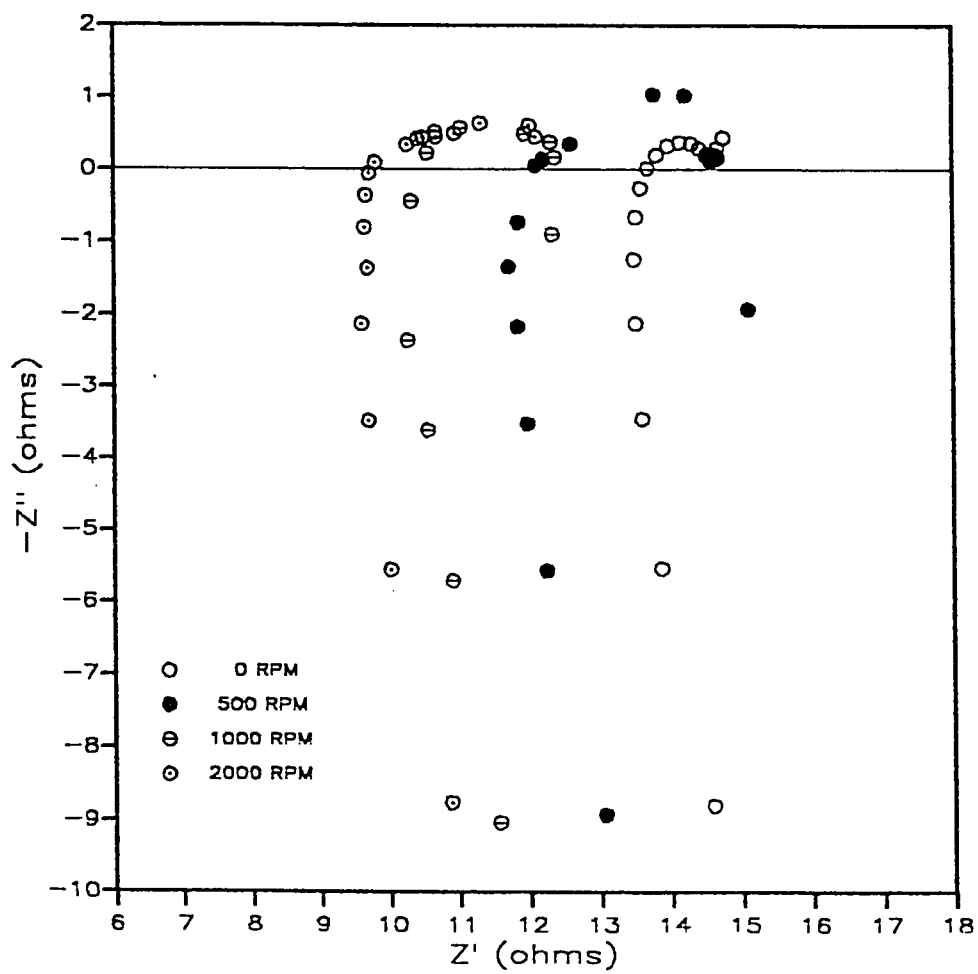


Figure 5.30: Impedance Spectra of Mild Steel (1018) in Water-Base Drilling Fluid at Different RPM and pH 4.1

agitation makes the mud more conductive and also aid the diffusion of electroactive species to the metal's surface. Figure 5.30 presents a decrease of R_{SO} with increased agitation, also an indication of increased mud conductivity. At 2000 rpm, two pseudo-capacitive loops are observed for mud pH 10.9 and 4.1 (Figs. 5.29 and 5.34). This again demonstrates that diffusion controls the corrosion process, although there are no clear evidence of low frequency end distortion of the semi-circle describing the charge transfer (Faradaic) process and diffusion impedance (the Warburg impedance). Charge transfer resistance, R_{ct} which is inversely proportional to the corrosion current and hence the corrosion rate, was found to be smaller in magnitude for mud pH 4.1 than for pH 10.9. This translates to high corrosion rate at pH 4.1 and low corrosion rate at pH 10.9. The magnitude of R_{ct} at 0 rpm is 1Ω for mud pH 4.1 compared to about 8Ω for pH 10.9.

The decrease of R_{SO} with increased RCE rotation speed shown in Figure 5.30 is an indication that the solution is non-homogenous. The solution however becomes more conductive as homogeneity improves with agitation. This again is a strong indication of agitation/flow rate dependency of the corrosive activity of the mud. Corrosion products are continually removed as the mud is agitated, resulting in renewal of metal surface and increased corrosion.

Impedance spectrum obtained under static condition at pH 4.1 (Fig. 5.31) shows a classical case of charge transfer process characterized by high frequency capacitive loop (semi-circle) and Warburg diffusion line^[24,26,31].

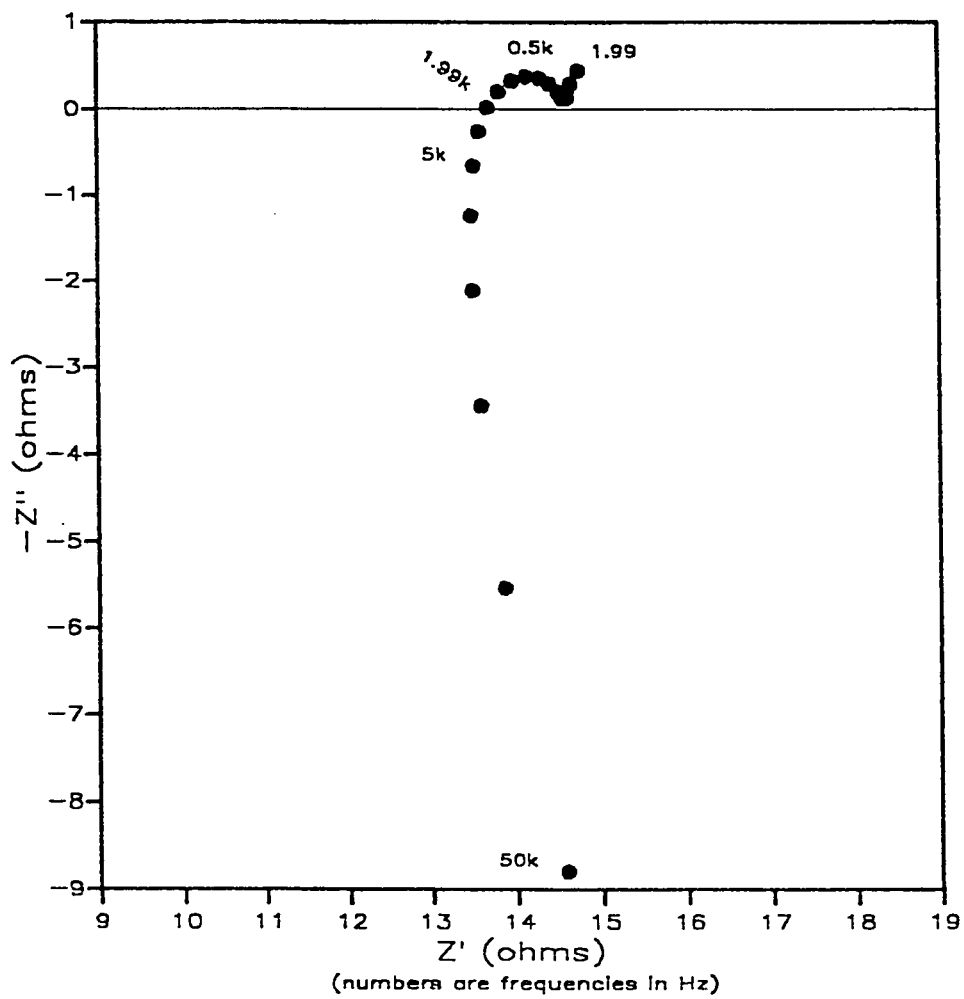


Figure 5.31: Impedance Spectrum of Mild Steel (1018) in Water-Base Drilling Fluid at Static Condition and pH 4.1

This is a combination of Faradaic process being limited by diffusion. Figures 5.32 and 5.33 at 500 and 1000 rpm respectively shows mostly one capacitive loop which likely corresponds to charge transfer process. The high frequency (50 kHz - 5 kHz) inductance effect characteristic of impedance spectra for mud pH of 4.1 could be due to extraneous ionic activities and/or occurrence of rapid and fast non-Faradaic processes.

Due to the renewal of metal surface at high flow rate and agitation, there is a possibility of the occurrence of erosion-corrosion.

5.6 Analysis of Scanning Electron Micrographs

Figures 5.35 through 5.41 show electron photomicrographs of mild steel (1018) sample exposed to drilling mud in the flow loop under various conditions. These micrographs indicate the extent of corrosion attack on the metal. Figure 5.35 shows an unexposed sample, which depicts the grain boundaries typical of carbon steel. The corrosion attack occurs generally at the grain boundaries. Figures 5.36 to 5.38 for mud pH 9.5 at different temperatures show deposition of non-conductive corrosion products on the surface of the metal.

The observed grain boundary attack is more pronounced at low pH. Figures 5.39 to 5.41 are samples exposed at pH 8, 6, and 4.1. They show severe attack at the grain boundaries. Figures 5.39 and 5.40 at pH 8 and 6 show that the attack is concentrated uniformly at the grain boundaries. This

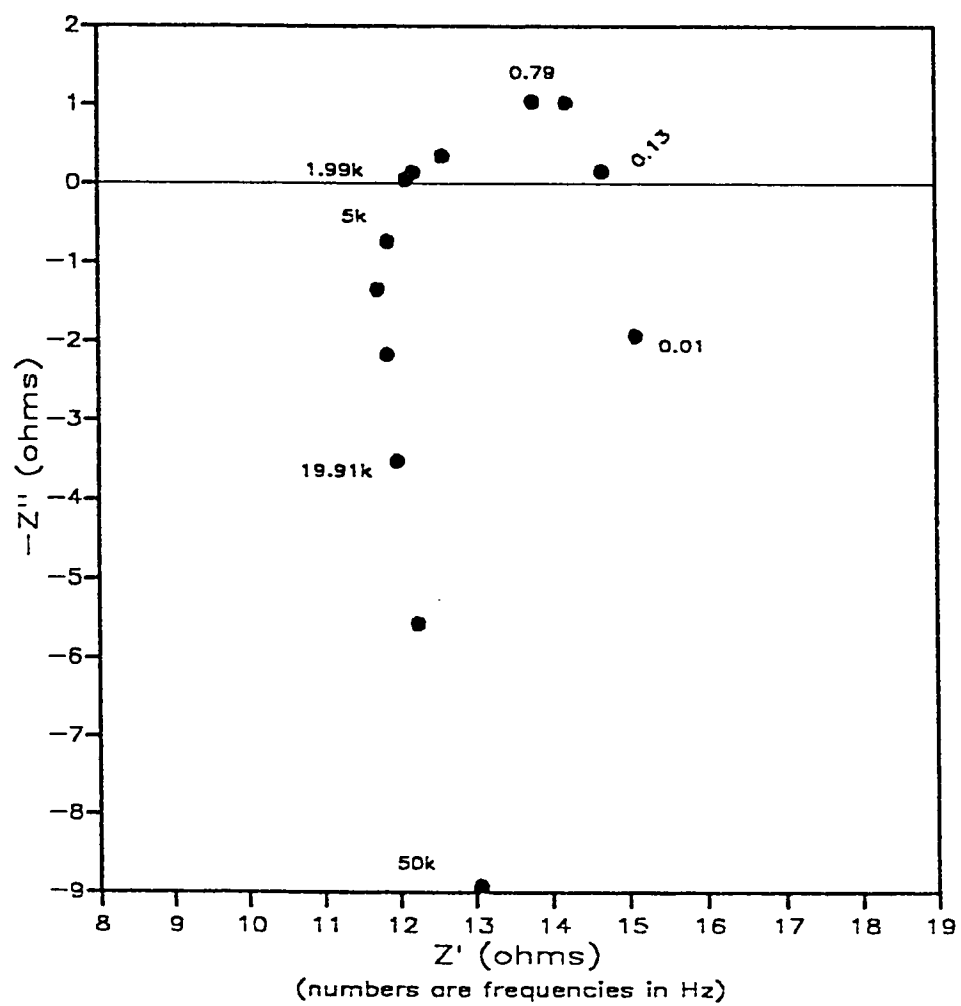


Figure 5.32: Impedance Spectrum of Mild Steel (1018) in Water-Base Drilling Fluid at 500 RPM and pH 4.1

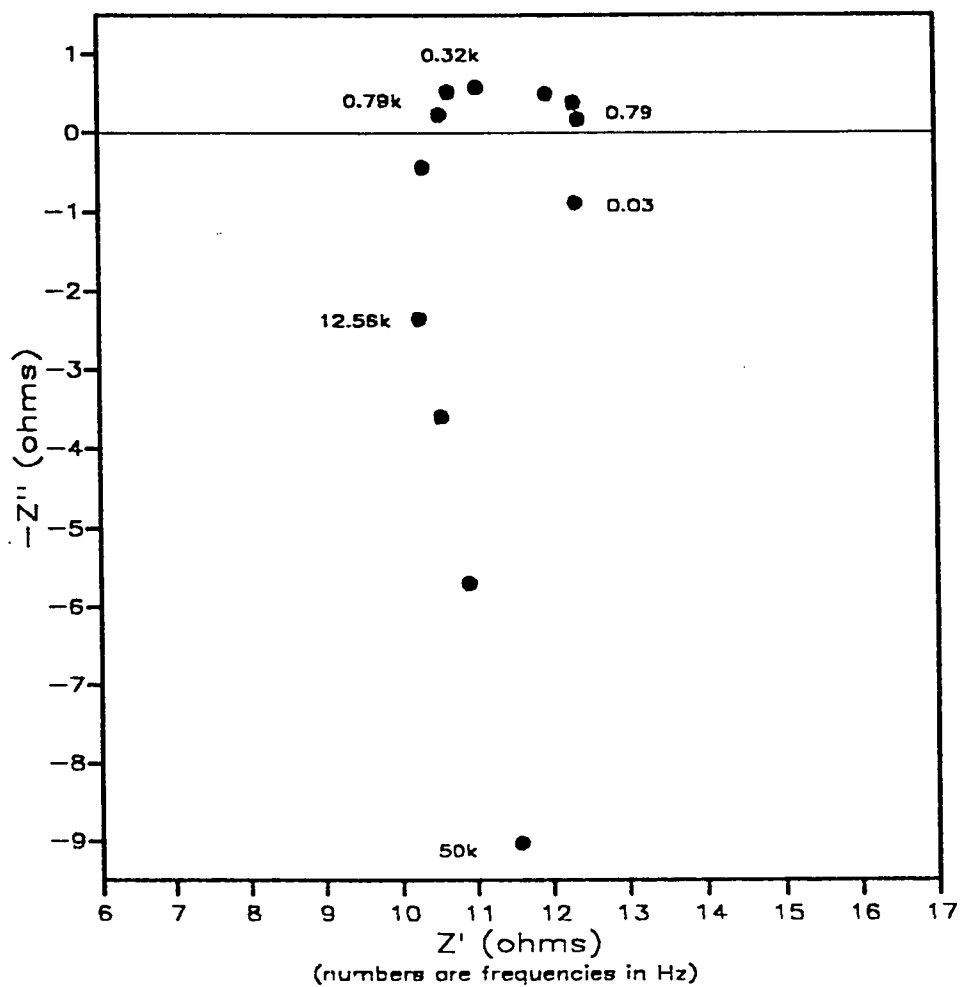


Figure 5.33: Impedance Spectrum of Mild Steel (1018) in Water-Base Drilling Fluid at 1000 RPM and pH 4.1

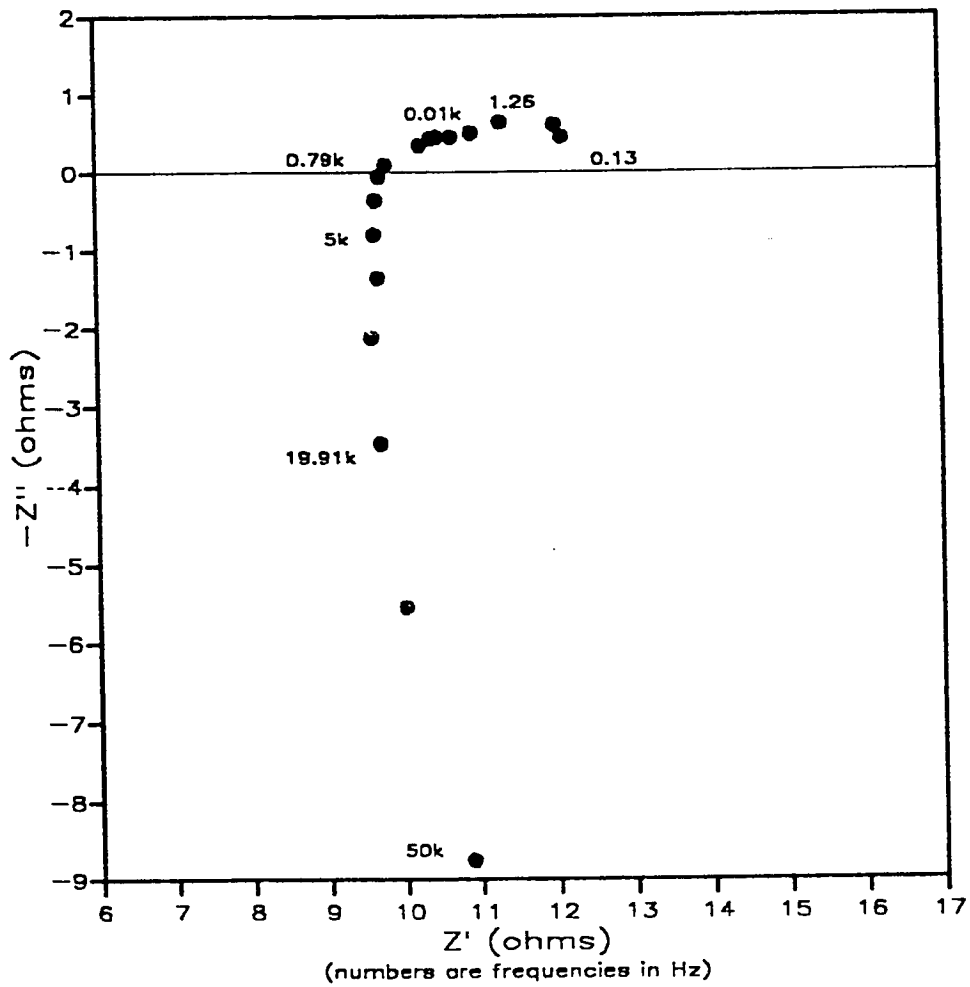


Figure 5.34: Impedance Spectrum of Mild Steel (1018) in Water-Base Drilling Fluid at 2000 RPM and pH 4.1

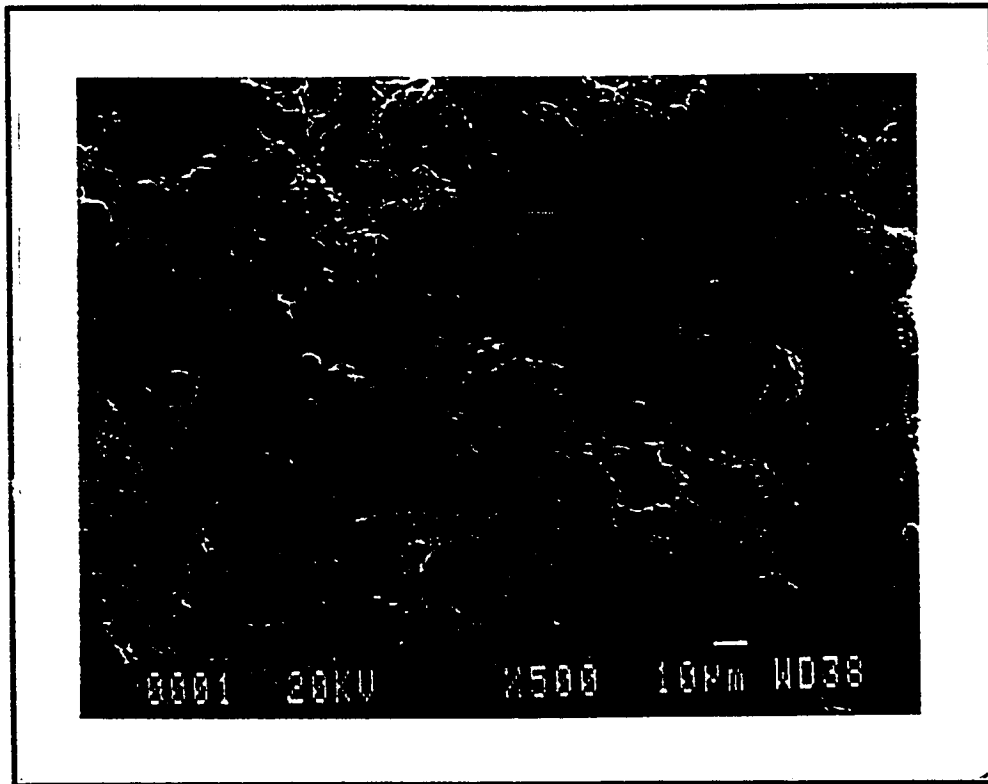


Figure 5.35: Scanning Electron Micrograph of an Unexposed Surface of Mild Steel (1018) Sample.

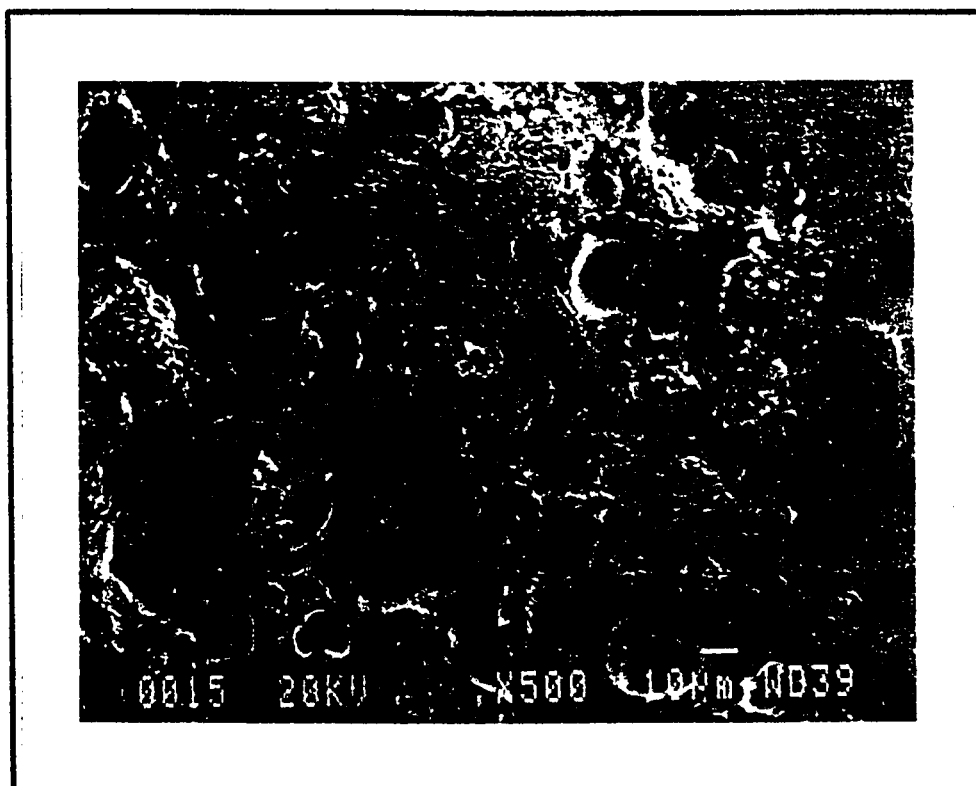


Figure 5.36: Scanning Electron Micrograph of a Corroded Surface of Mild Steel (1018) after Exposure to Drilling Mud in the Flow Loop at pH 9.5 and 98 °F for 8 hours.

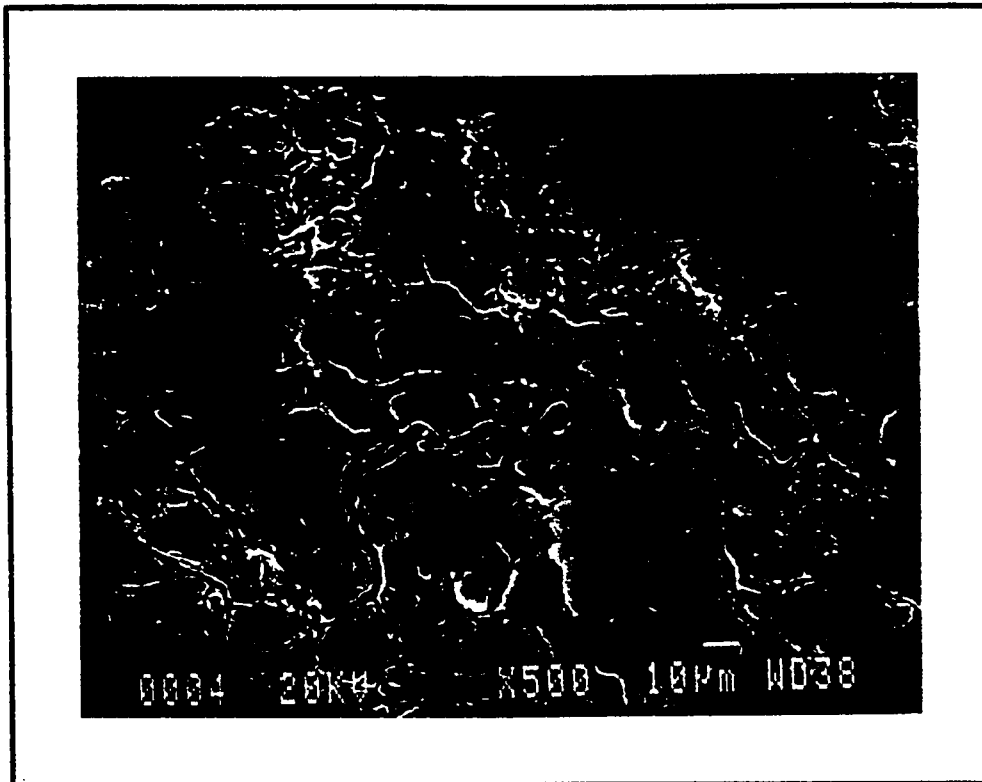


Figure 5.37: Scanning Electron Micrograph of a Corroded Surface of Mild Steel (1018) after Exposure to Drilling Mud in the Flow Loop at pH 9.5 and 161 °F for 8 hours.

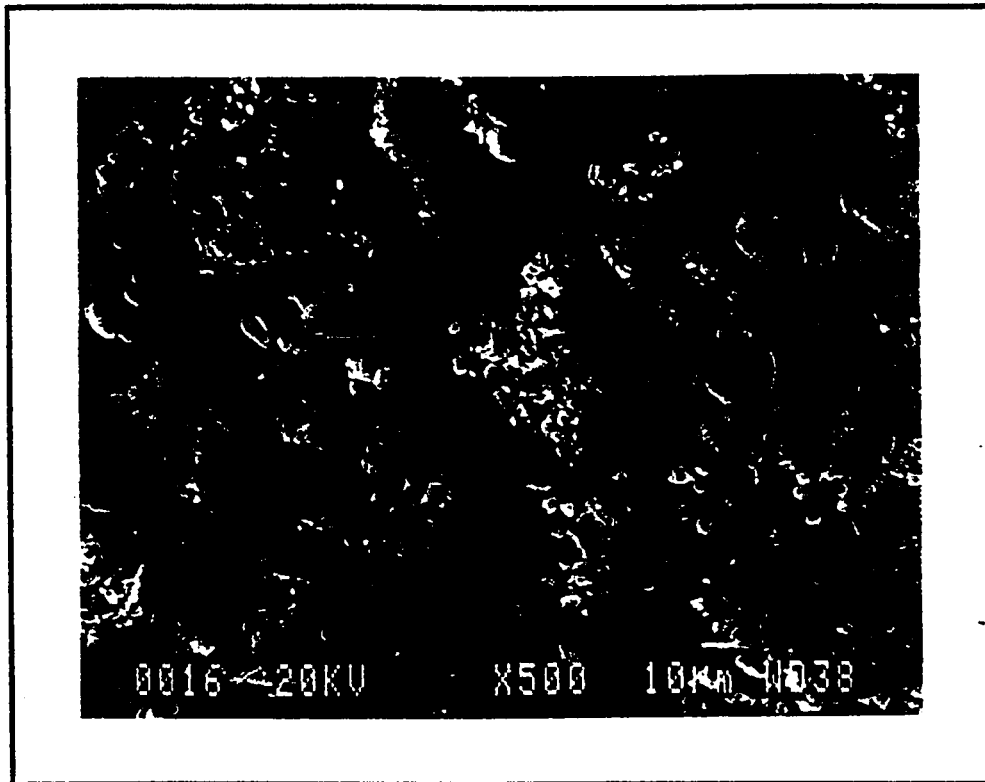


Figure 5.38: Scanning Electron Micrograph of a Corroded Surface of Mild Steel (1018) after Exposure to Drilling Mud in the Flow Loop at pH 9.5 and 253 °F for 8 hours.

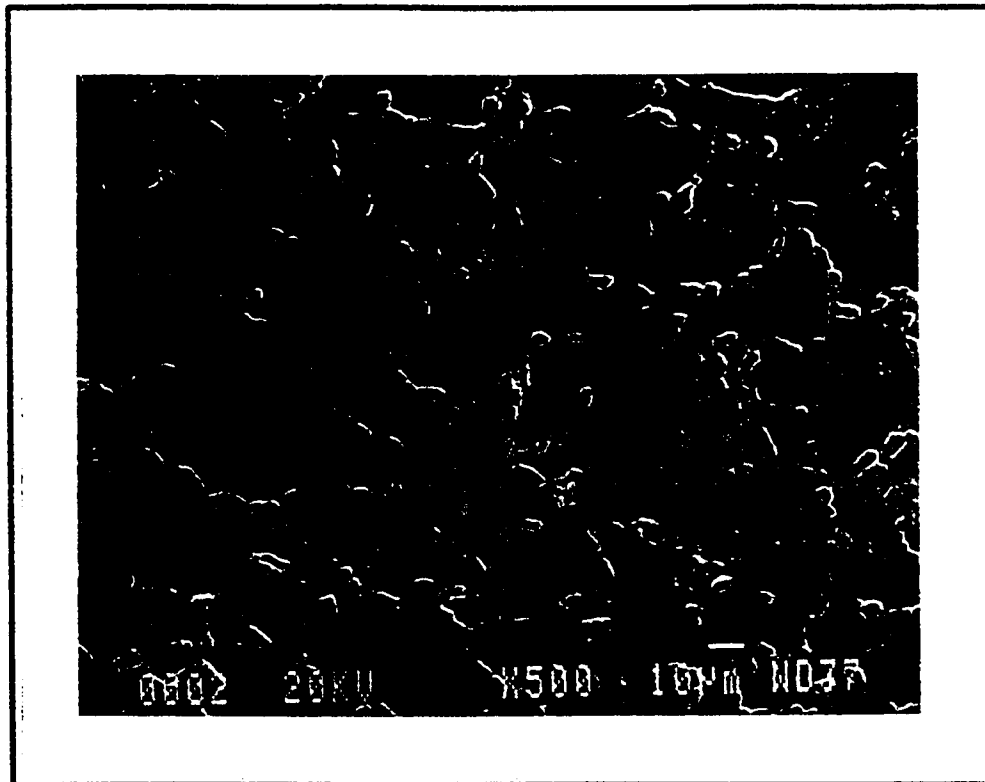


Figure 5.39: Scanning Electron Micrograph of a Corroded Surface of Mild Steel (1018) after Exposure to Drilling Mud in the Flow Loop at pH 8 and 161 °F for 8 hours.

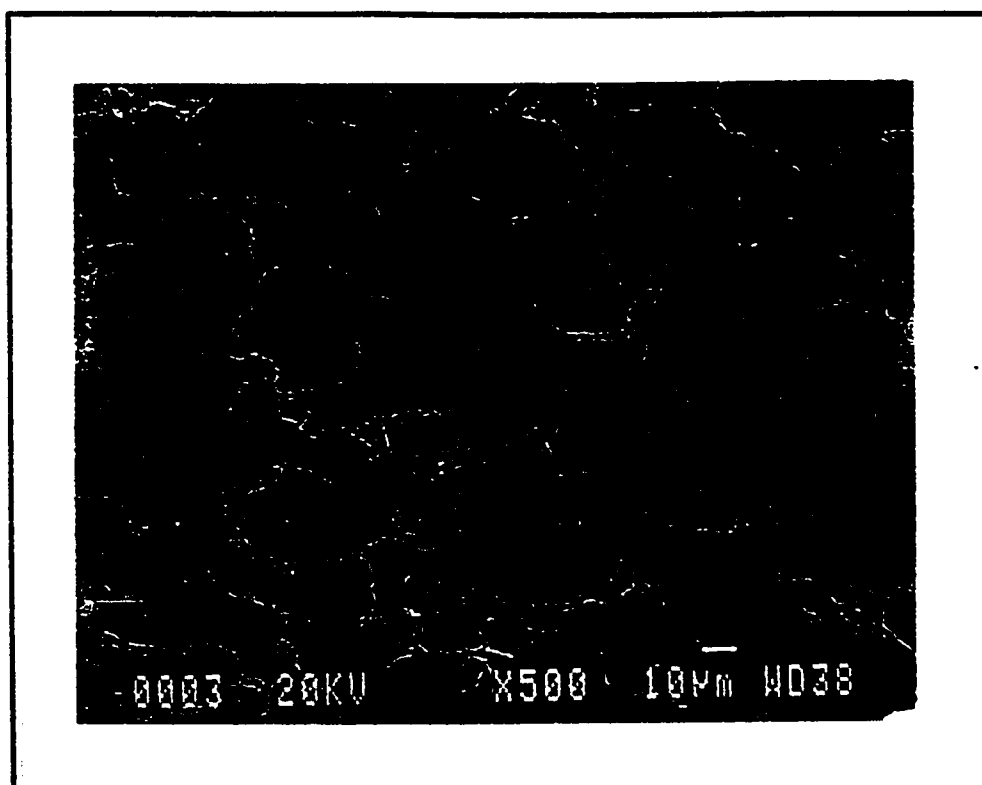


Figure 5.40: Scanning Electron Micrograph of a Corroded Surface of Mild Steel (1018) after Exposure to Drilling Mud in the Flow Loop at pH 6 and 161 °F for 8 hours.

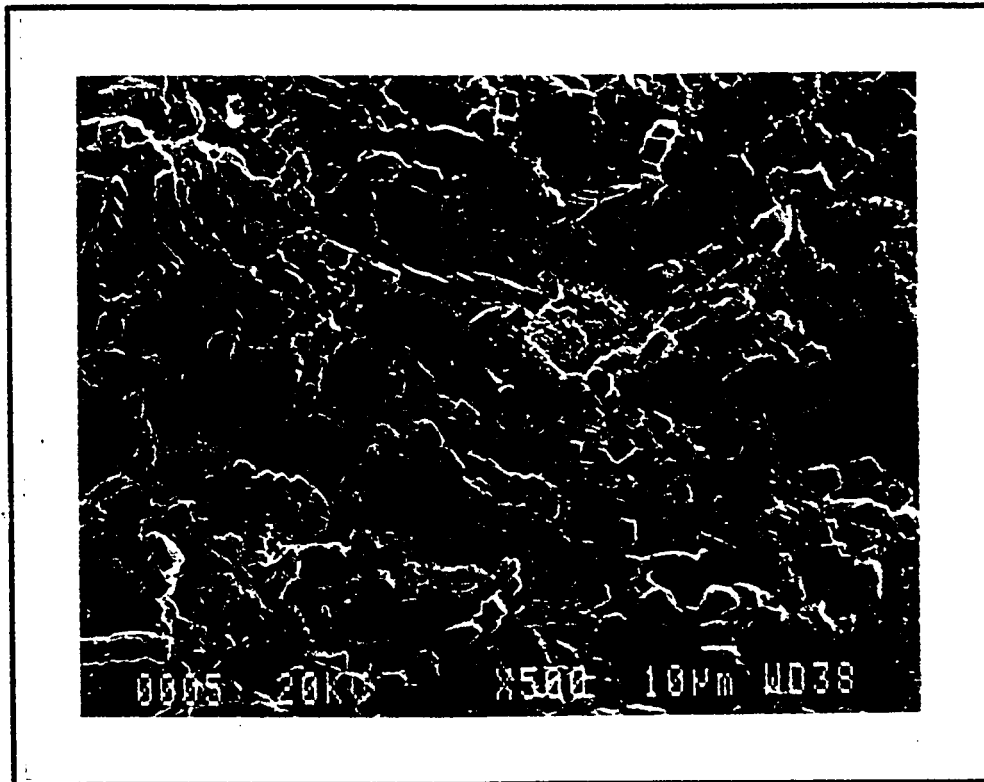


Figure 5.41: Scanning Electron Micrograph of a Corroded Surface of Mild Steel (1018) after Exposure to Drilling Mud in the Flow Loop at pH 4.1 and 161 °F for 8 hours.

is not unexpected since corrosion occurs preferentially at the grain boundaries, a stressful and weaker region of the steel matrix.

The grain boundaries have different atomic structures and chemical compositions compared to the rest of the matrix. Consequently, their electrochemical properties and corrosion resistance are different from those of the grains. The grain boundaries become anodic to the surrounding grains (which is cathodic), and attack is intensified by the small anode to large cathode area ratio^[25,34]. The intergranular attack is less at high pH compared to low pH. This corroborated the low corrosion rate described earlier.

The corrosion that occurred at pH 6 exerts a high stress on the grain boundaries, resulting in wide cracks that will lead to early disintegration of the grain and eventual failure of the steel. It could be recalled from potentiodynamic and flow loop results that corrosion rates are lowest around these pH. These micrographs, however, indicates the susceptibility to early failure of the steel at these pH, even though corrosion rates are low. The type of attack observed in Figure 5.41 at pH 4.1 is uniform over both the grain boundaries and the matrix. It shows severe attack over the entire surface of the steel and no tendency of localized attack is present.

CHAPTER 6

CONCLUSIONS AND RECOMMENDATIONS

6.1 CONCLUSIONS

The following conclusions may be drawn from this work:

1. The drilling mud used for this study is thermally stable for temperatures up to 400 °F.
2. Effective Viscosity, Plastic Viscosity and Yield Strength decreases with increase in temperature and increase in aging time. The effect of aging on rheological properties diminishes with increased aging time and increase in temperature.
3. Weight loss of mild steel (1018) increases with increase in drilling mud temperature. It also increase with increase in exposure time of steel to mud, albeit not significantly.
4. Corrosion is high at low pH and low at high pH while mud pH decreases with increase in temperature and increase in exposure time.
5. Diffusion is the corrosion rate limiting step. Once diffusion resistance is eliminated by increased agitation or high flow rate, corrosion reaction proceeds at a very fast rate.

6. Mild steel (1018) shows some degree of passivation in mildly alkaline to neutral pH region. This results in generally low corrosion rate around this region.
7. Corrosion attack on mild steel (1018) occurs generally at the grain boundaries. More stressful intergranular attack occurred at pH 6.
8. Weight loss and thus corrosion rates of coupons exposed in the flow loop for 8 hours is comparable in magnitude to that of coupons exposed in the roller oven for 10 days. It is, therefore, very important to study corrosion of drilling fluids under flow, temperature, and pressure conditions experienced in practice. It is also important to observe the physical nature of corrosion occurring under the scanning electron microscope.
9. pH is a critical factor whose effect should be investigated for any mud formulation to be used in practice. This work shows that low pH (< 8) is very corrosive.
10. The results obtained from all corrosion monitoring techniques used in this work are consistent.

6.2 RECOMMENDATIONS

The following are recommended based on the experience gathered from this work:

1. Based on our mud formulation, the use of mud in the mildly alkaline to mildly acidic pH range which is the current practice in the industry is not recommended.
2. Improvement in flow loop design and capabilities:
 - a) There is need to have a good control of fluid flow rate through the loop. Sequel to this, flow measurement instruments and controllers should be installed at several points in the loop.
 - b) Process control and data acquisition of measured parameters is very critical. Attempt should be made to automate this.
 - c) The corrosion measurement system needs to be updated.
 - d) Provision of facilities for fluid (liquid and gas) injection at selected points on the flow loop is essential to facilitate broad based study of drilling fluid corrosion and other properties.
3. Further studies essential for better understanding of drilling fluid corrosiveness:
 - a) Chemical and physical analysis of drilling fluid corrosion reaction products is essential for determination of its reaction mechanism.
 - b) Further electrochemical studies on the drilling mud used for this work and other water-base drilling fluid compositions should be

carried out. This in conjunction with (a) will enable the evolution of a general corrosion reaction mechanism for these fluids, and to obtain kinetic parameters useful in characterizing them.

- c) These studies should preferably be carried out on actual drill pipe/casing materials under flow rate/agitation typical of mud circulation when drilling a well.
- d) Electrochemical dc and AC impedance studies should be carried out at high rotation speeds to eliminate diffusion effect.
- e) Erosion-corrosion studies should be carried out to ascertain its contribution to drilling fluid corrosivity.

NOMENCLATURE

A	Exposed area available for corrosion, cm ²
E	Polarization potential, mV
E _{corr}	Corrosion (open circuit) potential, mV
EV	Effective viscosity, mPa.s
F	Faraday, 96487 coulombs
GS	Gel strength, dPa
I	Corrosion current, μA
I _{corr}	Corrosion current density, μA/cm ²
i _{lima}	Limiting current density, mA/cm ²
k	Consistency index (equivalent viscosity at unit shear rate), mPa.s
M	Molecular weight, g
m	Equivalent weight (M/n), g
mpy	Corrosion rate, mils per year
n	Number of electrons
n'	Power law exponent
PV	Plastic Viscosity, mPa.s
Q	Quantity of electric charge, coulombs
R _{ct}	Charge transfer resistance, Ω
R _{so}	Ohmic solution resistance, Ω
RCE	Rotating Cylinder Electrode
t	Time, seconds
W	Weight of electroactive species, g

YP	Yield strength, dPa
Z'	Real part of electrochemical impedance, Ω
Z''	Imaginary part of electrochemical impedance, Ω
β_a	Anodic Tafel slope
β_c	Cathodic Tafel slope
ρ	Density, g/cm^3
ω	Angular velocity (2π rpm), rad/s
θ_x	Viscometer dial reading at x rpm
θ	Phase Angle

REFERENCES

1. Simpson, J.P. and Barbee, R.D. "Corrosivity of Water Base Completion Muds." CO₂ Corrosion in Oil and Gas Production - Selected Papers, Abstracts, and References, NACE, Houston, Texas. 1984. pp. 407-416.
2. Zitter, H. "Corrosion Phenomena in Sour Gas Wells." Erdol, Erdgas, Zeitschrift, **89** (3) 1973. pp. 101-106.
3. Bush, H.E. "Treatment of Drilling Fluid to Combat Corrosion." SPE 5123. SPE of AIME 49th Annual Fall Meeting, Houston Texas. Oct. 6-9, 1974 pp. 1-11.
4. Carney, Leroy L. and Jones, Bob "Practical Solutions to Combat the Detrimental Effects of Hydrogen Sulfide During Drilling Operations." SPE 5198. SPE of AIME Symposium on Sour Gas and Crude, Tyler, Texas, Nov. 11-12, 1974 pp. 113-121.
5. Mauzy, Harry L. "Drillstem Maintenance in Sulfide Environments." SPE 5200. SPE of AIME Symposium on Sour Gas and Crude, Tyler, Texas, Nov. 11-12, 1974 pp. 137-141.
6. Azar, Jamal J. and Luminus, James L. "The Effect of Drill Fluid pH on Drill Pipe Corrosion Fatigue Performance." SPE 5516. SPE of

- AIME 50th Annual Fall Meeting, Dallas, Texas, Sept. 28-Oct. 1, 1975.
7. Woodroof, Robert A.; Baker, James R. and Jenkins Jr., Robert A. "Corrosion Inhibition of Hydrochloric-Hydrofluoric Acid/Mutual Solvent Mixtures at Elevated Temperatures." SPE 5645. SPE of AIME 50th Annual Fall Meeting, Dallas, Texas, Sept. 28-Oct. 1, 1975.
 8. Smith, C.F.; Dollarhide, F.E. and Byth, Nancy J. "Acid Corrosion Inhibition- Are We Getting What We Need?" JPT, May 1978. pp. 737-746.
 9. Ray, J.D.; Randall, B.V. and Parker, J.C. "Use of Reactive Iron Oxide to Remove H₂S From Drilling Fluid." JPT, June 1979. pp. 787-801.
 10. Azar, Jamal J. "How O₂, CO₂ And Chlorides Affect Drill Pipe Fatigue." Petroleum Engineer, Mar. 1979. pp. 72-78.
 11. Samuels, A. and Gupta, D.V.S. "Preventing Corrosion in Drilling." Proceedings of the International Symposium on Solving Corrosion and Scaling Problems in Geothermal Systems. San Francisco, California. Jan. 17-20, 1983. pp. 249-268.
 12. Moussa, M.M. "New Techniques To Measure and Control Corrosion and Thermal Stability of Drilling Fluids in Deep Wells." SPE 11512.

SPE Middle East Oil Technical Conference, Manama, Bahrain. Mar. 14-17, 1983. pp. 571-580.

13. Okoye, C.U.; Agusiegbe, C.V. and Hayatdavoudi, A. "Statistical Analysis of Factors that Promote Drilling Fluid Corrosion at Elevated Temperatures." SPE 17164. SPE Formation Damage Control Symposium, Bakersfield, California. Feb. 8-9, 1988 pp. 185-196.
14. Gilbert, Donald L. and Engen, Richard J. "Khuff Gas Well Downhole Scale and Corrosion- Experience and Evaluation." NACE 4th Middle East Corrosion Conference, Jan. 11-13, 1988. pp. 130-145.
15. Al-Marhoun, M.A. and Rahman, S.S. "Evaluation of Drilling Fluid Performance Under Simulated Bottom Hole Conditions." The Arabian Journal for Science and Engineering, 13 (3) 1988 pp. 343-54.
16. Kasnick, M.A. and Engen, R.J. "Iron Sulfide Scaling and Associated Corrosion in Saudi Arabian Khuff Gas Wells." SPE 17933, SPE Middle East Oil Technical Conference and Exhibition, Bahrain, Mar. 11-14, 1989. pp. 75-80.
17. Abdalla, M. Seham. "Appraisal of Techniques Applied to Stimulate the Deep Khuff Gas Wells." SPE 17950, SPE Middle East Oil Technical Conference and Exhibition, Bahrain, Mar. 11-14, 1989. pp. 199-206.

18. Ciaraldi, S.W. *et.al.* "Corrosion and Stress-Corrosion Cracking of Aluminium Alloy Drillpipe in a Water-Base, Low-Solids, Non-Dispersed Drilling Mud." SPE Drilling Engineering, June 1990. pp. 135-140.
19. Al-Marhoun, M.A. and Rahman, S.S. "Treatment of Drilling Fluid to Combat Drill Pipe Corrosion." Corrosion, Sept. 1990. pp. 778-782.
20. Darley, H.C.H. and Gray, George R. "Composition and Properties of Drilling and Completion Fluids." 5th Edition. Gulf Publishing Company, Houston. Feb. 1991.
21. Al-Marhoun, M.A. and Rahman, S.S. "Thermal Stability and Corrosivity of Drilling Fluids." Final Report, KACST Project No. AR-4-63, Mar.1988 (Revised) pp. 8-11, 102-230.
22. Uhlig, H. H., "Corrosion and Corrosion Control" 2nd ed. John Wiley & Sons, 1971.
23. Petrolite Instruments, Technical Manual for Model M-1010 Corrosion Data Acquisition System, 1981.
24. Kendig, M. "Corrosion Mechanism Using Electrochemical Impedance Spectroscopy." Perspectives on Corrosion. Prentice, G. and Smyrl, W.H. eds., AIChE Symposium Series. no 278, v.86, 1990.

25. Fontana, M.G. and Greene, N.D. "Corrosion Engineering." 2nd ed. Mc Graw-Hill, 1978.
26. Gabrielli, C. "Identification of Electrochemical Processes by Frequency Response Analysis" Technical Report Number 004/83. Solartron Instruments, 1984.
27. Personal Consultation with Dr. Oluwatoyin A. Ashiru, Research Institute, KFUPM. Saudi Arabia.
28. NACE Corrosion Engineer's Reference Book. R.S. Treseder, ed. National Association of Corrosion Engineers, Houston, Texas. 1980. pp.20-21.
29. Dean, S.W. "Overview of Corrosion Monitoring in Modern Industrial Plants." Corrosion Monitoring in Industrial Plants Using Nondestructive Testing and Electrochemical Methods. ASTM STP 908. Moran, G.C. and Labine, P. eds. ASTM, 1986. pp.197-220.
30. Magcobar Drilling Fluid Engineering Manual, Magcobar Division Oil Field Products Group, Dresser Industries Inc., Houston, Texas. Jan. 1977 (revised).
31. Ashiru, O. A. "Identification of Electrochemical Corrosion Processes Using Frequency Response Analysis." Proceedings of the First National Congress on Corrosion, Nigerian Corrosion Association, Jos, Nigeria. Nov. 30 - Dec. 2, 1988. pp. 187-202.

32. Princeton Applied Research, Operating Manual for Model 350A Corrosion Measurement System.
33. Mansfeld, F. "Recording and Analysis of AC Impedance Data for Corrosion Studies. I: Background and Methods of Analysis." *Corrosion* **36** (5) 1981.
34. Perry, B. "Corrosion Principles for Engineering Technicians." Department of Industry, London. 1982.

APPENDICES

Appendix A

EXPERIMENTAL DATA FOR THERMAL STABILITY TESTS

The following relationships were used to calculate the various parameters which describe the rheological properties of drilling fluids:

Effective Viscosity: measured as

$$EV = \theta_{600}/2 \text{ (mPa.s)}$$

where θ_{600} is the dial reading on the viscometer at 600 rpm. This implies that EV is measured at a shear rate of 1022 s^{-1} .

Plastic Viscosity: measured as

$$PV = \theta_{600} - \theta_{300} \text{ (mPa.s)}$$

where θ_{300} is the dial reading on the viscometer at 300 rpm.

Yield Strength: it is determined from

$$YP = 4.788026 * (\theta_{300} - PV) \text{ (dPa)}$$

Gel Strength: a measure of the minimum shear stress required to create the flow of the drilling fluid. It is measured immediately after the agitation of the mud, and shows the structural viscosity of the mud under circulation.

$$GS = 4.788026 * \theta_3 \text{ (dPa)}$$

where θ_3 is the dial reading at 3 rpm.

Power Law Exponent:

$$n' = 3.322 * \log (\theta_{600} / \theta_{300})$$

Consistency Index: This is equivalent to viscosity at unit shear rate

$$k = 4.788026 * \theta_{600} / (1022)^{n'} \text{ (mPa.s)}$$

Table A1: Consistency Curve Data Obtained at 3000 psi after Preparation of Mud (no aging)

Mud Density = 8.55 lb/gal

Mud pH = 10.9

Shear Rate (s^{-1})	Shear Stress (dPa)			
	200°F	250°F	300°F	400°F
1021.80	153.30	117.53	81.76	40.88
851.50	137.46	102.20	71.54	38.32
681.20	121.62	86.87	61.32	35.77
510.90	102.20	71.54	51.10	33.21
340.60	79.72	57.23	40.88	30.66
170.30	52.12	39.86	30.66	28.10
5.11	15.33	17.88	15.33	22.99

Table A2: Consistency Curve Data Obtained at 3000 psi after Aging for 5 days

Shear Rate (s^{-1})	Shear Stress (dPa)			
	200°F	250°F	300°F	400°F
1021.80	86.87	43.43	38.33	25.55
851.50	77.67	38.84	35.26	22.99
681.20	67.45	35.26	31.68	20.44
510.90	56.21	30.66	28.11	17.88
340.60	43.43	25.60	24.02	15.33
170.30	28.10	19.42	19.42	12.77
5.11	10.22	10.22	12.78	10.22

Table A3: Consistency Curve Data Obtained at 3000 psi after Aging for 10 days.

Shear Rate (s^{-1})	Shear Stress (dPa)			
	200°F	250°F	300°F	400°F
1021.80	71.54	33.21	35.77	25.55
851.50	62.34	29.13	32.19	22.99
681.20	52.12	24.53	28.62	20.44
510.90	43.43	20.44	25.55	17.88
340.60	31.68	16.35	21.97	15.33
170.30	19.93	12.26	18.91	12.77
5.11	5.11	7.66	12.78	10.22

Table A4: Consistency Curve Data Obtained at 3000 psi after Aging for 15 days

Shear Rate (s^{-1})	Shear Stress (dPa)			
	200°F	250°F	300°F	400°F
1021.80	61.32	28.10	30.66	17.88
851.50	53.65	24.55	28.10	16.35
681.20	45.48	21.44	25.55	14.82
510.90	35.77	17.88	22.99	12.77
340.60	25.55	15.33	20.44	11.24
170.30	15.33	11.24	17.88	9.71
5.11	5.11	7.66	15.33	7.66

Table A5: Consistency Curve Data Obtained at 3000 psi after Aging for 20 days

Shear Rate (s^{-1})	Shear Stress (dPa)			
	200°F	250°F	300°F	400°F
1021.80	58.76	20.44	30.66	15.33
851.50	50.08	18.86	28.10	14.56
681.20	41.39	17.27	25.55	13.54
510.90	33.21	15.33	22.99	12.78
340.60	24.02	12.78	20.44	10.63
170.30	13.80	10.22	17.88	7.92
5.11	5.11	7.67	15.33	5.11

Table A6: Consistency Curve Data Obtained at Ambient Conditions after Aging at 250°F.

Shear Rate (s^{-1})	Shear Stress (dPa)				
	0 day	5 days	10 days	15 days	20 days
1021.80	281.05	140.52	99.64	66.43	48.55
851.50	260.61	123.66	86.87	56.21	41.65
681.20	232.50	106.29	71.54	47.01	34.08
510.90	204.40	89.42	58.76	38.32	28.11
340.60	168.63	68.98	45.99	28.10	20.80
170.30	122.64	45.99	28.10	17.88	12.78
5.11	40.88	5.11	5.11	5.11	2.56

Table A7: Effective Viscosity Data Obtained at 3000 psi, Different Temperatures and Aging period.

Temperature (°F)	Effective Viscosity (mPas)				
	0 day	5 days	10 days	15 days	20 days
200	15.00	8.50	7.50	6.00	5.75
250	11.50	4.25	3.25	2.75	2.00
300	8.00	3.75	3.50	3.00	3.00
400	4.00	2.50	2.50	1.75	1.50

Table A8: Plastic Viscosity Data Obtained at 3000 psi, different Temperatures and Aging period.

Temperature (°F)	Plastic Viscosity (mPas)				
	0 day	5 days	10 days	15 days	20 days
200	10.0	6.0	5.5	5.0	5.0
250	9.0	2.5	2.5	2.0	1.0
300	6.0	2.0	2.0	1.5	1.5
400	1.5	1.5	1.5	1.0	0.5

Table A9: Yield Strength Data Obtained at 3000 psi, Different Temperatures and Aging period.

Temperature (°F)	Yield Strength (dPa)				
	0 day	5 days	10 days	15 days	20 days
200	47.88	23.94	14.36	9.58	7.18
250	23.94	16.76	7.18	7.18	9.58
300	19.15	16.76	14.36	14.36	14.36
400	23.94	9.58	9.58	7.18	9.58

Table A10: Gel Strength Data Obtained at 3000 psi, Different Temperatures and Aging period.

Temperature (°F)	Gel Strength (dPa)				
	0 day	5 days	10 days	15 days	20 days
200	14.36	9.58	4.79	4.79	4.79
250	16.76	9.58	7.18	7.18	7.18
300	14.36	11.97	11.97	14.36	14.36
400	21.55	9.58	9.58	7.18	4.79

Table A11: Power Law Exponent, n' Obtained from all Tests at 3000 psi, Different Temperatures and Aging period.

Temperature (°F)	n'				
	0 day	5 days	10 days	15 days	20 days
200	0.5850	0.6280	0.7199	0.7776	0.8231
250	0.7162	0.5025	0.7005	0.6521	0.4151
300	0.6781	0.4475	0.4854	0.4151	0.4151
400	0.2996	0.5146	0.5146	0.4854	0.2630

Table A12: Consistency Index, k Obtained from all Tests at 3000 psi, Different Temperatures and Aging period.

Temperature (°F)	k (mPas) equivalent viscosity at unit shear rate				
	0 day	5 days	10 days	15 days	20 days
200	0.025	0.011	0.005	0.003	0.002
250	0.008	0.013	0.002	0.003	0.011
300	0.007	0.016	0.012	0.016	0.016
400	0.048	0.007	0.007	0.006	0.023

Appendix B

EXPRIMENTAL DATA FOR ROLLER OVEN AND FLOW LOOP CORROSION TESTS

Table B1: Corrosion Rate Data of Mild Steel (1018) Coupons Exposed to Mud in the Roller Oven at 200°F. pH of Mud = 10.9

Time (days)	Coupon #	Initial weight (g)	Final Weight (g)	Weight Loss (g)	Average weight Loss (mg)	Weight Loss per unit area (mg/cm ²)	pH after test
5	1	4.590	4.588	0.002	2.3	0.260	9.43
	2	4.400	4.399	0.001			
	3	4.742	4.738	0.004			
10	1	4.605	4.600	0.005	6.7	0.757	9.29
	2	4.461	4.455	0.006			
	3	4.509	4.500	0.009			
15	1	4.640	4.631	0.009	11.0	1.243	9.05
	2	4.192	4.184	0.008			
	3	4.510	4.494	0.016			
20	1	4.912	4.893	0.019	18.7	2.112	8.75
	2	4.893	4.875	0.018			
	3	4.561	4.542	0.019			

Table B2: Corrosion Rate Data of Mild Steel (1018) Coupons Exposed to Mud in the Roller Oven at 250°F. pH of Mud = 10.9

Time (days)	Coupon #	Initial weight (g)	Final Weight (g)	Weight Loss (g)	Average weight Loss (mg)	Weight Loss per unit area (mg/cm ²)	pH after test
5	1	4.400	4.392	0.008	11.0	1.243	9.0
	2	4.743	4.732	0.011			
	3	4.592	4.581	0.011			
10	1	4.457	4.437	0.020	18.7	2.112	9.0
	2	4.500	4.481	0.019			
	3	4.600	4.583	0.017			
15	1	4.576	4.548	0.028	24.7	2.790	8.8
	2	4.563	4.541	0.022			
	3	4.573	4.549	0.024			
20	1	4.636	4.605	0.031	33.0	3.728	8.0
	2	4.578	4.544	0.034			
	3	4.599	4.565	0.034			

Table B3: Corrosion Rate Data of Mild Steel (1018) Coupons Exposed to Mud in the Roller Oven at 300°F. pH of Mud = 10.9

Time (days)	Coupon #	Initial weight (g)	Final Weight (g)	Weight Loss (g)	Average weight Loss (mg)	Weight Loss per unit area (mg/cm ²)	pH after test
5	1	4.636	4.603	0.033	30.7	3.468	8.5
	2	4.613	4.582	0.031			
	3	4.670	4.642	0.028			
10	1	4.593	4.556	0.037	38.3	4.326	8.00
	2	4.607	4.567	0.040			
	3	4.606	4.568	0.038			
15	1	4.658	4.619	0.039	39.0	4.406	6.30
	2	-	-	-			
	3	4.639	4.600	0.039			
20	1	4.645	4.598	0.047	46.3	5.230	5.90
	2	4.632	4.585	0.047			
	3	4.491	4.446	0.045			

Table B4: Corrosion Rate Data of Mild Steel (1018) Coupons Exposed to Mud in the Roller Oven at 400°F. pH of mud = 10.9

Time (days)	Coupon #	Initial weight (g)	Final Weight (g)	Weight Loss (g)	Average weight Loss (mg)	Weight Loss per unit area (mg/cm ²)	pH after test
5	1	4.624	4.559	0.065	83.7	9.455	5.90
	2	4.660	4.559	0.101			
	3	4.620	4.535	0.085			
10	1	4.670	4.579	0.091	90.3	10.200	5.90
	2	4.533	4.441	0.092			
	3	4.598	4.510	0.088			
15	1	4.526	4.427	0.099	96.0	10.844	5.82
	2	4.587	4.498	0.089			
	3	4.683	4.583	0.100			
20	1	4.675	4.587	0.088	101.3	11.443	5.60
	2	4.663	4.545	0.118			
	3	4.187	4.089	0.098			

Table B5: Corrosion Rate Data of Mild Steel (1018) Coupons Exposed to Mud in the Roller Oven at pH of 7.9. Temperature = 250°F

Time (days)	Coupon #	Initial weight (g)	Final Weight (g)	Weight Loss (g)	Average weight Loss (mg)	Weight Loss per unit area (mg/cm ²)	pH after test
5	1	4.734	4.722	0.012	10.0	1.130	7.7
	2	4.585	4.577	0.008			
	3	4.395	4.385	0.010			
10	1	4.609	4.591	0.018	21.7	2.451	7.5
	2	4.603	4.577	0.026			
	3	4.634	4.613	0.021			
15	1	4.444	4.405	0.039	35.5	4.010	8.1
	2	4.493	4.461	0.032			
	3	-	-	-			
20	1	4.572	4.503	0.069	60.3	6.812	6.8
	2	4.584	4.533	0.051			
	3	4.582	4.521	0.061			

Table B6: Corrosion Rate Data of Mild Steel (1018) Coupons Exposed to Mud in the Roller Oven at pH of 6.1. Temperature = 250°F

Time (days)	Coupon #	Initial weight (g)	Final Weight (g)	Weight Loss (g)	Average weight Loss (mg)	Weight Loss per unit area (mg/cm ²)	pH after test
5	1	4.686	4.676	0.010	9.5	1.073	7.7
	2	4.350	4.341	0.009			
	3	-	-	-			
10	1	4.564	4.547	0.017	22.0	2.485	6.9
	2	4.603	4.574	0.029			
	3	4.538	4.518	0.020			
15	1	4.563	4.506	0.057	51.7	5.840	6.7
	2	4.557	4.509	0.048			
	3	4.532	4.482	0.050			
20	1	4.571	4.436	0.135	135.3	15.284	6.8
	2	4.132	3.990	0.142			
	3	4.540	4.411	0.129			

Table B7: Corrosion Rate Data of Mild Steel (1018) Coupons Exposed to Mud in the Roller Oven at pH of 4.9. Temperature = 250°F

Time (days)	Coupon #	Initial weight (g)	Final Weight (g)	Weight Loss (g)	Average weight Loss (mg)	Weight Loss per unit area (mg/cm ²)	pH after test
5	1	4.694	4.684	0.010	9.7	1.096	6.4
	2	4.537	4.524	0.013			
	3	4.353	4.347	0.006			
10	1	4.596	4.576	0.020	23.3	2.632	6.5
	2	4.559	4.531	0.028			
	3	4.160	4.138	0.022			
15	1	4.460	4.338	0.122	116.3	13.137	6.3
	2	4.609	4.490	0.119			
	3	4.595	4.487	0.108			
20	1	4.601	4.239	0.362	399.7	45.151	6.3
	2	4.539	4.249	0.290			
	3	4.671	4.124	0.547			

Table B8: Corrosion Rate Data of Mild Steel (1018) Coupons Exposed to Mud in the Cold Section of Flow Loop at 3000 psi for 8 hours. pH of mud = 9.5

Temp. (°F)	Coupon #	Initial weight (g)	Final weight (g)	Weight Loss (g)	Exposed area (cm ²)	Corrosion Rate (mpy)	Average Corrosion Rate (mpy)	Flow rate (cm ³ /s)	pH after Test
98	1R	2.705	2.694	0.011	5.6420	106.50	124.34	60.97	9.3
	1L	2.616	2.605	0.011	5.5480	108.29			
	2R	2.303	2.291	0.012	4.8830	134.25			
	2L	2.658	2.643	0.015	5.5245	148.32			
104	1R	2.353	2.349	0.004	5.0394	43.36	37.24	32.78	8.9
	1L	2.344	2.341	0.003	4.9722	32.96			
	2R	2.321	2.318	0.003	4.9278	33.26			
	2L	2.650	2.646	0.004	5.5480	39.38			
109	1R	2.367	2.364	0.003	4.9950	32.82	32.32	22.44	8.9
	1L	2.585	2.582	0.003	5.9300	27.63			
	2R	2.582	2.578	0.004	5.4538	40.06			
	2L	2.718	2.715	0.003	5.7003	28.75			
120	1R	2.658	2.658	0	5.5593	-	40.56	50.86	9.1
	1L	2.651	2.646	0.005	5.6662	48.20			
	2R	2.401	2.396	0.005	5.1518	53.02			
	2L	2.505	2.503	0.002	5.3370	20.47			

Table B9: Corrosion Rate Data of Mild Steel (1018) Coupons Exposed to Mud in the Hot Section of Flow Loop at 3000 psi for 8 hours. pH of mud = 9.5

Temp. (°F)	Coupon #	Initial weight (g)	Final weight (g)	Weight Loss (g)	Exposed area (cm ²)	Corrosion Rate (mpy)	Average Corrosion Rate (mpy)	Flow rate (cm ³ /s)	pH after Test
105	1R	2.473	2.463	0.010	5.2434	104.18	130.72	60.97	9.3
	1L	2.251	2.237	0.014	4.7941	159.51			
	2R	2.555	2.543	0.012	5.4290	120.74			
	2L	2.654	2.640	0.014	5.5246	138.44			
161	1R	2.488	2.480	0.008	5.3130	82.24	66.0	32.78	8.9
	1L	2.309	2.303	0.006	4.9054	66.82			
	2R	2.313	2.308	0.005	4.9358	55.32			
	2L	2.571	2.565	0.006	5.4980	59.61			
196	1R	2.350	2.342	0.008	4.995	87.49	93.74	50.86	9.1
	1L	2.656	2.646	0.010	5.5728	99.09			
	2R	2.589	2.579	0.010	5.3951	101.25			
	2L	2.653	2.644	0.009	5.6432	87.12			
253	1R	2.310	2.301	0.009	4.9390	99.54	110.53	22.44	8.9
	1L	2.287	2.276	0.011	4.8931	122.80			
	2R	2.343	2.331	0.012	5.0150	130.71			
	2L	2.299	2.291	0.008	4.9056	89.08			

Table B10: Corrosion Rate Data of Mild Steel (1018) Coupons Exposed to Mud in the Cold Section of Flow Loop at 3000 psi for 8 hours.

Mud pH	Coupon #	Initial weight (g)	Final weight (g)	Weight Loss (g)	Exposed area (cm ²)	Corrosion Rate (mpy)	Average Corrosion Rate (mpy)	Flow rate (cm ³ /s)	pH after Test
9.5 (104 °F)	1R	2.353	2.349	0.004	5.0394	43.36	37.24	32.78	8.9
	1L	2.344	2.341	0.003	4.9722	32.96			
	2R	2.321	2.318	0.003	4.9278	33.26			
	2L	2.650	2.646	0.004	5.5480	39.38			
8.1 (99 °F)	1R	2.299	2.296	0.003	4.9056	33.39	37.19	29.11	8.1
	1L	2.265	2.261	0.004	4.8342	45.19			
	2R	2.546	2.542	0.004	5.4540	40.07			
	2L	2.586	2.583	0.003	5.4423	30.11			
6.0 (103 °F)	1R	2.512	2.509	0.003	5.4186	30.24	18.87	34.96	6.5
	1L	2.265	2.263	0.002	4.8170	22.68			
	2R	2.246	2.245	0.001	4.7010	11.62			
	2L	2.358	2.357	0.001	4.9944	10.93			
4.1 (96 °F)	1R	2.632	2.608	0.024	5.5480	236.29	218.43	31.48	4.4
	1L	2.631	2.608	0.023	5.5363	226.93			
	2R	2.643	2.622	0.021	5.6072	204.60			
	2L	2.643	2.622	0.021	5.5715	205.91			

Table B11: Corrosion Rate Data of Mild Steel (1018) Coupons Exposed to Mud in the Hot Section of Flow Loop at 3000 psi for 8 hours. Temperature = 161 °F

Mud pH	Coupon #	Initial weight (g)	Final weight (g)	Weight Loss (g)	Exposed area (cm ²)	Corrosion Rate (mpy)	Average Corrosion Rate (mpy)	Flow rate (cm ³ /s)	pH after Test
9.5	1R	2.488	2.480	0.008	5.3130	82.24	66.0	32.78	8.9
	1L	2.309	2.303	0.006	4.9054	66.82			
	2R	2.313	2.308	0.005	4.9358	55.32			
	2L	2.571	2.565	0.006	5.4980	59.61			
8.1	1R	2.648	2.644	0.004	5.5836	39.11	47.74	29.11	8.1
	1L	2.606	2.600	0.006	5.4775	59.83			
	2R	2.199	2.196	0.003	4.6826	35.00			
	2L	2.229	2.224	0.005	4.7886	57.03			
6.0	1R	2.414	2.413	0.001	5.0933	10.71	14.36	34.96	6.5
	1L	2.440	2.438	0.002	5.1140	21.37			
	2R	2.369	2.368	0.001	4.9710	11.01			
	2L	2.597	2.597	0.000	5.5010	-			
4.1	1R	2.666	2.645	0.021	5.6671	202.42	202.09	31.48	4.4
	1L	2.520	2.500	0.020	5.3198	305.35			
	2R	2.574	2.552	0.022	5.4498	220.51			
	2L	2.733	2.714	0.019	5.7630	180.09			

Table B12: Polarization Resistance Corrosion Rate Data of Mild Steel
(1018) Coupons Exposed to Mud in the Cold Section of Flow
Loop at Different Temperature and 3000 psi over an 8 hour
period. pH of Mud = 9.5

Temperature (°F)	Corrosion Rate (mpy)	Flow Rate (cm ³ /s)	pH after Test
98	29.50	60.97	9.3
104	25.75	32.78	8.9
120	29.50	50.86	9.1
109	27.50	22.4	8.9

Table B13: Polarization Resistance Corrosion Rate Data of Mild Steel
(1018) Coupons Exposed to Mud in the Hot Section of Flow
Loop at Different Temperature and 3000 psi over an 8 hour
period. pH of Mud = 9.5

Temperature (°F)	Corrosion Rate (mpy)	Flow Rate (cm ³ /s)	pH after Test
105	33.75	60.97	9.3
161	28.90	32.78	8.9
196	36.50	50.86	9.1
253	18.75	22.40	8.9

Table B14: Polarization Resistance Corrosion Rate Data of Mild Steel
(1018) Coupons Exposed to Mud in the Cold Section of Flow
Loop at Different pH and 3000 psi over an 8 hour period.

Mud pH	Corrosion Rate (mpy)	Flow Rate (cm ³ /s)	pH after Test
9.5 (104 °F)	25.75	32.78	8.9
8.1 (99 °F)	17.75	29.11	8.1
6.0 (103 °F)	14.00	34.96	6.5
4.1 (96 °F)	180.00	31.48	4.4

Table B15: Polarization Resistance Corrosion Rate Data of Mild Steel
(1018) Coupons Exposed to Mud in the Hot Section of Flow
Loop at Different pH and 3000 psi over an 8 hour period.
Temperature = 161 °F

Mud pH	Corrosion Rate (mpy)	Flow Rate (cm ³ /s)	pH after Test
9.5	28.90	32.78	8.9
8.1	22.50	29.11	8.1
6.0	8.00	34.96	6.5
4.1	127.00	31.48	4.4

Appendix C

EXPERIMENTAL DATA FOR POTENTIODYNAMIC AND AC IMPEDANCE POLARIZATION TESTS

Table C1: Potentiodynamic Polarization Data Measured Under Static and Ambient Conditions at Different Mud pH.

Mud pH	E_{corr} (mV SCE)	Tafel Slopes		R_p (ohm)	I_{corr} ($\mu\text{A}/\text{cm}^2$)	Corrosion Rate (mpy)
		β_a	β_c			
10.9	-482	0.417	0.155	2816	17.42	8.047
8.0	-712	0.230	0.148	2441	16.05	7.414
6.0	-680	0.225	0.151	2315	16.93	7.921
5.1	-696	0.253	0.151	1349	30.44	14.060
4.1	-686	0.293	0.264	483.2	124.90	57.690

Table C2: Hydrodynamic Data Obtained at Equilibrium Corrosion Potential of 500 mV for Mud pH 4.1

RPM	Angular Velocity, ω ($\text{rad}^{1/2}\text{s}^{1/2}$)	Limiting Current Density, i_{lim} (mA/cm^2)
500	7.236	25.80
800	9.153	29.02
1000	10.233	31.37
1500	12.533	27.75
2000	14.472	26.09

Table C3: Hydrodynamic Data Obtained at Equilibrium Corrosion
Potential of 500 mV for Mud pH 10.9

RPM	Angular Velocity, ω ($\text{rad}^{1/2}\text{s}^{1/2}$)	Limiting Current Density, i_{lim} (mA/cm ²)
100	3.236	9.324
500	7.236	3.479
1000	10.233	9.451
1500	12.533	5.160
2000	14.472	7.438

Table C4: AC Impedance Data Obtained Under Static Condition for Mud
pH 10.9

Frequency, kHz	Real Impedance, Z' (ohm)	Imaginary Impedance, Z''
50.00	40.86	2.711
31.55	41.13	1.906
19.91	41.32	1.429
12.56	41.49	1.070
7.92	41.57	0.903
5.00	41.70	0.804
3.15	41.86	0.807
1.99	42.06	0.835
1.26	42.27	0.899
0.79	42.53	1.010
0.50	42.82	1.114
0.32	43.16	1.251
0.20	43.54	1.413
0.08	44.37	1.752
0.05	44.96	1.730
0.03	45.50	1.763
0.02	45.93	1.722
0.01	46.31	1.697
7.92 Hz	46.37	1.695

Table C5: AC Impedance Data Obtained at 500 rpm for Mud pH 10.9

Frequency, kHz	Real Impedance, Z' (ohm)	Imaginary Impedance, Z''
50.00	43.72	2.335
31.55	44.05	1.966
19.91	44.47	1.534
5.00	45.33	1.055
1.99	45.70	1.126
0.79	47.04	1.580

Table C6: AC Impedance Data Obtained at 1000 rpm for Mud pH 10.9

Frequency, kHz	Real Impedance, Z' (ohm)	Imaginary Impedance, Z''
50.00	65.26	11.213
31.55	67.59	8.978
19.91	69.21	7.487
12.56	70.74	6.900
7.92	72.58	6.735
5.00	74.82	6.553
3.15	76.89	5.987
1.26	79.61	3.970
0.79	81.02	2.617
0.50	81.10	2.569
0.32	83.30	3.140
0.03	85.54	4.830
0.01	89.57	5.863
1.99 Hz	95.03	7.219
0.79 Hz	100.30	8.239
0.20 Hz	107.70	7.522
0.13 Hz	121.86	5.054

Table C7: AC Impedance Data Obtained at 2000 rpm for Mud pH 10.9

Frequency, kHz	Real Impedance, Z' (ohm)	Imaginary Impedance, Z''
50.00	54.46	6.170
31.55	55.46	4.569
19.91	56.09	3.480
12.56	56.69	2.930
7.92	57.24	2.478
5.00	57.89	2.250
3.15	58.03	2.531
1.99	58.86	2.304
1.26	59.24	2.457
0.79	60.18	2.634
0.50	60.96	2.575
0.20	63.88	3.842
0.03	67.83	5.701
0.02	70.61	6.932
0.01	72.40	8.285
7.92 Hz	75.18	8.338
5.00 Hz	76.60	9.855
3.16 Hz	79.80	9.915
1.26 Hz	82.92	11.812
0.79 Hz	84.96	16.751
0.50 Hz	85.73	18.288
0.32 Hz	87.65	23.763

Table C8: AC Impedance Data Obtained Under Static Condition for Mud
pH 4.1

Frequency, kHz	Z'	Z''
50.00	14.59	-8.787
31.55	13.87	-5.523
19.91	13.60	-3.437
12.56	13.51	-2.108
7.92	13.49	-1.232
5.00	13.52	-0.651
3.15	13.59	-0.253
1.99	13.69	0.024
1.26	13.82	0.209
0.79	13.98	0.333
0.50	14.15	0.382
0.32	14.31	0.363
0.20	14.42	0.304
0.13	14.52	0.209
0.08	14.55	0.206
0.05	14.56	0.148
0.03	14.57	0.133
0.02	14.63	0.137
0.01	14.59	0.143
7.92 Hz	14.62	0.166
5.00 Hz	14.63	0.214
3.15 Hz	14.67	0.299
1.99 Hz	14.76	0.449

Table C9: AC Impedance Data Obtained at 500 rpm for Mud pH 4.1

Frequency, kHz	Real Impedance, Z' (ohm)	Imaginary Impedance, Z''
50.00	13.06	-8.914
31.55	12.25	-5.559
19.91	11.98	-3.509
12.56	11.85	-2.161
7.92	11.72	-1.335
5.00	11.86	-0.729
1.99	12.11	0.053
0.20	12.21	0.146
0.08	12.60	0.354
0.79 Hz	13.78	1.043
0.20 Hz	14.22	1.029
0.13 Hz	14.68	0.160
0.01 Hz	15.10	-1.918

Table C10: AC Impedance Data Obtained at 1000 rpm for Mud pH 4.1

Frequency, kHz	Real Impedance, Z' (ohm)	Imaginary Impedance, Z''
50.00	11.57	-9.021
31.55	10.91	-5.692
19.91	10.56	-3.597
12.56	10.27	-2.349
3.15	10.33	-0.436
0.79	10.56	0.235
0.50	10.68	0.524
0.32	11.05	0.582
1.99 Hz	11.96	0.499
1.26 Hz	12.32	0.387
0.79 Hz	12.38	0.174
0.03 Hz	12.34	-0.886

Table C11: AC Impedance Data Obtained at 2000 rpm for Mud pH 4.1

Frequency, kHz	Real Impedance, Z' (ohm)	Imaginary Impedance, Z''
50.00	10.88	-8.746
31.55	10.02	-5.542
19.91	9.70	-3.462
12.56	9.60	-2.120
7.92	9.69	-1.355
5.00	9.65	-0.797
3.15	9.67	-0.356
1.99	9.72	-0.049
0.79	9.81	0.099
0.32	10.27	0.348
0.13	10.42	0.433
0.05	10.50	0.453
0.01	10.69	0.456
3.16 Hz	10.96	0.507
1.26 Hz	11.33	0.647
0.32 Hz	12.02	0.614
0.13 Hz	12.11	0.458

VITA

Personal Information

Name: Olawale Surajudeen Shokoya
Born: July 9, 1965 in Lagos, Nigeria to Mr. and Mrs. A.O. Shokoya.
Permanent Address: 27 Araromi Street, P.O. Box 771, Somolu, Lagos. Nigeria.

Education

- Diploma in Science Technology (June, 1985) from Yaba College of Technology, Yaba, Lagos. Nigeria.
- Bachelor of Science in Chemical Engineering (Sept., 1990) from University of Lagos, Akoka, Lagos. Nigeria.
- Master of Science in Petroleum Engineering (Jan., 1995) from King Fahd University of Petroleum and Minerals, Dhahran, Saudi Arabia.

Member of

Nigerian Society of Chemical Engineers